5-2015

The fabrication of micro- and nano- scale deterministic and stochastic pillar arrays for planar separations

Teresa Byers Kirchner
University of Tennessee - Knoxville, tbyers@vols.utk.edu

Recommended Citation

To the Graduate Council:

I am submitting herewith a dissertation written by Teresa Byers Kirchner entitled "The fabrication of micro- and nano- scale deterministic and stochastic pillar arrays for planar separations." I have examined the final electronic copy of this dissertation for form and content and recommend that it be accepted in partial fulfillment of the requirements for the degree of Doctor of Philosophy, with a major in Chemistry.

Michael J. Sepaniak, Major Professor

We have read this dissertation and recommend its acceptance:

Charles S. Feigerle, Ben (Ziling) Xue, Robert N. Compton

Accepted for the Council:
Dixie L. Thompson

Vice Provost and Dean of the Graduate School

(Original signatures are on file with official student records.)

The fabrication of micro- and nano- scale deterministic and stochastic pillar arrays for planar separations

A Dissertation Presented for the

Doctor of Philosophy

Degree

The University of Tennessee, Knoxville

Teresa Byers Kirchner

May 2015

Dedication

To Matt, Reed,

Mom, Dad,

Candace, Steven,

and Alison

For your guidance, love and, most importantly, your patience.

Acknowledgements

I would like to acknowledge the gratitude that I have for God in all things that I have accomplished. I know that these accomplishments are not mine but through your grace. May I request that in my next life you grant me the good sense to aim for a less painful existence and contentment with a Bachelor's degree. Also, I would like to live in one of the realities with dragons – thanks.

I would like to thank my mentor and research advisor Dr. Michael J. Sepaniak. Regardless of my stubbornness and infinite shortcomings you have somehow managed to get me to this point in my career. I cannot fully express my appreciation for your patience, guidance and commitment to my success.

Also, I would like to thank the members of my committee. The input that each of you have given at the varying stages of my professional development has been invaluable.

The Sepaniak Group: Lisa, Sabrina, Deepak, Zhou, Jim, Nahla, Jennifer, Nichole, Chris, Danielle, Ryan, Rachel. You have all been great friends, therapy and support. I recognize that I would not be here without all of your contributions. I look forward to following your career successes and celebrating all of your accomplishments.

I would like to acknowledge the Center for Nanophase and Materials Sciences, Oak Ridge National Laboratories, and the phenomenal research team that I had the privilege of collaborating with for this research. Particularly, I would like to thank Dr. Nickolay V. Lavrik for your research guidance and mentoring.

Finally, I would like to thank:

My husband, Matt, for your support and patience during this incredible and challenging journey. You have made numerous sacrifices in both your professional and personal life so that I could follow this dream. You have my gratitude, respect and love; from this life into the next. You are my lobster.

My son Reed, you are only 1.5 years old but you are a daily inspiration for greatness. You are the greatest joy in my life. I hope to inspire you to dream big, and to take chances. Do not be afraid of failing. The only real failure in life is to let fear keep you

from trying to achieve your goals. The greater danger for most of us lies not in setting our aim too high and falling short; but in setting our aim too low, and achieving our mark (Michelangelo). I love you.

My parents, Glenn & Judy Byers; my sister, brother-in-law and nephew, Candace, Scott and Ford Simmons; my brother and nephew; Steven and Ian Byers. You have all supported, encouraged, and believed in me through this process and through all of the challenges that I have set (and caused) for myself. Thank you.

The most bittersweet acknowledgement: My sister, Alison L. Byers. You helped me register for my first college course so you were there when all of this began. It is incredibly unfair that you are not here at the end. Thank you for teaching me that life is to short to worry about what people think at the expense of happiness, an appreciation for all things "girly", and most of all thank you for inspiring me to attempt great things. I miss you daily.

Abstract

Planar chromatography, unlike high performance liquid chromatography (HPLC), has not experienced a significant evolution in stationary phase media since the development of the technique. This has lead HPLC to become a much more popular and robust analytical method. Main factors that contribute to improved performance of chromatographic systems include a reduction in particle size, homogeneity of the stationary phase, and an increase in velocity of the mobile phase. In general, a reduction in particle size should lead to an improvement in the performance of all chromatography systems. However, the main obstacle of improving the performance of planar chromatography systems is that a reduction in particle size leads to a reduction in the capillary flow that governs solvent velocity. This decrease in solvent velocity leads to band broadening resulting in poor efficiency and resolution which are critical performance parameters for chromatographic systems.

The research presented herein investigates the scaling down of dimensions to the micro- and nano-scale for pillar arrays in order to investigate the effect on plate height and chromatographic efficiency of these capillary action driven micro- and nano-fluidic systems. Sample application is a critical parameter that effects band broadening in Ultrathin-Layer Chromatography (UTLC) systems. By taking advantage of the superhydrophobic nature of these arrays the development of a spotting method that demonstrates the ability to create reproducible sample spots that are less than 200 microns (micro- scale arrays) and 400 nanometer (nano- scale arrays) within these arrays are highlighted in this dissertation.

We have demonstrated the fabrication of deterministic micro-scale arrays that exhibit plate heights as low as 2 microns as well as deterministic and stochastic nanothin-layer chromatographic platforms. Most significantly these nano-thin layer systems resulted in bands that were highly efficient, with plate heights in the nanometer range. This resulted in significant separations of analytical laser test dyes, environmentally significant NBD-derivatized amines, and, biologically relevant chemotherapy drugs (Adriamycin and Daunorubicin).

Table of Contents

List of Tables

List of Figures

Nomenclature

A	Eddy diffusion term
B	Longitudinal dispersion term
CAD	Computer Assisted Drawing
CCD	Charge Coupled Device
C_M	Resistance to mass transfer in the mobile phase
$\cos \theta$	Cosine of the contact angle of the mobile phase
C_S	Resistance to mass transfer in the stationary phase
d_f	Average film thickness of the stationary phase
D_M	Diffusion coefficient for the mobile phases
d_p	Particle diameter
dp	Particle size
DPA	Deterministic Pillar Array
DRIE	Deep Reactive Ion Etching
D_S	Diffusion coefficient for the stationary phase
EBL	Electron Beam Lithography
g	Surface Tension
g	Surface tension of the mobile phase
GLAD	Glancing angle deposition
H	Plate Height
h	Viscosity
h	Viscosity of the mobile phase
H_{DF}	Band Dispersion from Development Factors
HPLC	High Performance Liquid Chromatography
HPTLC	High-performance Thin-Layer Chromatography
H_{SS}	Band Dispersion from Spot Solvation
ICP	Inductively Coupled Plasma
k'	Partition factor
K0	Permeability Constant
K_C	Fundamental partition coefficient
k_o	Permeability constant
L^2	Solvent front displacement
MP	Mobile Phase
N	Number of theoretical plates
n	Peak Capacity
NP	Normal Phase
N_P	Number of Pillars
NTLC	Nano-Thin Layer Chromatography
OPLC	Overpressured Layer Chromatography
OTS	Octadecyltricholorsilane

PACS	Pillar arrays chemical separations
PC	Paper chromatography
PDMS	Polydimethylsiloxane
PEB	Post Exposure Bake
PECVD	Plasma Enhanced Chemical Vapor Deposition
PSO	Porous Silicon Oxide
R_f	Retardation (Retention) Factor
RIE	Reactive Ion Etching
RP	Reverse Phase
R_{ST}	Retention of the standard
SA_P	Surface Area per Pillar
SA_T	Total Surface Area
SEM	Scanning Electron Microscope
SP	Stationary Phase
SPA	Stochastic Pillar Array
t	Time
TLC	Thin-Layer Chromatography
µ or µf	Mobile phase velocity
UTLC	Ultrathin-Layer Chromatography
UV	Ultraviolet
V_C	Total Volume per Pillar Array
V_P	Pillar Volume
V_S/V_M	Volume ratio of stationary (V_S) to mobile phase (V_M)
W_B	Width of the peak
Z_0	distance between the original solvent level and the original spot
Z_F	distance travelled by the solvent front
Z_S	distance travelled by the sample
Z_{ST}	distance travelled by the standard
β	Phase volume ratio
θ	Contact angle of the mobile phase

Chapter 1

Introduction to planar chromatography

1.1 Introduction:

Planar Chromatography is a rapid and nondestructive analysis method that is commonly used in order to determine sample purity, reaction completion, and the identity of organic and inorganic compounds. Examples of planar chromatography include Paper Chromatography (PC), Thin-layer chromatography (TLC), and Ultrathin-Layer chromatography (UTLC). Planar Chromatography requires minimal sample preparation and equipment. The most common types of planar chromatography (TLC & UTLC) consists of a stationary phase (usually silica gel, cellulose or aluminum oxide) that is suspended onto a solid support. A small amount of analyte is spotted onto the TLC plate which is then sealed inside of a development chamber that has been pre-saturated with an appropriate mobile phase for the analyte/stationary phase system. The mobile phase moves across the TLC plate by means of capillary action. Chemicals are separated in this system by adsorbing onto the stationary phase with different selectivities. An analyte that has a higher affinity for the stationary phase will be more retained.

Generally speaking, chromatographic theory predicts that decreasing particle size will allow for an increase in separation speed and efficiency. Traditional TLC has particle sizes in the 10 micron range with a layer thickness that is typically larger than 1mm (for glass supported plates)[1]. Reducing the particle sizes in this system should lead to an increase in efficiency, however, this reduction in particle size causes a decrease in the capillary action driven mobile phase velocity. This velocity decrease counteracts gains in efficiency due to smaller particle sizes. UTLC uses a monolithic stationary phase that is around 10 microns thick. These layers are significantly more thin than traditional TLC plates. This monolithic phase is composed of meso- and macro- pores that allow for analyte and mobile phase partitioning. UTLC has demonstrated that a reduction in plate thickness combined with alternative stationary phases shows an improvement in efficiencies and has shown a reduction in development times. This indicates that exploring planar chromatographic stationary

phases with reduced thickness and smaller particle size should yield improved efficiencies.

Deterministic silicon pillar arrays have been used in pressurized chromatography and the results from these studies indicate that, for these highly ordered systems, a reduction in particle size does not result in a reduction in mobile phase velocity. The fabrication methods for these arrays allow for precise control of pillar morphology, size, placement and height. This dissertation focuses on the effect of scaling planar chromatography systems down to the low micron and nano- scale in non-pressurized, capillary flow driven systems . Effects on velocities, and efficiency were studied using the low micron plates and velocity, efficiency and resolution was evaluated using both deterministic and stochastic nano- scale systems.

1.2 The development of traditional thin-layer chromatography

Planar chromatography has a long history from its initial development to modern analytical applications. This chapter serves as a brief overview of that history as well as the theory associated with modern planar chromatography. Particular attention will be given to treatments concerning UTLC and current advancements in analytical methods pertaining to UTLC.

Thin-layer chromatography was derived from the drop chromatographic method developed by Nikolai Izmailov and Maria Shraiber in 1938[2]. A variation of the original drop chromatography method was used by T. I. Williams which is described as a sandwich method where the original TLC plate is covered by a second glass slide and the sample is applied through a hole drilled in slide. Meinhard and Hall introduced a binder that adhered the sorbent medium to the glass slide and, also added Celite powder to improve the uniformity of the layer[3].

Justus G. Kirchner et. al. developed a method of separating terpenes on a medium that he named a chromatostrip in 1951[4]. Kirchner's method used the adsorbent coated glass slides developed by Meinard and Hall but instead of using a drop of developing solvent he developed the plates in the same ascending mode

manner as paper chromatography[3]. This is the method that is still used today where the chromatographic plate is sealed inside of a saturated development chamber that has a small amount of solvent in the bottom. The solvent then moves up the plate using capillary action and separates chemicals based on the preference for the stationary or mobile phase. Another significant breakthrough made by J. Kirchner was the demonstration of performing quantitative analysis using absorbance detection of the separated analytes.

Egon Stahl's contributions to the field of thin-layer chromatography pushed the technique into the widespread use that is seen today[3-5]. Stahl was the first to make popular the term thin-layer chromatography and he was fundamental in optimizing and standardizing the adsorbent medium and the technique. Stahl developed standard adsorbents for TLC and he designed equipment to apply a uniform thin layer of the adsorbent onto a glass layer[3] which was introduced at an exhibition for chemical equipment in Germany by E. Merck and Desaga. Stahl also worked to expand the applications for TLC. This standardized method and expansion of applications lead to a substantial increase in the popularity of this technique[3].

Advantages to using TLC for sample analysis include multiple sample analysis in a single run (i.e. multiple spots are applied to a chromatographic plate and developed simultaneously). Minimal sample preparation is required in that "dirty" samples do not cause column occlusion as is the case for HPLC. Also, orthogonal separations are easily performed on planar chromatographic platforms.

1.3 Modern thin-layer chromatography

Traditional thin-layer chromatograph is still often performed in the same manner that was standardized by Stahl in the late 1950's. TLC is one of the simplest and fastest methods to test for sample purity and identification. Developments in the field include high-performance thin-layer chromatography and ultrathin-layer chromatography.

High-performance thin-layer chromatography (HPTLC) is an improvement in traditional TLC sampling techniques that has assisted in moving this method to a more quantitative type of analysis. HPTLC generally combines methods for spot automation, advanced separation layers (which include smaller particle size separation medium) and software controlled sample analysis. This combination allows for highly controlled and reproducible chromatographic experiments.

Ultra-thin layer chromatography consists of a monolithic stationary phase that is approximately 10 microns in thickness. In contrast, HPTLC layers are generally between 100 and 250 microns. Another major difference between these two TLC methods is that the development distance for HPTLC can be around 8 to 10 cm and is only 1 to 3 cm for UTLC. These differences contribute to improved separation efficiencies and greater sensitivity for UTLC when compared to HPTLC[6]. Plate numbers (N) for conventional TLC are often reported in the range of several hundred, whereas HPTLC can be around a thousand[7]. Table 1.3.1 is a comparison of traditional TLC parameters and the pillar array chemical separation systems (PACS) presented in this research.

More recent advancements in the field of planar chromatography has involved development of UTLC stationary phases where micro-machined methods have been investigated for separation efficiencies. To date, significant contributions have been made to the field by Saha, Olesik and Brett[8-10]. Saha has investigated using SU8, which is a negative tone photoresist, and polydimethylsiloxane (PDMS), a silicon based organic polymer to fabricate pillars. This research investigated the relationship between capillary flow and aspect ratio, pillar diameter and inter-pillar spacing. Olesik's research group has created new stationary phases for UTLC using electrospun nano-fibers. Varying stationary phase thicknesses were investigated and the fiber diameters for these UTLC stationary phases are 400nm in diameter. It was determined that these electrospun fibers exhibited an improved efficiency when compared to commercially available UTLC plates while decreasing development time. Brett used a glancing angle deposition (GLAD) method in order to create an

5

Table 1.3.1: Comparison of TLC Plates and Pillar Array Systems.

Type	Thickness	Particle Size	Sample Size
Traditional TLC	250µm	10-12µm	≥ 1µL
HPTLC	± 150µm	5-6µm	50-500 nL
µ PACS	~ 20µm	1-3µm	pL - nL
n PACS	~ 2 µm	150-300 nm	pL – nL
Miller, J. M., *Chromatography: Concepts and Contrasts*. John Wiley & Sons, Inc.: Hoboken, NJ, 2005.			

HPTLC nanostructured stationary phase by depositing silicon oxide onto glass substrates.

Combining TLC with forced flow mobile phase chambers has also been used, resulting in much lower plate heights when compared to traditional TLC and HPTLC. This type of chromatography is called Overpressured Layer Chromatography (OPLC)[11]. The setup for this method is that a TLC or HPTLC plate is covered by a thin flexible sheet inside of an S-chamber and then pressurized to remove any headspace above the chromatographic plate. The mobile phase is then forced across the plate at a constant rate. Radial or linear flow is used in these devices. Published Van Deemter plots indicate that for capillary TLC and HPTLC the minimum plate height is ~60mm and ~50mm, respectively. The forced flow TLC and HPTLC methods yield plates heights that are reduced to ~40mm and ~15mm[11, 12].

Advancements in the area of micromaching pillar arrays and fluid dynamics which greatly influenced this research have been made by Desmet, Regnier and Tallarek[13-28]. These researchers have provided numerous studies on fluid flow dynamics in nanostructured systems that has been a large motivation for exploring pillar arrays as planar chromatographic substrates. Further discussion on the influence of micromaching to band broadening and micromaching methods are discussed in detail in Chapter 2 of this dissertation.

1.4 Types of chromatographic systems

Chromatographic systems are classified as one of two types. Normal phase (NP) systems consist of a hydrophilic stationary phase (SP) combined with more non-polar mobile phase (MP) solvents. Conversely, reverse phase (RP) systems are comprised of a hydrophobic stationary phase coupled with relatively polar mobile phase solvents. The research presented in this dissertation focuses on reverse phase chromatographic systems, however, these substrates also could be used for normal phase chromatography. The decision to use a RP system was based on this being the more popular separation system historically utilized which provides the

7

opportunity to more easily compare these chromatographic platforms with currently available technologies.

1.5 Common Stationary Phases for Reverse Phase Planar Chromatography

The most common stationary phase used for RP planar chromatography are silica spheres that have undergone surface modification with a carbon phase. The spheres are combined with a binder and then made into a slurry and spread onto a solid support. Sizes for these spheres range from 5-7 µm for HPTLC and 8-10 µm for conventional TLC[29]. Common binders include calcium sulfate (Gypsum)and is denoted by a G in labeling (silica gel G)[7]. Other common SP chemicals include alumina, cellulose polyamide, and magnesium oxide[7]. UTLC layers using monolithic stationary phases are 7-8 µm for particle-loaded membranes and around 15 µm for particle-embedded membranes[29]. Phosphors are also common additives to commercial TLC plates. Manufacturers use the notation of F (silica gel F) to indicate that when viewed under 254nm UV light the analyte will appear as a dark spot against a phosphorescent background[7].

Other common UTLC stationary phases include nanofibrous layers which are created by electrospinning polymeric fibers[9, 29] and the use of nanostructured films prepared by using lithographic methods developed in the semiconductor industry[8, 23, 29]. The research presented in this manuscript focuses on this last concept of using lithographic technologies to precisely control the apparent particle size and inter-particle spacing in order to investigate the impact of manipulating these parameters on the metrics used to evaluate the performance of planar chromatographic systems.

1.6 Equipment and techniques

Planar chromatography equipment generally includes the chromatographic substrate, the solvent system, and the development chamber. The chromatographic substrate consists of the stationary phase that is attached to a solid support and the solvent system, which is picked according to the analytes to be separated, normally

from a literature review combined with trial and error[30]. The development chamber is a critical piece of equipment and should be picked to minimize volume to discourage evaporation of the mobile phase.

1.7 Solvent Systems

Solvent systems should be selected so that they adequately dissolve the analytes, give retardation factors (R_f) values (defined in 1.10) that are close to $0.25^{[11]}$, and are selective to the analytes being separated. Other factors to consider when selecting a solvent system include low viscosity, vapor pressure that is neither high nor low and, generally, the system should generate a linear partition isotherm[5]. Toxicity, purity and stability should also be taken into consideration when selecting a solvent system.

The eluotropic series for solvent strength was introduced by Trappe in the 1940's with the most commonly used adaptation developed by Halpaap and is intended to assist in determining an appropriate solvent system for a silica stationary phase[5, 31, 32]. Other means of selecting mobile phases include using solvent strength as calculated by Snyder[33], or the Prism model[34, 35]. The general rule is that if there are no literature examples of mobile phases available for the stationary phase and analyte system then selecting pure solvents with medium elution strength is recommended[5].

1.8 Development Chambers for Planar Chromatography

Development chambers for planar chromatography include ascending, descending and horizontal devices. Examples of these can be seen in Figure 1.8.1. This research used both ascending and horizontal development chambers. The ascending development chamber was beneficial for rapid development of analytes when visualization of the developed bands would be analyzed post development. However, for real-time analysis of band development a horizontal development chamber can be used and coupled with a fluorescent microscope. There are many commercially available development chambers, however for the micro- and nano-
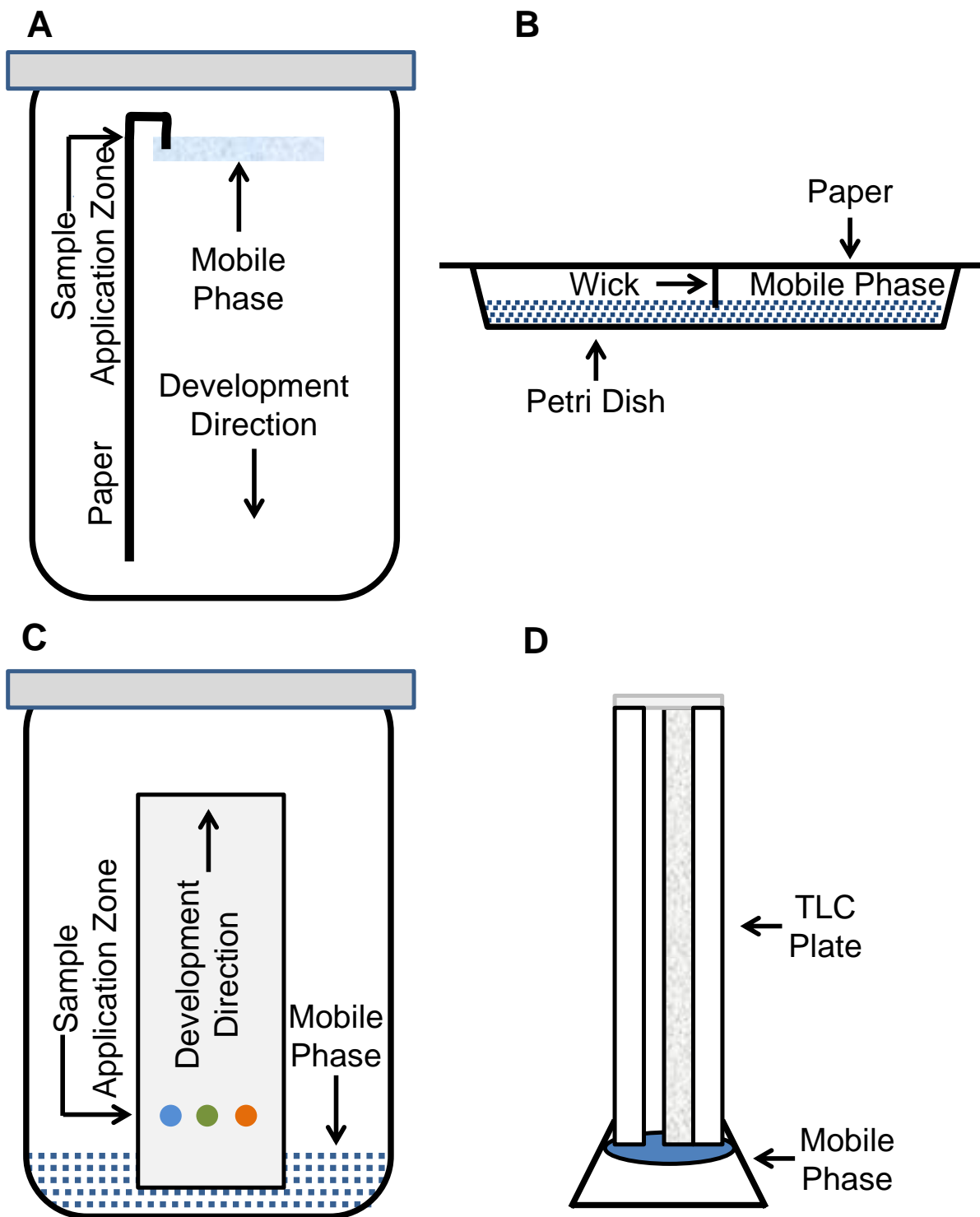
Figure 1.8.1: Development chambers for planar chromatography. A: Descending (paper chromatography), B: Horizontal (paper & HPTLC), C: Ascending (TLC & PC), D: Sandwich (TLC).
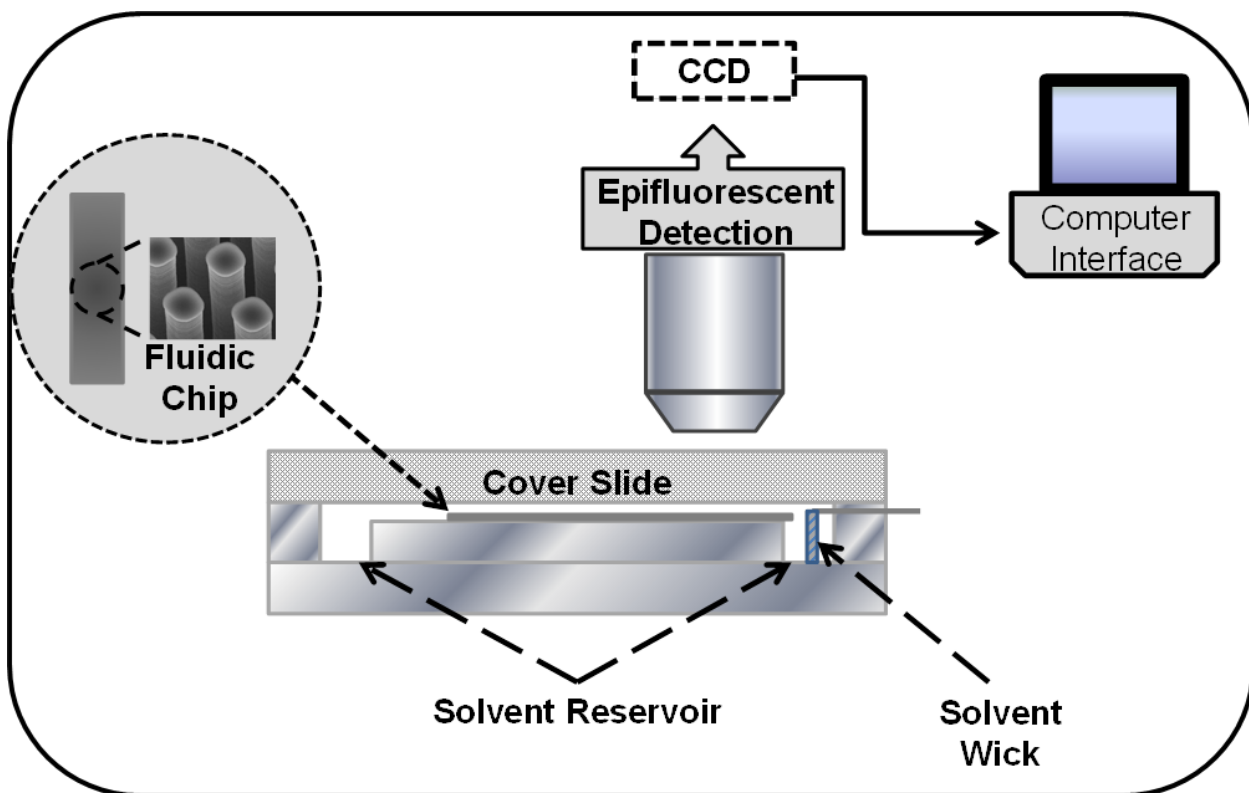
Figure 1.8.2: Schematic of horizontal development chamber interfaced with epifluorescent microscope.
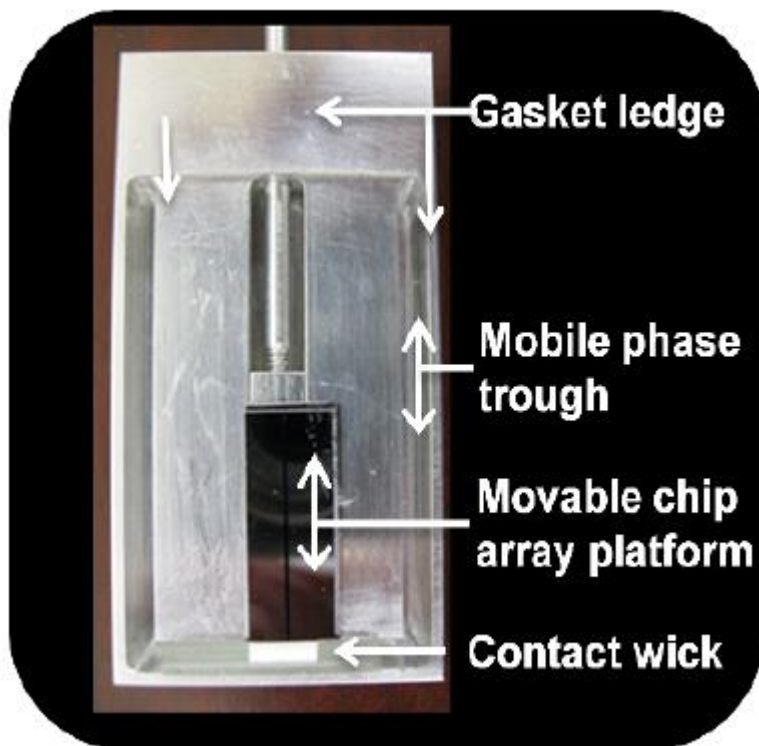
Figure 1.8.3: Image of horizontal development chamber with pillar array mounted.

systems presented in this dissertation the large volumes of these commercially available chambers would have exacerbated evaporation issues observed within the systems. Examples of the chambers used in this work are shown in figures 1.8.2. and 1.8.3.

1.9 Mobile phase flow in capillary driven systems

Mobile phase flow in capillary driven systems is dependent on the surface tension (g) and viscosity (h) of the mobile phase[11]. More importantly it is believed that the ratio of these two parameters (g/h) is more important than the individual parameters[36, 37]. It is common to think of the chromatographic bed as series of connected capillaries. Prior to development this capillary bed is dry and the liquid is applied at one end. The mobile phase then moves across the bed, driven by capillary action forced flow. This causes the solvent front velocity to be greater than the bulk mobile phase. An increase in homogeneity across the bed improves the inhomogeneity of the mobile phase velocity, however, there is always a gradient of solvent volume from the solvent front to the solvent reservoir. This gradient has less volume at the solvent front when compared to the mobile phase closer to the reservoir[11]. This indicates that evaporation rates across the mobile phase are inconsistent, causing a phase ratio. Further exacerbating this phase ratio is the nature of the mixed solvents used in chromatography. As a mixed solvent travels across the bed of the systems one of the solvents will be more volatile and will evaporate at a faster rate. There is also the issue that the solvents will have different affinities to the stationary phase, further increasing this phase ratio as development increases. Factors that contribute variations in phase ratio can be described using Equations [1.9.1] and [1.9.2]

$$ k' = K_C \frac{V_S}{V_M} \ \text{ or } \ \frac{K_C}{\beta} \qquad \text{[1.9.1]} $$

$$ V_{zone} = \frac{V_M}{(1 + k')} \qquad \text{[1.9.2]} $$

13

Where:

k' = retention factor

K_C = fundamental partition coefficient

$\frac{V_S}{V_M}$ = the volume ratio of stationary (V_S) to mobile phase (V_M)

β = the phase volume ratio $\left(\frac{V_M}{V_S}\right)$

Equations [1.9.1] and [1.9.2], indicate that as values for the phase ratio, β, increase we observe smaller k' values for a given partition coefficient (Kc). This results in a relative increase in the mobile phase velocity (v_{mp}) for the zone experienced by the band involved. This results in the zone behind the band center moving faster than the zone in front. This can result in a reduction in band broadening as this faster moving region carries part of the band into the slower moving zone in front. More on this concept is discussed in Chapters 4 and 5.

For capillary driven system it is predicted that solvent front migration distance (Z_F) is proportional to the square root of the migration time (t) as shown in Equation [1.9.3].

$$Z_F = \sqrt{kt} \qquad [1.9.3]$$

Where the proportionality constant is described using Equation [1.9.4].

$$k = \frac{2K_0 d_p g}{h \cos \theta} \qquad [1.9.4]$$

Where:

K_0 = Permeability Constant

d_p = is the particle size

θ = contact angle of the mobile phase

g = surface tension of the mobile phase

h = viscosity of the mobile phase

for most common solvents used in planar chromatography this value is nearly always 0 and the $\cos\theta$, goes to unity[11]. This indicates that factors that contribute to capillary flow is strongly influenced by particle size, and the permeability constant regarding factors that are unique to the chromatographic platform. The surface tension to viscosity ratio is also a factor that greatly influences capillary flow and can be manipulated by picking appropriate solvents.

The velocity of the solvent front (μ_f) is defined by Equation [1.9.5]:

$$\mu_f = \frac{k}{2Z_F} \qquad [1.9.5]$$

This equation indicates that the solvent front velocity is directly related to the surface tension of the mobile phase and inversely related to the viscosity combined with the distance that the solvent front has moved. This equation further highlights that the solvent velocity is not constant and that the velocity decreases as solvent front distance is increased.

Overall it should be noted that capillary flow is not constant and is influenced by mobile phase selection, combined with the stationary phase medium[11].

1.10 Chromatographic evaluation metrics

One of the most important metrics used in planar chromatography is R_f and is defined using the following equation[5]:

$$R_f = \frac{Z_s}{Z_F - Z_0} \qquad [1.10.1]$$

Where, Z_s is the distance between the developed band and the original spot, Z_F is the distance the solvent front has traveled from the original solvent level and Z_0

15

represents the distance between the original solvent level and the original spot. This is analogous to retention time in high performance liquid chromatography (HPLC) and allows for analyte identification when compared to standards. This value is always ≤ 1.0 and, ideally, one picks a chromatographic system so that the value for the analyte to be identified is close to 0.5 in order to avoid drastic changes in phase ratio across the separation zone[38].

Another useful metric is the retention of the standard substance (R_{ST}), which is calculated by[5]:

$$R_{ST} = \frac{Z_S}{Z_{ST}} \qquad [1.10.2]$$

Where, Z_S and Z_{ST} represent the distance the sample and the standard have travelled, respectively. This is a useful metric to compare the reproducibility between different chromatographic plates.

Another metric for evaluating the performance of a chromatographic system under isocratic conditions is the calculation of the number of theoretical plates(N) in the separation field and the theoretical plate height (H). The following two equations are commonly recognized as valid for planar chromatography.

$$N = 16 \left(\frac{Z_S}{W_B}\right)^2 \qquad [1.10.3]$$

$$H = \frac{N}{Z_S} \qquad [1.10.4]$$

Where, Z_S, is the distance that the band has traveled from the original spot (measured at the center) and, W_B, is the width of the peak.

Peak Capacity (n), is often used to describe gradient systems and can be calculated using the following equation, formulated by Guiochon for TLC[39]:

$$n = 1 + \frac{\left(\sqrt{N}\right)}{2} \qquad \text{[1.10.5]}$$

Where, N, is the number of theoretical plates as defined in equation [1.10.3].

1.11 Contributions to band broadening

Random porosity and nanoscale morphology associated with conventional TLC indicates that heterogeneity within the morphology of these stationary phases result in mass transfer issues causing band broadening. A reduction in band broadening is desired when optimizing a chromatographic system. This can be achieved by maximizing the number of theoretical plates (N) or peak capacity (n), which reduces plate height (H).The Van Deemter equation (Equation 1.11.1) is traditionally used to describe the factors that contribute to band broadening.

$$H = A + \frac{B}{u} + (C_S + C_M)u \qquad \text{[1.11.1]}$$

This equation shows that plate height is controlled by a number of contributions to band broadening. These terms are defined below:

A = Eddy diffusion term; this is used to define the random path that an analyte travels through a heterogeneous packed column.

B = is the longitudinal dispersion term

u = mobile phase velocity

C_S = resistance to mass transfer in the stationary phase

C_M = resistance to mass transfer in the mobile phase

Expanding this equation to include the kinetic contributions to band broadening gives the following equation:

$$H = 2\lambda d_p + \frac{2\gamma D_M}{u} + (\frac{qk'd_f^2 u}{(1+k')^2 D_S} + \frac{wd_p^2 u}{D_M} \qquad \text{Eq [1.11.2]}$$

With the terms defined as follows:

d_p = particle diameter

k'= partition coefficient

d_f= average film thickness of the stationary phase

D_S and D_M, diffusion coefficient for the stationary and mobile phases, respectively.

$q, \lambda, \gamma \; and \; w$ are independent factors that are conditional to the packing or ordering of the column.

Since flow velocity is prominent in Equation 1.11.2., equation 1.11.3 is commonly used to predict the relative velocity trend among different solvents[40, 41] for planar chromatographic systems.

$$L^2 = k_0 d_p t \left(\frac{g}{h}\right) \cos\theta \qquad \text{[1.11.3]}$$

With the terms defined as follows:

L^2 = solvent front displacement

k_0= permeability constant

t = time

$\frac{g}{h}$ = surface tension to viscosity ratio of the mobile phase

$\cos\theta$ = cosine of the contact angle of the mobile phase

From Equations [1.11.1], [1.11.2] and, [1.11.3]it is apparent that dominant terms may lead to plate heights that are either inversely or directly proportional to mobile phase velocity. For example, a reduction in particle size should lead to a decrease in band broadening due to contributions from Eddy diffusion (A-term). However, in traditional thin-layer chromatography a reduction in particle size leads to a decrease in mobile phase velocity which contributes to band broadening from longitudinal dispersion (B- term).

For the deterministic (highly ordered) pillar arrays initially studied in this work it has been shown that band broadening from the eddy diffusion term is negligible and can, therefore be disregarded[42-45]. Also, it has been shown that for these pillar array systems that the reduction in mobile phase velocity that is observed as particle size decreases in traditional TLC is not observed due to a favorable permeability constant [8, 9, 30, 37, 46-48]. This indicates that for these systems decreasing pillar size or, more accurately, inter-pillar gap is expected to decrease plate height and improve efficiency for these chromatographic systems.

1.12 Analyte application

Sample spotting is a critical parameter in planar chromatography. If quantitative values are to be obtained small, consistent spots of known volume must be applied to the chromatographic plate.

According to a recent research profile further development of spotting methods for use in UTLC is a relevant area of research [49].   More specifically, minimizing the size of the original analyte spot or band applied to the planar chromatography substrate is an important area of research to advance the field. Examples of current advances in sample spot application in the mm regime include the use of modified inkjet printer cartridges which produce spot sizes in the range of 0.45-0.87mm[50].
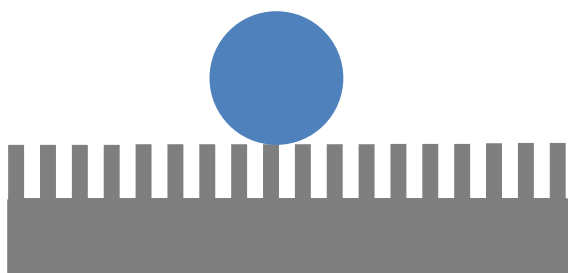
Cassie State
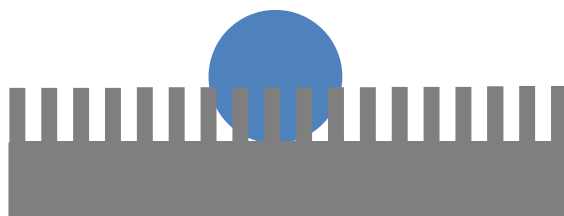
Wenzel State

Figure 1.12.1: Illustration of the Cassie and Wenzel states for a droplet.
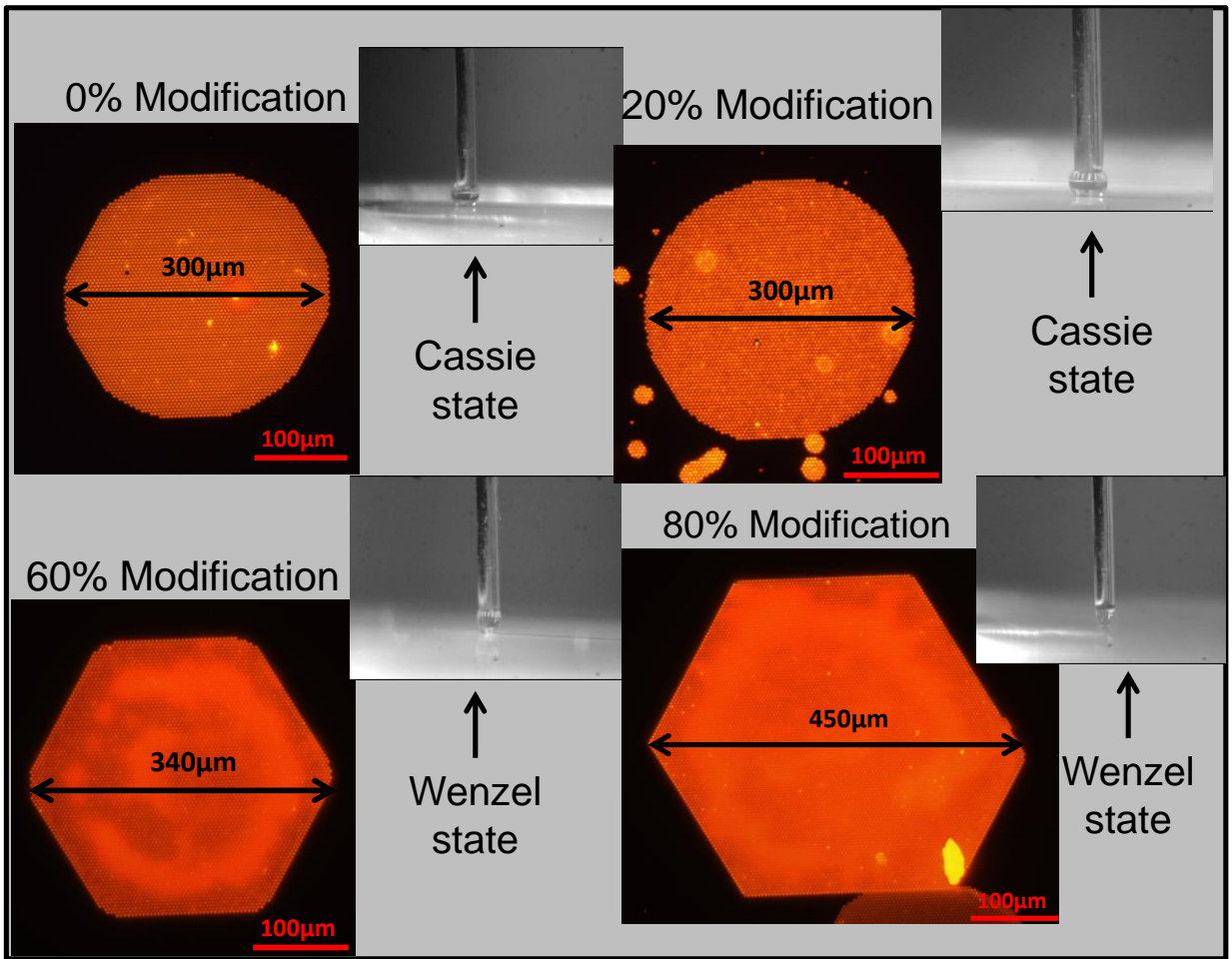
Figure 1.12.2: Effect of methanol modification on spot size and Cassie to Wenzel transition.

Submillimeter methods include a contact spotting method reported by Fennimore in 1979[51], an electroosmosis-based nano pipette,[52] and a piezoelectric nanojet printing method[53]. Other commercial spotting tools include the Nanomat and the Camag Linomat[11].

The spotting method developed for use with these lithographic substrates utilized the hydrophobic nature of these micro- and nano- scale features. These features, when coupled with the hydrophobic carbon RP, resulted in a super-hydrophobic surface that allowed for concentration of the analyte into reproducibly small spots. Initial spotting attempts were performed where the droplet was released from a pipette and allowed to fall onto the array surface. This resulted in difficult to control spot placement and, more problematic, with the droplet drying onto the pillar tops instead of depositing into the pillar array. To resolve this issue analyte was dissolved into a methanol/water mixture of increasing organic percentage to determine an appropriate ratio that would allow for the droplet to transition from the Cassie state (riding on the pillars) to the Wenzel state (descending into the pillars). An illustration of these two states are shown in Figure 1.12.1. The results of this study determined that a mixture of 50-60% methanol with water allowed for the application of spots that were reproducibly smaller than 200 µm that consistently transitioned to the Wenzel state. Figure 1.12.2 shows the resulting spot sizes from this study. Reproducibility is shown in Figure 3.8.1.

1.13 Methods of detection and identification

For traditional TLC direct visualization of the analyte is a common method for detection for colored analytes. This can be done either directly or with a UV lamp. For non-colored and non-fluorescing samples TLC plates with a fluorescent additive can be combined with a 285nm UV lamp for band visualization. The analyte causes fluorescent quenching which results in a dark area (analyte) on a bright fluorescent background. Alternatively, for analytes that self fluoresce illumination under 365nm UV light will result in a fluorescing analyte on a dark background[5]. Detection using a

TLC scanner combined with fluorescence measurement can be used for obtaining quantitative data.

Densitometry is often used as a means of detection for quantitative TLC. Densitometry can operate in either transmission or reflectance modes and can take either absorbance or fluorescence measurements. Typical wavelengths are 190-800nm with full spectra availability for qualitative analysis and precision is generally within 1-3% RSD[11].

Recent advancements in TLC detection include using diode-array scanners, image analyzers, mass spectrometry and SERS analysis[11, 54-56].

For the research presented herein, the analytes were either self-fluorescing or were derivatized to fluoresce and then visualized directly using an epifluorescent microscope as illustrated in the set-up in Figure 1.8.1.

1.14 Conclusion

The random porosity and morphology associated with conventional TLC system indicates system heterogeneity will result in mass transfer induced band broadening based on the Van Deemter equation. A reduction in particle size diameter should result in a decrease in band broadening but the resulting decrease in mobile phase velocity observed with traditional systems negates any such advantages. The work presented in this dissertation builds upon the fundamental principles of traditional planar chromatography and has coupled this theory with recent advancements in lithographic pillar array fabrication. These advancements indicate that a decrease in pillar size does not show a reduction in mobile phase velocity. This allows for a unique study of the effects of decreasing particle diameter (inter-pillar gap) on band broadening and plate height. The chromatographic techniques that had to be optimized for this research to be successful included analyte spotting methods, development chamber fabrication and detector interface as well as MP phase ratio gradients and spot solvation kinetics and the aforementioned chromatography fundamentals. Non-chromatographic obstacles discussed in the following chapters

include chromatographic substrate fabrication (i.e. pillar robustness and adequate surface area for retention which is discussed in Chapter 2) and carbon phase surface chemistry modification.

1.15 References

1. in *Sigma Aldrich*, ed. Supelco.
2. N. O. Mchedlov-Petrossyan, Professor Nikolai IZMAILOV (1907–1961): Scientific career, main results and achievements, http://www-chemistry.univer.kharkov.ua/files/PAC-Izmailov_1.pdf.
3. L. S. Ettre and H. Kalász, *LCGC*, 2001, 19, 712-721.
4. M. F. Striegel and J. Hill, *Thin-Layer Chromatography for Binding Media Analysis*, The J. Paul Getty Trust, United States of America, 1996.
5. E. Hahn-Deinstrop, *Applied Thin-Layer Chromatography - Best Practice and Avoidance of Mistakes*, Wiley-VCH, Federal Republic of Germany, 2007.
6. S. Mennickent, M. d. Diego and M. Vega, *Chromatographia*, 2013, 76, 1233-1238.
7. J. M. Miller, in *Chromatograhpy: Concepts and Contrasts*, John Wiley & Sons, Inc., Hoboken, NJ, 2005.
8. L. W. Bezuidenhout and M. J. Brett, *Journal of Chromatography A*, 2008, 1183, 179-185.
9. J. E. Clark and S. V. Olesik, *Analytical Chemistry*, 2009, 81, 4121-4129.
10. A. A. Saha, S. K. Mitra, M. Tweedie, S. Roy and J. McLaughlin, *Microfluidics and Nanofluidics*, 2009, 7, 451-465.
11. J. M. Miller, *Chromatography: Concepts and Contrasts*, John Wiley & Sons, Inc., Hoboken, NJ, 2005.
12. C. F. Poole and S. K. Poole, *Journal of Chromatography A*, 1995, 703, 573-612.
13. D. Clicq, R. W. Tjerkstra, J. G. E. Gardeniers, A. v. d. Berg, G. V. Baron and G. Desmet, *Journal of Chromatography A*, 2004, 1032, 185-191.
14. A. Daneyko, S. Khirevich, A. Holtzel, A. Seidel-Morgenstern and U. Tallarek, *Journal of Chromatography A*, 2011, 1218, 8231-8248.
15. W. De Malsche, D. Clicq, V. Verdoold, P. Gzil, G. Desmet and H. Gardeniers, *Lab on a Chip*, 2007, 7, 1705-1711.
16. W. De Malsche, S. De Bruyne, J. O. De Beeck, S. Eeltink, F. Detobel, H. Gardeniers and G. Desmet, *Journal of Separation Science*, 2012, 35, 2010-2017.
17. W. De Malsche, H. Eghbali, D. Clicq, J. Vangelooven, H. Gardeniers and G. Desmet, *Analytical Chemistry*, 2007, 79, 5915-5926.
18. W. De Malsche, H. Gardeniers and G. Desmet, *Analytical Chemistry*, 2008, 80, 5391-5400.
19. J. De Smet, P. Gzil, N. Vervoort, H. Verelst, G. V. Baron and G. Desmet, *Analytical Chemistry*, 2004, 76, 3716-3726.
20. G. Desmet and S. Eeltink, *Analytical Chemistry,* 2012, 85, 543−556.
21. H. Eghbali, W. D. Malsche, D. Clicq, H. Gardeniers and G. Desmet, *LC»GC Europe*, 2007, 208-222.
22. H. Eghbali, S. Matthijs, V. Verdoold, H. Gardeniers, P. Cornelis and G. Desmet, *Journal of Chromatography A*, 2009, 1216, 8603-8611.

23. P. Gzil, N. Vervoort, G. V. Baron and G. Desmet, *Analytical Chemistry*, 2003, 75, 6244-6250.
24. P. Gzil, N. Vervoort, G. V. Baron and G. Desmet, *Journal of Separation Science*, 2004, 27, 887-896.
25. B. He and F. Regnier, *Journal of Pharmaceutical and Biomedical Analysis*, 1998, 17, 925–932.
26. W. D. Malsche, D. Clicq, V. Verdoold, P. Gzil, G. Desmet and H. Gardeniers, *Lab on a Chip*, 2007, 7, 1705–1711.
27. W. D. Malsche, H. Gardeniers and G. Desmet, *Analytical Chemistry*, 2008, 80, 5391-5400.
28. R. M. Tiggelaar, V. Verdoold, H. Eghbali, G. Desmet and J. G. E. Gardeniers, *Lab on a Chip*, 2008, 9, 456–463.
29. S. K. Poole and C. F. Poole, *Journal of Chromatography A*, 2010, 1218, 2648-2660.
30. J. Sherma, *Analytical Chemistry*, 2004, 76, 3251-3262.
31. W. Trappe, *Biochem. Z.*, 1940, 305.
32. H. Halpaap and J. Ripphahn, *Kontakte (Mercke)*, 1976, 3, 16-34.
33. L. R. Snyder, *Journal of Chromatographic Science*, 1978, 16, 223-234.
34. J. J. Kirkland, J. L. Glajch in Gertz, Ch, W. Fellman and Z. Fresenius, *Analytical Chemistry*, 1986, 323, 342-349.
35. S. Nyierdy, K. Dallenbach-Toelke and O. Sticher, *Journal of Planar Chromatography*, 1988, 4, 336-342.
36. C. F. Poole, *Journal of Chromatography A*, 2003, DOI: 10.1016 /S0021-9673(03)00435-7, 963-984.
37. S. K. Poole and C. F. Poole, *Journal of Chromatography A*, 2011, 1218, 2648-2660.
38. P. S. Variyar, S. Chatterjee and A. Sharma, in *High-Performance Thin-Layer Chromatography*, ed. M. Srivastava, Springer, 2011.
39. , eds. L. Komsta, M. Waksmundzka-Hajnos and J. Sherma, CRC Press, Dec 20, 2015.
40. G. Guiochon, *Journal of Chromatography A*, 2007, 1168, 101-168.
41. G. Guiochon, G. Korosi and A. Siouffi, *Journal of Chromatographic Science*, 1980, 18, 324-329.
42. N. V. Lavrik, L. C. Taylor and M. J. Sepaniak, *Lab on a Chip*, 2010, 10, 1086-1094.
43. N. V. Lavrik, L. T. Taylor and M. J. Sepaniak, *Analytica Chimica Acta*, 2011, 694, 6-20.
44. L. C. Taylor, Ph.D., University of Tennessee, 2012.
45. L. C. Taylor, N. V. Lavrik and M. J. Sepaniak, *Analytical Chemistry*, 2010, 82, 9549-9556.
46. T. J. Kauppila1, N. Talaty, P. K. Salo, T. Kotiaho, R. Kostiainen and R. G. Cooks, *Rapid Communications in Mass Spectrometry*, 2006, 20, 2143-2150.
47. C. F. Poole, *Journal of Chromatography A*, 2003, 1000, 963-984.

48. S. Tuomikoski, K. Huikko, K. Grigoras, P. Östman, R. Kostiainen, M. Baumann, J. Abian, T. Kotiaho and S. Franssila, *Lab on a Chip*, 2002, 2, 247-253.
49. S. C. Powell, *Analytical Chemistry*, 2010, DOI: 10.1021/AC100625S, 3408.
50. G. E. Morlock, C. Oellig, L. W. Bezuidenhout, M. J. Brett and W. Schwach, *Analytical Chemistry*, 2010, 82, 2940-2946.
51. D. C. Fenimore and C. J. Meyer, *Journal of Chromatography*, 1979, 186, 555-561.
52. C. K. Byun, X. Wang, Q. Pu and S. Liu, *Analytical Chemistry*, 2007, 79, 3862-3866.
53. W. Streule, T. Lindemann, G. Birkle, R. Zengerle and P. Koltay, *Journal of the Association for Laboratory Automation*, 2004, 9, 300-306.
54. C. E. Freye, N. A. Crane, T. B. Kirchner and M. J. Sepaniak, *Analytical Chemistry*, 2013, 85, 3991-3998.
55. S. Nyiredy, *Journal of Chromatography A*, 2003, 1000, 985-999.
56. C. F. Poole, *Journal of Chromatography A*, 2003, 1000, 963-984.

Chapter 2

Introduction to lithographic techniques

2.1 Introduction:

Lab-on-chip technologies have become increasingly popular as a robust and powerful analytical tool. Microfabrication methods that were developed for use in the semiconductor industry have been adapted to fabricate miniaturized devices that have applications in the healthcare industry as point-of-care devices, environmental applications for use as in-field measurement devices and have been developed for use in space exploration as miniaturized biological laboratories. Silicon wafer technology is the most commonly adapted technique because it is possible to tune these systems down to the nanometer scale and to precisely control the positioning of the desired features within these systems. As described in the previous chapter using the Van Deemter equation parameters that influence band broadening such as pillar diameter and spacing are critical when fabricating these chromatographic substrates. Due to this we have applied microfabrication methods that allow us to precisely control these parameters. This chapter is focused on the microfabrication process used for the research presented herein and includes photo and electron beam lithography. Recognizing that lithographic methods can be expensive and time consuming anon-lithographic fabrication method was also investigated. These fabrication methods are not trivial and require a number of precise steps to successfully fabricate the desired features. These steps generally include a patterning step which makes a mask of the desired features followed by reactive ion etching. In order to perform the desired surface chemistry and to improve surface area for the stationary phases a room temperature silicon oxide deposition was performed as the final step. Further information on microfabrication methods can be found in textbooks and journal articles related to these processes[1-8].

2.2 Photolithography

Photolithography is a relatively economical and rapid lithographic process when compared to electron beam lithography. Limitations of this technique are that features can only be scaled to approximately a 1 micron limit with resolution limits of
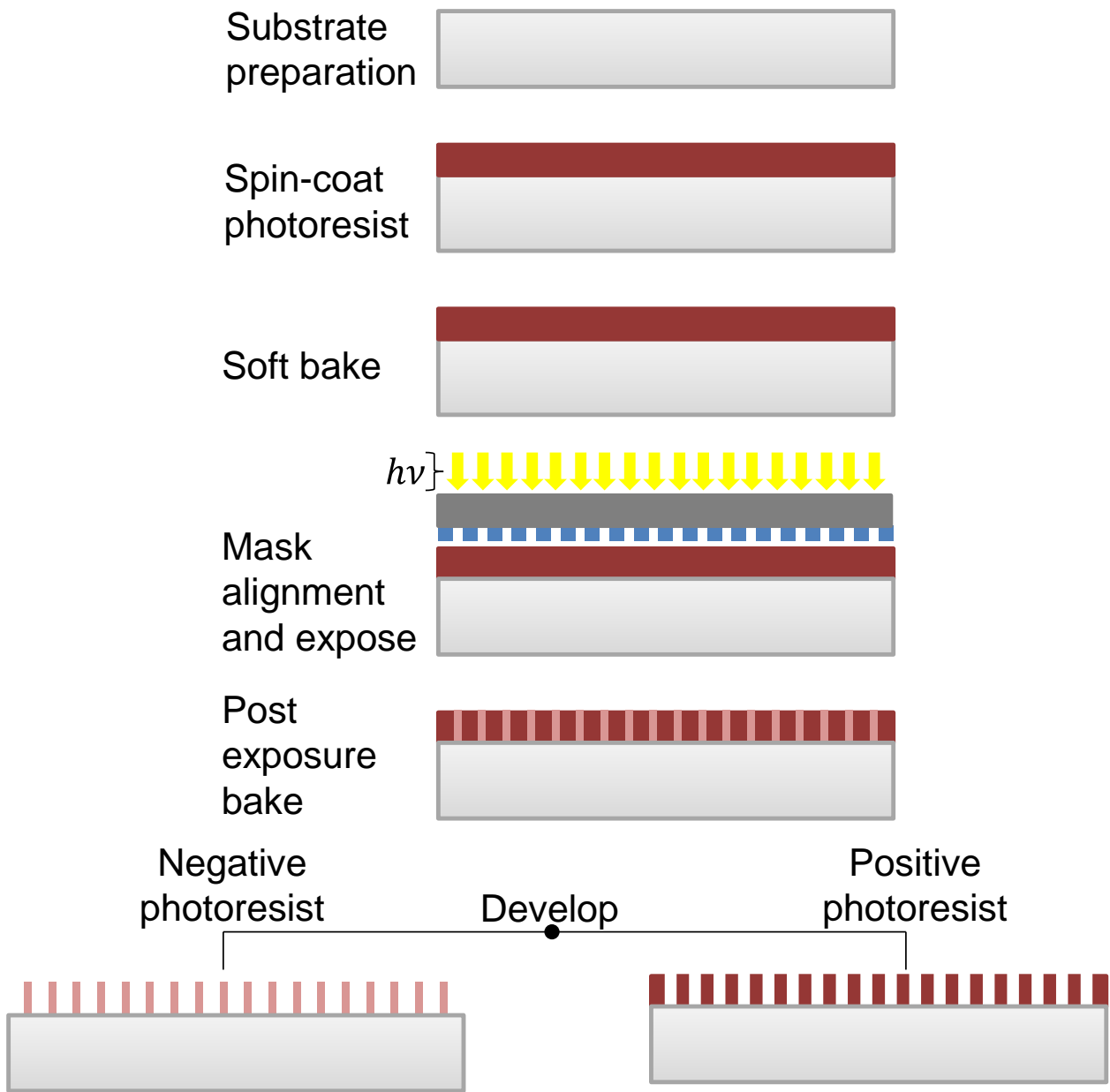
Figure 2.2.1: Typical photolithographic process

± 0.5μm[9, 10]. A typical photolithographic process is illustrated in Figure 2.2.1. The substrate is prepared to insure that the photoresist adheres uniformly to the surface.

Examples of substrate preparation include dehydration bake, cleaning procedures, or coating with a primer that encourages adhesion. After substrate preparation the wafer is coated with a uniform layer of photoresist that is of a specified thickness. The thickness is controlled by spin-coating at a predetermined rate that is photoresist specific (i.e. for photoresist LOR-1A spin rates between 2500-4500rpm produces resist layers of 100-150nm thick). Photoresist is a photosensitive polymer. When exposed to an appropriate wavelength of light the polymer either solubilizes (positive photoresist) or, alternatively, for negative photoresist the masked off regions that are protected from light remain soluble. After spin-coating the photoresist is baked (soft bake) to improve adhesion to the wafer surface. The wafer is then ready for light exposure. In order to print the features onto the wafer the substrate is aligned with a quartz plate mask that has been previously laser written and developed with the desired features. The exposure time is photoresist dependent and is also dependent on the variable strength of the light source. A test wafer is usually exposed in order to determine the correct exposure time for each process.

Exposure can be performed using one of three types of methods which is based off of the spacing of the mask and lithographic substrate. For this research the contact method was used. Contact exposure gives superior resolution, however the contact between the mask and substrate can cause damage which results in feature imperfections. These imperfections can be avoided for systems where resolution is not as critical by using projection lithography. Projection lithography provides adequate resolution using a dual lens optical system which projects the pattern onto the wafer to be patterned[11, 12]. The third type of exposure is proximity exposure. This method prevents contact feature damage but loses resolution when compared to the other two exposure options.

The post exposure bake (PEB) is critical for reducing the standing wave effect. This occurs when monochromatic light which has been projected onto a lithographic

2 layer photoresist

silicon wafer

UV exposure or EBL

Develop

Hard mask deposition
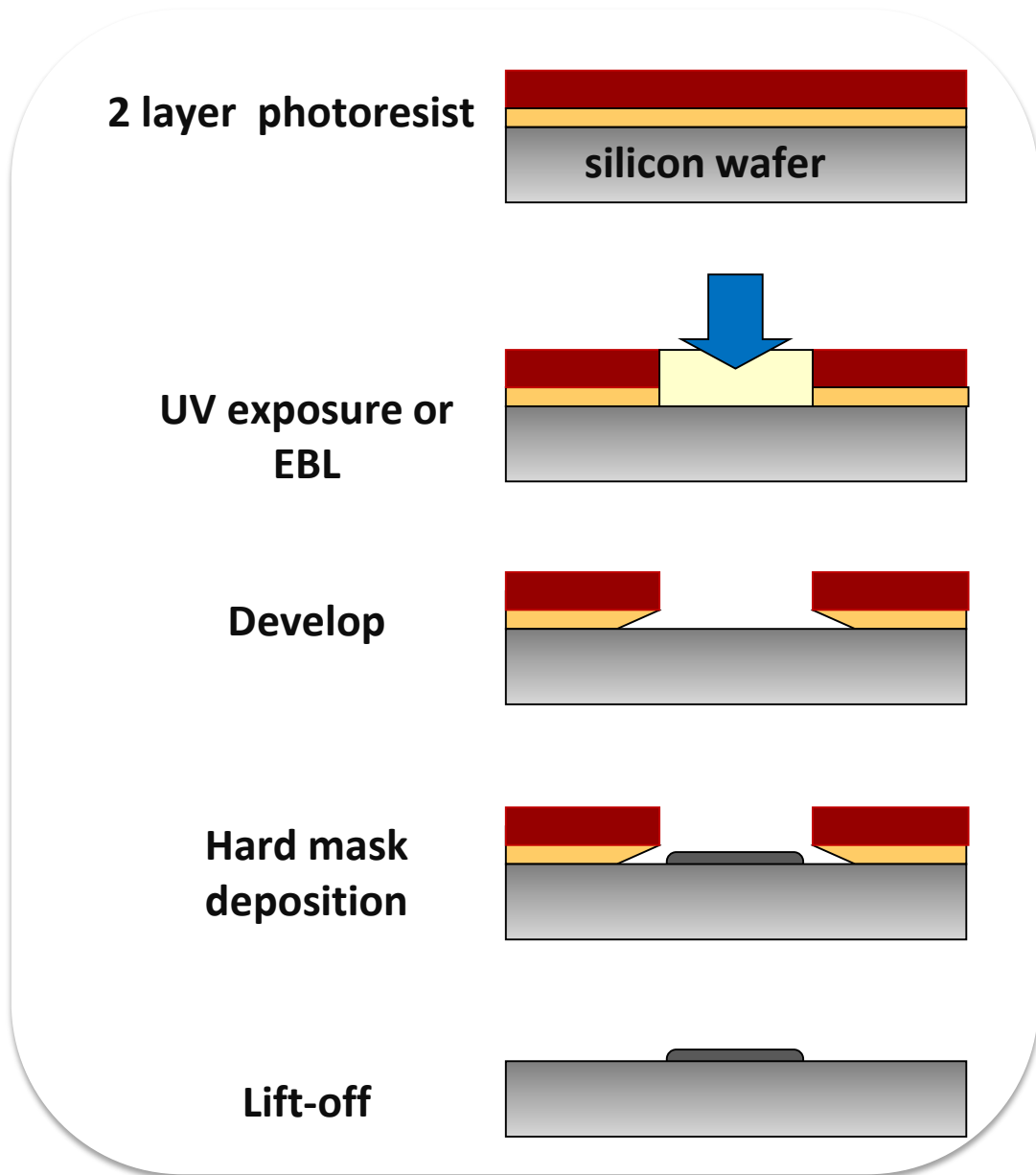
Lift-off

Figure 2.2.2: Double layer lift-off photoresist for improved lithographic resolution.

surface impacts the substrate at multiple angles. The light ravels through the photoresist and is then reflected off of the wafer surface. This interference pattern causes high and low intensity waves which results in ridge formation in the sidewalls causing a reduction in feature quality[8, 12]. Some photoresists are chemically amplified and for these resists the PEB helps to increase the solubility of the polymer. After the PEB the photoresist is developed (i.e. the uncrosslinked polymer is dissolved from the wafer surface) in an appropriate solvent and the result is a wafer layered with polymerized photoresist which has the desired pattern.

The photolithographic substrates developed for this research were exposed using a Quintel Contact Mask Aligner that uses a G-line (436 nm) exposure system. To improve the resolution of our features we modified the typical lithographic methods shown in Figure 2.2.1 to include a double layer photoresist system combined with a chromium metal deposition step to create a hard mask prior to etching the silicon wafer which is illustrated in Figure 2.2.2. The chromium is deposited using a dual electron beam physical vapor deposition method. Once the chromium is deposited a lift-off process is then performed and all of the remaining photoresist is removed along with any excess chromium. At this point the wafer is ready for etching of the patterned features (details in Section 2.5).

2.3 Electron beam lithography

The deterministic nano-scale pillar arrays studied in this research were fabricated using electron beam lithography (EBL). The fabrication steps to produce these nano-scale arrays are similar to the process discussed for photolithography in Section 2.2 but instead of UV light patterning electron beam patterning is used. Care must be taken when selecting a photoresist for each of these methods in that differing resists have feature size limitations. Both of these techniques are top-down lithographic approaches but, as discussed earlier, photoresist size limitations are approximately 1 micron. In order to investigate deterministic arrays with features less than 1 micron it was necessary to utilize electron beam lithography. EBL, like photolithography, can generate chromatographic substrates that are highly ordered
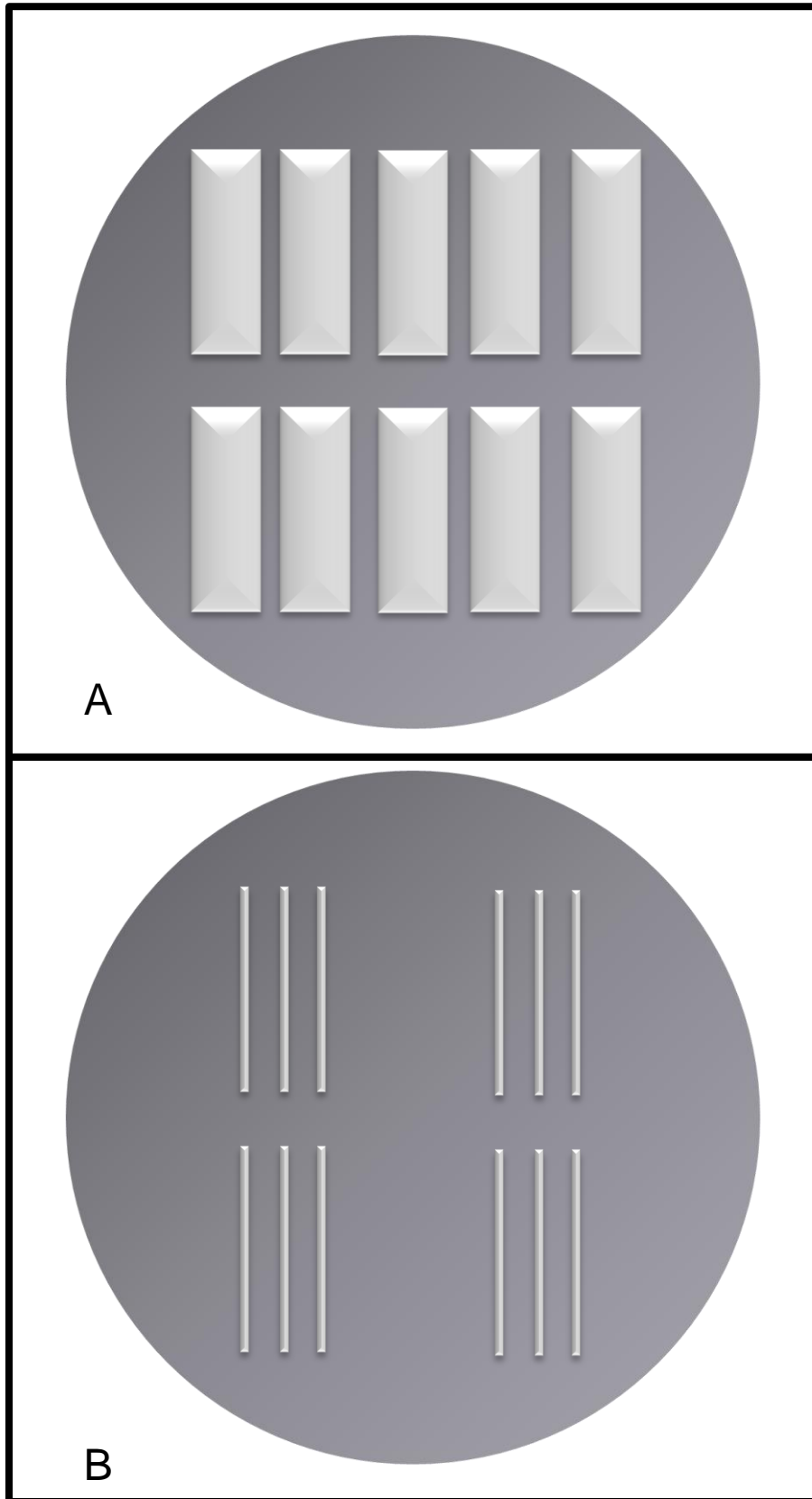
Figure 2.3.1: (A) Wafer layout of photolithographic pillar arrays and, (B) layout of EBL arrays on a 4" silicon wafer.

and are reproducible for this study. Notable drawbacks of this method are cost and time constraints to produce these substrates. However, these limitations are irrelevant to this small scale analysis for theoretical investigation of the effects of scaling down these chromatographic systems to the nano-scale.

EBL patterned chromatographic substrates allows for the investigation of small, highly reproducible and tunable pillar dimensions and spacing. The first use of EBL for patterning was in the 1960's with the use of modified electron microscopes[10, 13]. Like photolithography, the semiconductor industry has been responsible for developing modern EBL methods where applications have developed rapid due the desirability of device miniaturization and circuit integration[10]. Obvious limitations to using EBL in this application is long patterning times due to the serial patterning process. For example the lithographic patterning times for the deterministic EBL arrays presented in this dissertation required 3-4 days of open instrument time to pattern 2 wafers in comparison to the photolithographic arrays that were patterned within 5-7 minutes per wafer. The wafer layout for both the photolithographic and the EBL arrays are shown in Figure 2.3.1. Advancements to increase the throughput of EBL include electron projection lithography, variable-shaped beam lithography and low-energy electron beam proximity projection lithography[10, 14-17]. However, it should be noted that although these developments do improve throughput for production purposes there is a sacrifice of resolution when compared to traditional EBL.

A schematic of a typical EBL system is illustrated in Figure 2.3.2 and consists of an electron gun and focusing column for the electron beam, all under vacuum, which is also connected to a computer system. The electrons are generated by electron emitters or cathodes and accelerated by an electrostatic field. The focusing column focuses these electrons into a beam and is directed onto the wafer by electric and magnetic lenses. The computer system is loaded with a CAD design which controls the pattern writing process.

EBL patterning is performed using directed electrons instead of photons, as is the patterning light source for photolithography discussed earlier. Because of this the
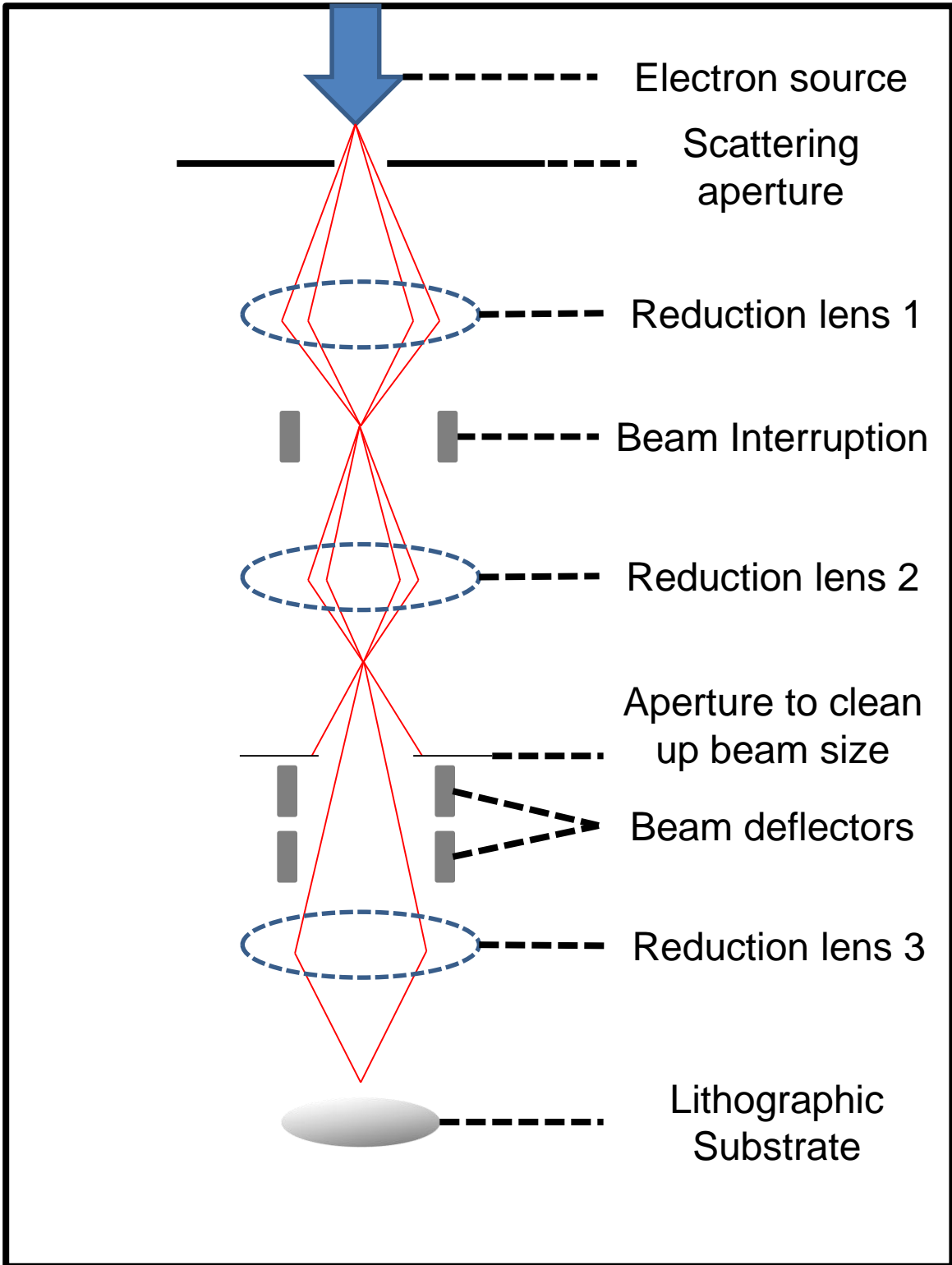
Figure 2.3.2: Schematic of a typical EBL instrument.

pattern is written serially as opposed to exposing the entire surface of the wafer. This direct write method allows for patterning to be performed without a mask onto the wafer that has been coated with an appropriate photoresist for nanoscale features. Photoresist resolution limits need to be considered when scaling down from photolithography to EBL but the same types of considerations can be given when picking either negative or positive photoresist discussed in Section 2.2. Resolution for EBL can be optimized ±10nm with a beam spot size that can be focused to approximately 1nm[9, 10]. Dosage studies must be performed to optimize the system to insure that the features are patterned as desired. High or low energy electrons can cause exposure issues. High energy electrons cause exposure bleed where more photoresist is exposed than desired and low energy electrons cause a lack of homogeneity in exposure of desired areas. The high energy electrons would cause a loss of feature resolution due to overexposure and the low energy electrons would create resolution issues due to lack of homogeneity for photoresist development times. Dosage studies, resist choices and development solvents are critical parameters when optimizing lithographic features and as the size of the features are reduced these parameters become even more critical to achieve the desired resolution. Figure 2.3.3 A and B show examples of pillars with poor electron dosage and C and D show the same pattern after dosage has been optimized.

2.4 Lithography free fabrication

Due to the cost and throughput limitations of EBL we have also studied stochastic nano-scale pillar arrays. This unique lithographic free process is performed by depositing a thin layer of platinum onto the wafer surface using physical vapor deposition onto a p-type silicon wafer with 100nm of thermally grown silicon oxide. Thermal annealing of the thin platinum film is performed in a 10:1 mixture of argon/hydrogen at 735 Torr is a cold wall furnace which is equipped with a radiative heat source. The heat source for the annealing process was set for the maximum power of 22kW for 8 seconds which heated the wafer and thin film to an estimated 900°C. This thermally induced metal film dewetting process causes the metal to form platinum islands on the wafer surface which act as the hard mask for the etching
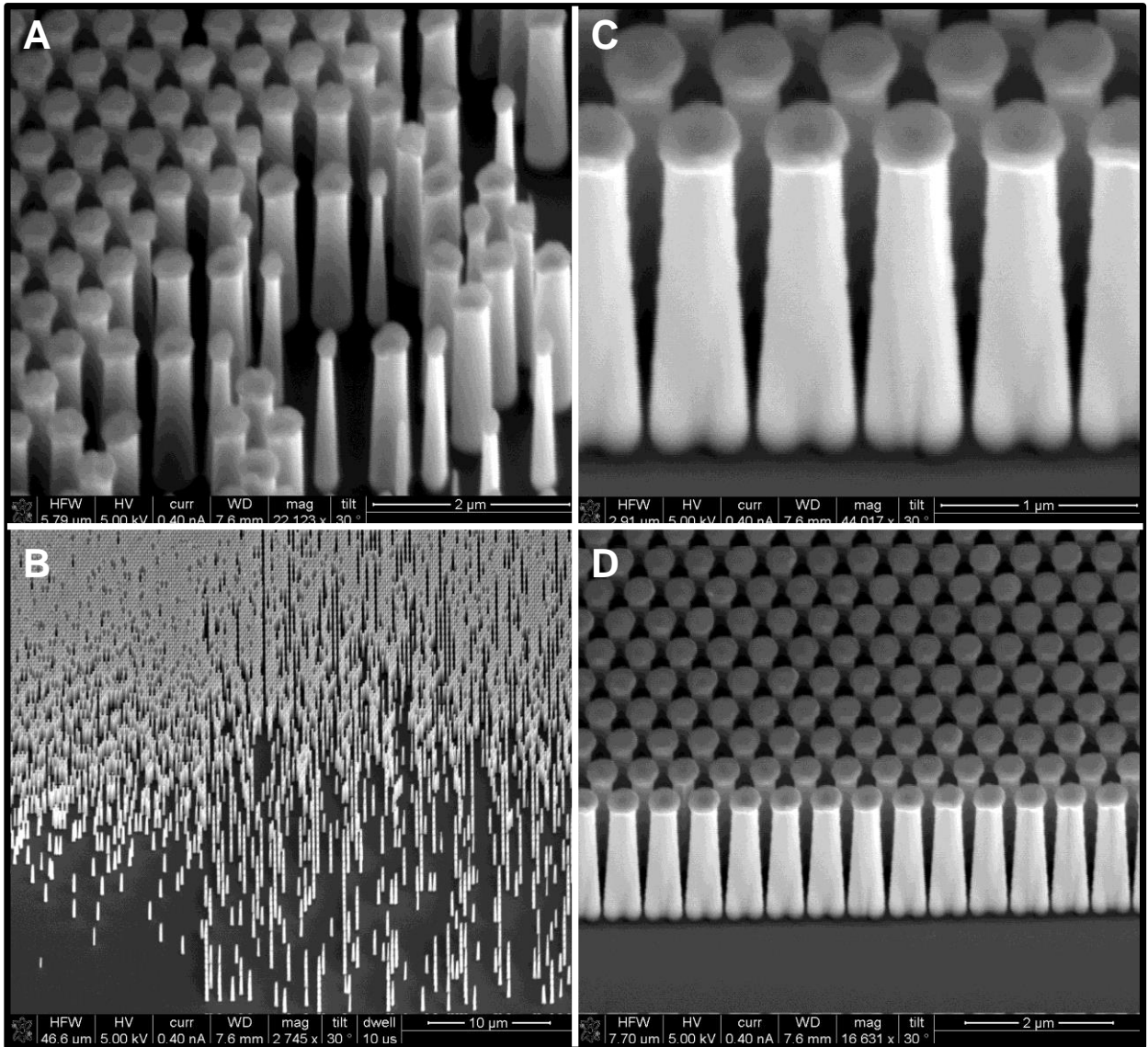
Figure 2.3.3: A & B are examples of EBL pillars with poor dosage. C&D are the same pattern with appropriate electron dosage.
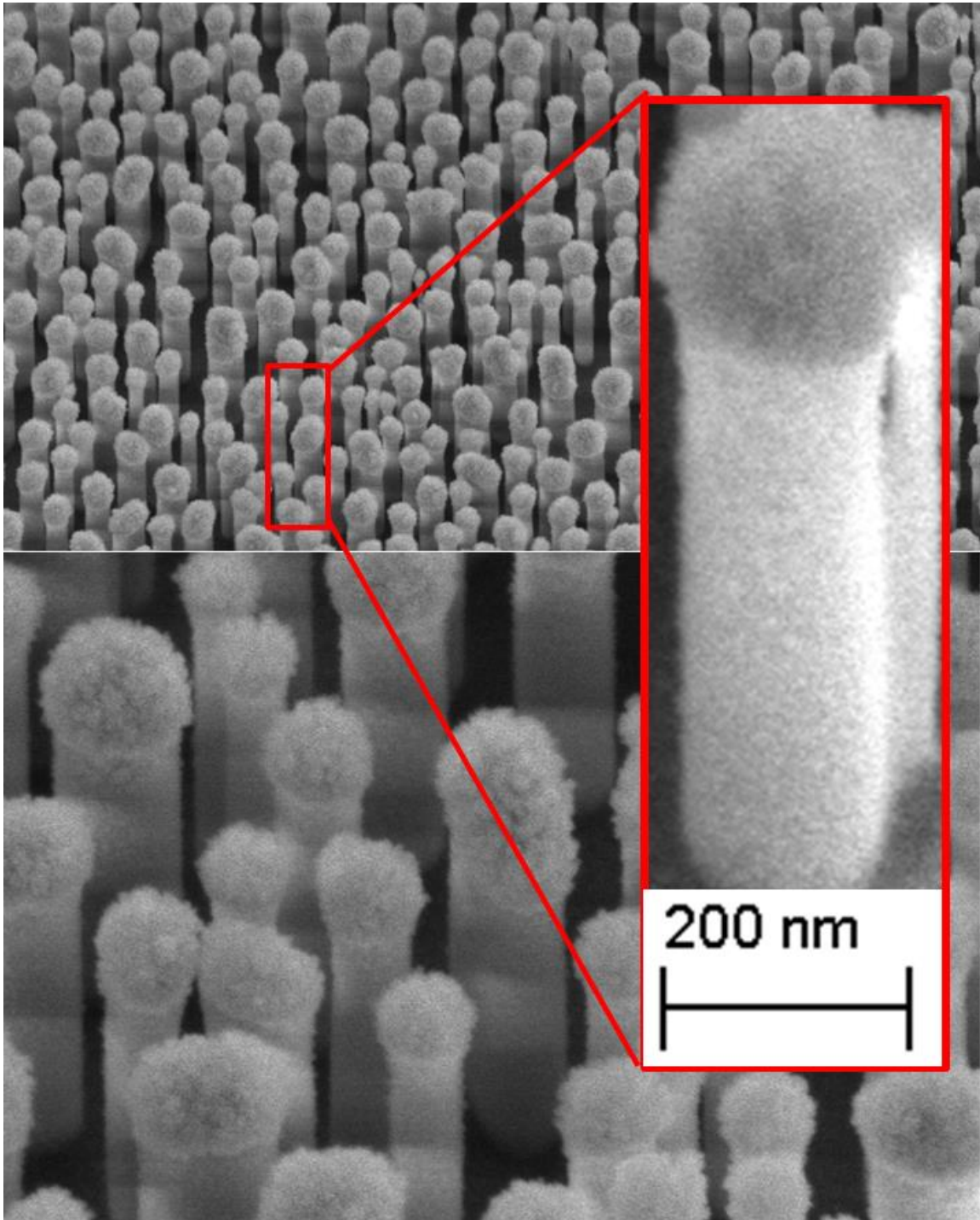
Figure 2.4.1: SEM of stochastic pillar array.

process discussed in Section 2.5[20, 21]. Although the position and size of these pillars cannot be controlled to the same level as lithographic pillar arrays there is a reasonable amount of tunable pillar features regarding size and spacing which is dependent on the platinum layer deposition thickness[5, 18, 19]. Figure 2.4.1 show stochastic nano-scale pillar arrays that have been fabricated to closely mimic the smallest EBL patterns that were investigated in this study[20, 21].

2.5 Reactive ion etching

The chromium metal acts as the hard mask for the pattern to be etched into the silicon wafer. Etching methods can be achieved through either a wet chemical or dry plasma etching process. Profiles of both etching process can either be isotropic or anisotropic. An isotropic profile is one in which the etch is independent of position and direction. Anisotropic profiles are generated when the vertical etch rate is higher than the horizontal etch rate. These two etching profiles are illustrated in Figure 2.5.1. Anisotropic profiles are generally the preferred profile because of the improved feature shape whereas isotropic etch profiles tend to create undercutting in features decreasing the stability of very small features[12]. Examples of common wet chemical etchants include buffered hydrofluoric acid for silicon dioxide deposited onto a silicon substrate, and, for anisotropic etching, potassium hydroxide and tetramethylamonium hydroxide.

The etching method used in this research to a dry plasma etch method that removes material using ion bombardment at the surface. In this case, inductively coupled plasma (ICP) reactive ion etching (RIE) was used, where chemically reactive ions are generated in plasma using an RF powered magnetic field and a gaseous mixture. The reactive ion chamber is illustrated in Figure 2.5.2. In RIE both physical and chemical etching occurs as ions are accelerated towards the surface of the silicon wafer. The main process is the chemical process where the ions have a chemical reaction with the surface layer of material. However, some of the material is removed by a physical process where high energy ions remove atoms from the

Anisotropic   **Isotropic**

Figure 2.5.1: Etching profiles indicating the round sidewalls generated by isotropic etching methods and the vertical sidewalls generated by anisotropic methods.
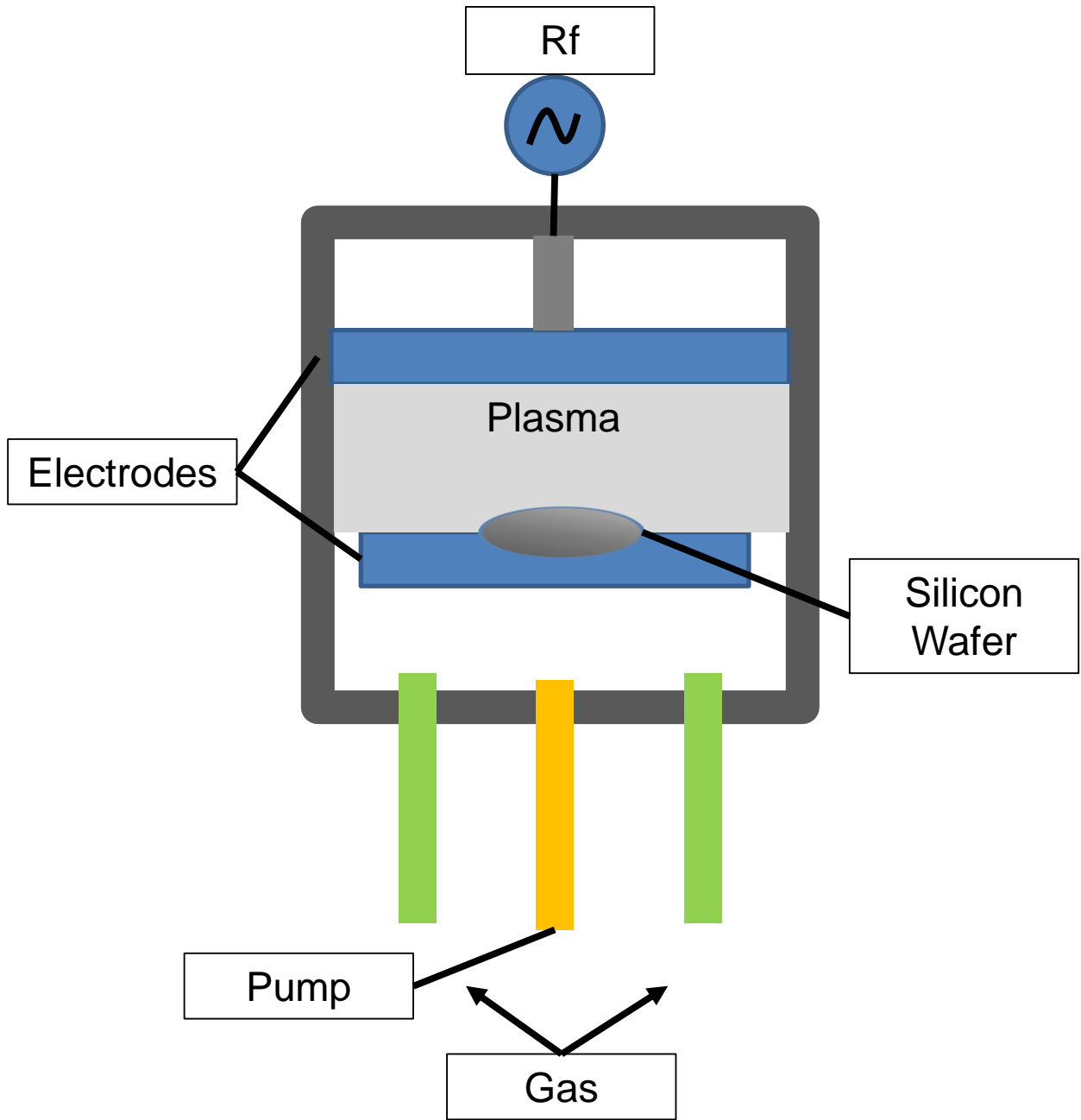
Figure 2.5.2: Schematic of basic RIE.

Bosch Etching Process

A

B

Etch

Passivate
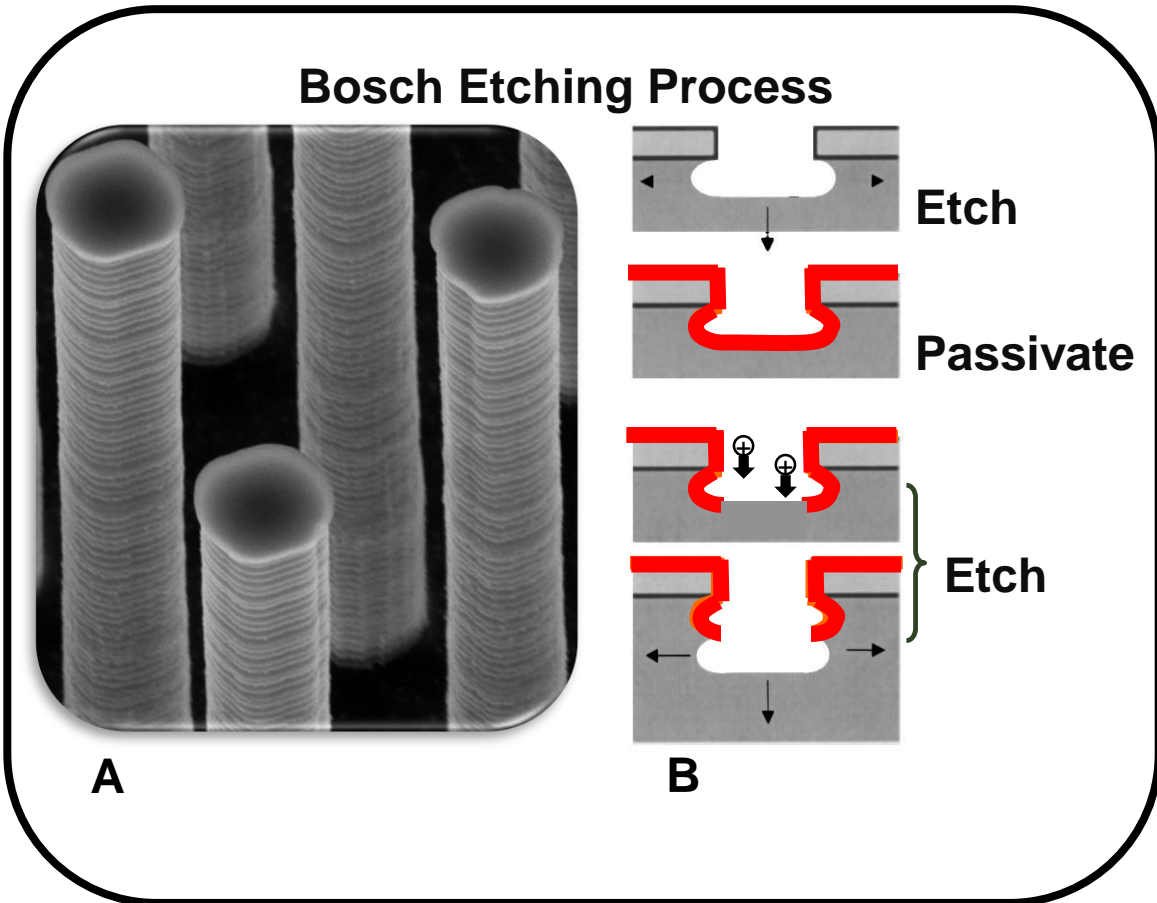
Etch

Figure 2.5.3: (A) SEM of Bosch etched pillars and, (B), schematic of Bosch process

material by kinetic energy transfer. Depending on the features desired undercutting can be controlled by balancing these two processes.

For the photolithographic pillars studied in this research a special recipe for deep reactive ion etching (DRIE) called the Bosch recipe has been utilized to enhance both surface area and to further reduce undercutting of the pillars to improve pillar stability. The Bosch recipe utilizes an etching step followed by a passivation step. This process is used to create vertical sidewalls and high-aspect ratio features in silicon wafers due to the high etch rate and silicon selectivity of the recipe. The etch step is performed on exposed silicon using isotropic SF_6 gas. The passivation step follows the etch step and is performed by a deposition of C_4F_8 polymer onto the entire wafer surface. This cycle is then repeated with the result that the physical portion of the etch process rapidly removes the fluoropolymer it directly contacts (i.e. the unmasked portions of the wafer). However, as the etch cycle switches from the physical etch to the chemical etch (RIE) the fluoropolymer is not as rapidly etched. This results in the accumulation of fluoropolymer on the pillar sidewalls which protects the pillars during the etching process. This cyclic process is optimized for each substrate (time of SF_6 to C_4F_8) and the cycle is then repeated to achieve the desired height for the features. In the case of our high-aspect arrays the photolithographic arrays were etched to a height of ~20μm and the EBL array were etched to ~2μm. Figure 2.5.3 shows an example of pillars that have been etched using this process as well as a schematic of the process.

2.6 Thin film deposition

Thin film deposition was used to deposit a layer of silicon oxide onto the wafer surface in order to perform the surface chemistry to covalently bond the RP carbon phase to the chromatographic substrate. Initial work on the photolithographic pillars used a low rate deposition process at elevated temperatures for the deposition process. Subsequent work with the nano-scale arrays has been performed using a room temperature deposition process. The advantage of the room temperature

Porous Silicon Oxide (PSO)
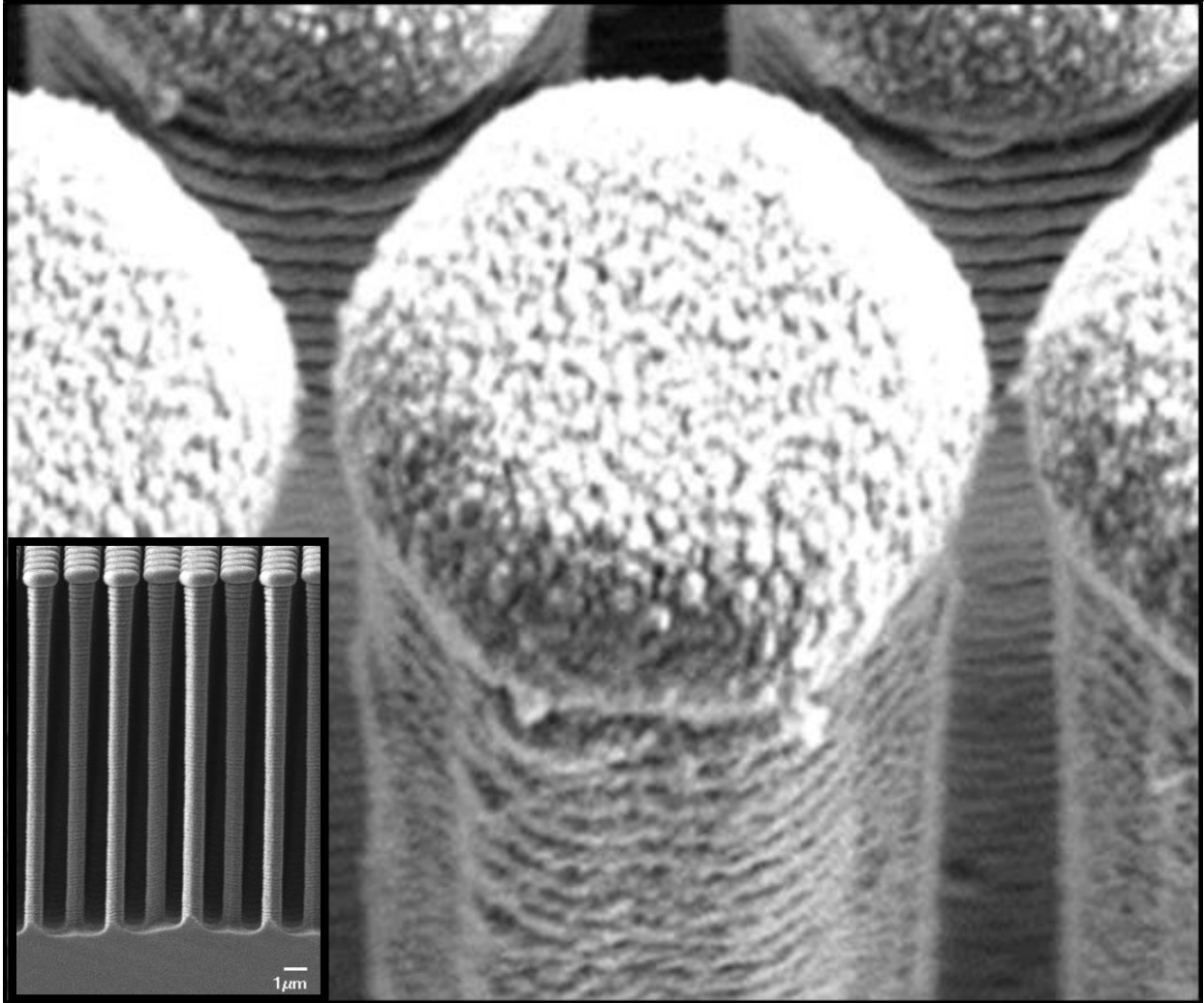
Figure 2.6.2:SEM image of pillar arrays before (inset) and after porous silicon oxide deposition.
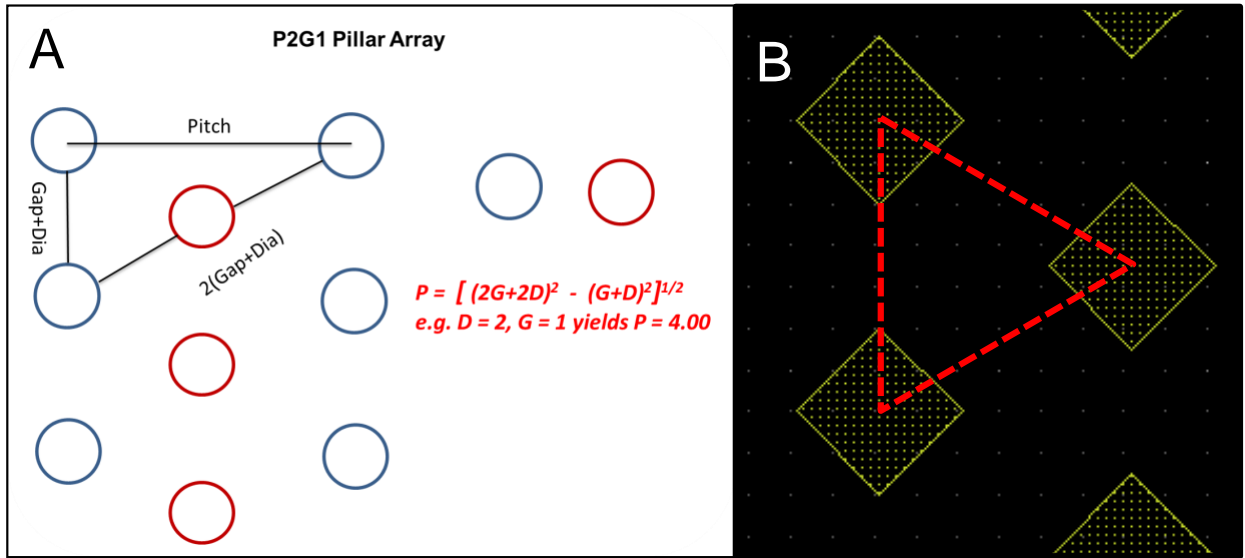
Figure 2.7.1: Illustration of CAD design for fabrication of deterministic pillar arrays for optimized capillary flow.

deposition process is that it generates a porous silicon oxide that increases our surface area.

Thin film deposition are films with layers that range to several nanometers to 100 microns. The most common types of deposition processes are classified as either chemical or physical depositions. In the chemical process a chemical reaction producing a solid occurs within the evaporation chamber and then begins to condense within the chamber. The chemical process yields a highly conformal layer of the material being deposited. Alternatively, physical methods rely on a sputtering technique that does not produce as conformal of a layer.

It is possible to achieve high quality thin films using thermal oxidation or thermal chemical vapor deposition if your material is not limited by temperature. Plasma enhanced chemical vapor deposition (PECVD) is a method that can be used when temperature is of concern. This is the method used to deposit the films discussed within this research. A plasma reactor causes gases to dissociate into reactive molecules which can be used to deposit silicon oxide at room temperature up to several hundred degrees C.

For the photolithographic deposition process we used the higher temperature range (200 °C) to deposit conformal thin layers of silicon oxide. Upon determining that the surface area was inadequate for analyte retention in these chromatographic systems we then discovered in the literature a room temperature recipe that deposited a porous silicon oxide layer that would increase surface area in these systems. Figure 2.6.1 is an SEM image of pillar arrays before and after porous silicon oxide deposition.

2.7 Design of lithographic substrates

Desmet et. Al. has performed extensive fluid dynamic research regarding the geometric parameters required to optimize solvent velocity within pillar arrays. Equation 2.7.1 was used in our CAD design of the deterministic pillar arrays to meet these requirements.

47
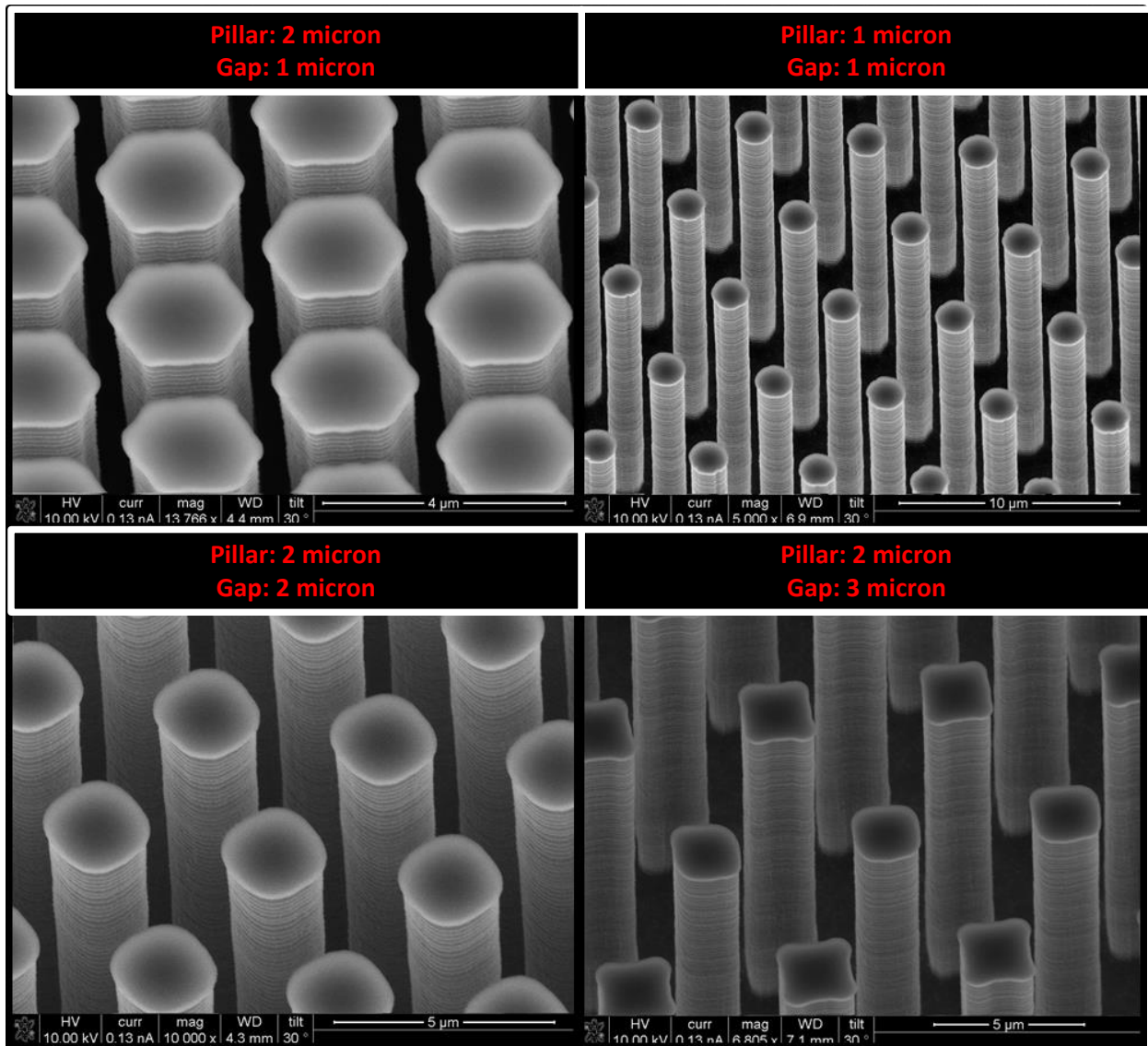
Figure 2.7.2: SEM images of the deterministic pillar arrays optimized for capillary flow.

$$P = [(2G + 2D)^2 - (G + D)^2]^{1/2} \tag{2.7.1}$$

This equation yields equilateral triangles between the pillars within the array which is critical for the capillary driven flow within these systems[22, 23]. This equation is illustrated in Figures 2.7.1A with a screen capture of the CAD file shown in Figure 2.7.1B. SEM images of the varying pillar diameters and interpillar spacing of the deterministic photolithographic pillar arrays is shown in Figure 2.7.2.

2.8 Conclusion

The fabrication methods discussed in this chapter are non-trivial and require multiple optimization steps to achieve the fabrication of substrates that are appropriate for chromatographic separations. Many of these steps must be optimized for each generation of arrays fabricated due to differences in photoresist or changes in fabrication machine environments over time.

Deterministic micro- and nano- scale pillar arrays were fabricated using traditional lithographic techniques developed in the semiconductor industry. Alternatively, recognizing the throughput challenges and financial costs of EBL, a non-lithographic fabrication method was used to fabricate stochastic nano-scale arrays. After determining that the Bosch process did not create sufficient surface area for retention on the pillar sidewalls a room temperature silicon oxide deposition process was used that deposits porous silicon oxide. This porous silicon oxide increased the surface area for the RP stationary phase to retain analytes and also increases the structural stability of the arrays.

2.9 References

1.	*Nanotechnology*, Springer-Verlag, New York, 1999.
2.	, ed. D. R. Lide, 81st edn., 2000-2001.
3.	*Springer Handbook of Nanotechnology*, Springer-Verlag Berlin, Heidelberg, Germany, 2003.
4.	*Nanofabrication fundamentals ans applications*, World Scientific Publishing Co., Toh Tuck Link, Singapore, 2008.
5.	R. L. Agapov, B. Srijanto, C. Fowler, D. Briggs, N. V. Lavrik and M. J. Sepaniak, *Nanotechnology*, 2013, 24, 505302-505311.
6.	P. Gzil, N. Vervoort, G. V. Baron and G. Desmet, *Analytical Chemistry*, 2003, 75, 6244-6250.
7.	N. V. Lavrik, L. T. Taylor and M. J. Sepaniak, *Analytica Chimica Acta*, 2011, 694, 6-20.
8.	C. A. Mack, *Fundamental Principles of Optical Lithography: the science of microfabrication*, Wiley, Hoboken, NJ, 2007.
9.	D. M. Tennant, *Limits of Conventional Lithography*, Springer, New York, 1999.
10.	S. M. Wells, Ph.D. Dissertation, University of Tennessee, 2012.
11.	M. Rothschild, T. M. Bloomstein, T. H. Fedynyshyn, R. R. Kimz, V. Liberman, M. Switkes, N. N.E. Jr., S. T. Palmacci, J. H. C. Sedladek, D. E. Hardy and A. Greenville, *Lincoln Laboratory Journal*, 2003.
12.	L. C. Taylor, Ph.D., University of Tennessee, 2012.
13.	G. Mollenstedt, *Important problems of the electron microscope*, 1961.
14.	S. D. Berger, J. M. Gibson, R. M. Camarda, R. C. Farrow, H. A. Huggins, J. S. Kraus and J. A. Liddle, *Journal of Vacuum Science & Technology B*, 1991, 9, 2996-2999.
15.	H. C. Pfeiffer, *Journal of Vacuum Science & Technology B*, 1978, 15, 887-890.
16.	N. Saitou, *International Journal of the Japan Society for Precision Engineering*, 1996, 30, 107-111.
17.	T. Utsumi, *Japanese Journal of Applied Physics Part 1 - Regular Papers Short Notes & Review Papers*, 1999, 38, 7046-7051.
18.	J. J. Charlton, N. Lavrik, J. A. Bradshaw and M. J. Sepaniak, *ACS Applied Materials & Interfaces*, 2014.
19.	T. B. Kirchner, N. A. Hatab, J. J. Charlton, R. B. Strickhouser, I. I. Kravchenko, N. V. Lavrik and M. J. Sepaniak, *Pending*, 2014.
20.	L. A. Rebecca, S. Bernadeta, F. Chris, B. Dayrl, V. L. Nickolay and J. S. Michael, *Nanotechnology*, 2013, 24, 505302.
21.	J. J. Charlton, N. Lavrik, J. A. Bradshaw and M. J. Sepaniak, *ACS Applied Materials & Interfaces*, 2014, 6, 17894-17901.
22.	W. D. Malsche, D. Clicq, V. Verdoold, P. Gzil, G. Desmet and H. Gardeniers, *Lab on a Chip*, 2007, 7, 1705-1711.
23.	W. D. Malsche, H. Eghbali, D. Clicq, J. Vangelooven, H. Gardeniers and G. Desmet, *Analytical Chemistry*, 2007, 79, 5915-5926.

Chapter 3

Deterministic micro-scale silicon pillar arrays as platforms for reverse phase planar chromatography

The research presented in Chapter 4 has been adapted from a research article published in *Analytical Chemistry*, 2013, 85 (24), pp 11802–11808. This chapter focuses on band broadening and plate height in capillary flow driven micro-scale planar chromatographic systems. These unique systems exhibit plate heights around 2 microns and show promise that scaling planar chromatographic systems to these dimensions can offer improvements in efficiency and band broadening when compared to traditional TLC systems.

3.1 Abstract:

Unlike HPLC, there has been sparse advancement in the stationary phases used for planar chromatography. Nevertheless, modernization of planar chromatography platforms can further highlight the technique's ability to separate multiple samples simultaneously, utilize orthogonal separation formats, image (detect) separations without rigorous temporal demands, and its overall simplicity. This paper describes the fabrication and evaluation of ordered pillar arrays that are chemically modified for planar chromatography and inspected by fluorescence microscopy to detect solvent development and analyte bands (spots).

Photolithography, in combination with anisotropic deep reactive ion etching, is used to produce uniform high aspect ratio silicon pillars. The pillar heights, diameters, and pitch variations are approximately 15 to 20 µm, 1 to 3 µm, and 2 to 6 µm, respectively, with the total pillar array size typically 1 by 3 cm. The arrays are imaged using scanning electron microscopy in order to measure the pillar diameter and pitch as well as analyze the pillar sidewalls after etching and stationary phase functionalization. These fluidic arrays will enable exploration of the impact on mass transport and chromatographic efficiency caused by altering the pillar array morphology. A C18 reverse stationary phase (RP), common RP solvents that are transported by traditional but uniquely rapid capillary flow, and Rhodamine 6G (R6G) as the preliminary analyte are used for this initial evaluation. The research presented in this article is aimed at understanding and overcoming the unique challenges in developing and utilizing ordered pillar arrays as a new platform for planar chromatography; focusing on fabrication of expansive arrays, studies of solvent

transport, methods to create compatible sample spots, and an initial evaluation of band dispersion.

3.2 Introduction

Modification of fabrication processes traditionally designed for the semiconductor industry has been shown to have advantages in the development of on-chip separation techniques. Using these techniques allows for the fabrication of micro- and nano- structured on-chip separation media that have been proven to be successful using computational analysis and actual separations by Desmet et. al. [1-4]. This approach was pioneered by Regnier and coworkers in the late 1990s [5, 6], who fabricated pillar arrays within channels in a reproducible and controlled manner. The advantages of using ordered arrays comprised of high aspect ratio pillars as a separation medium over traditional packed and monolithic columns have been well documented [1, 6-8]. Significantly, separation efficiency with these engineered systems is usually improved when replacing relatively polydisperse and heterogeneous packing particles with lithographically-fabricated pillars. The separation media in packed and monolithic columns realize benefits in mass transfer related efficiency as the size of the media particles or domains becomes smaller. However, scaling down traditional systems generally exasperates non-uniformity of the packing itself and the beds created with them and also increases pressure demands. Conversely, an advantage identified in recent studies is that nearly perfect ordered pillar arrays exhibit less flow resistance than comparable traditional packed and monolithic columns [9]. The improved flow resistance of these pillar array systems coupled with the ability to greatly reduce the pillar size to low-micro- or nano-scale indicates that this separation platform should exhibit an improvement over traditional separation media. Moreover, in a practical sense, these diminutive lab-on-a-chip platforms are expected to be particularly useful for in-field monitoring or point-of-care diagnostics due to the overall simplicity of the device. The footprint of the device is small, allowing for ease of transport, the system is reusable which offsets production costs, and only small sample volumes are required for analysis.

Appropriately designed pillar arrays have enabled novel separation mechanisms. An example is the use of deterministic lateral displacement discovered for particle separation accomplished by manipulating pillar positions to cause separations by altering the path taken by varying particles [10]. More conventional separation methods have also been used that are more similar to packed bed liquid chromatography which combines a mobile phase-stationary phase partitioning type separation which is controlled by the retentive nature of the solute within the system. Examples of these include pressure driven separations in pillar array systems explored by Desmet and coworkers using C8 and C18 liquid phase modifications with both porous and nonporous pillar arrays [3, 7, 11, 12]. These examples highlight the possibility of using pillar array separation platforms on real world samples while recognizing the challenges that impede these substrates from being competitive with traditional packed bed columns. These challenges include increasing the pillar surface area in order to obtain a similar mass loadability as conventional HPLC columns, mechanical stability, and stationary phase creation. Theory predicts that by increasing the pillar surface area of these ordered arrays, results similar to HPLC can be achieved [1, 4]. Electrochemical anodization has been proven to be a successful treatment to increase the surface area of pillar arrays [2, 13] and more recently sol-gel chemistry has been effectively used on silicon pillar arrays for separations[14]. Stationary phase functionalization in pillar array systems using standard reverse phases can be complicated in that occlusion can occur in the system obstructing solvent flow so advances in this area are critical.

Our research group has addressed methods to increase mechanical stability and phase functionalization using pillar arrays for separations in pressurized systems [15]. These include capping the pillar array with silicon oxide in order to increase the robustness of the array and using a gas phase stationary phase modification to functionalize the pillar array surface creating a reverse phase. However, due to the challenges of sealing these pressurized devices we have expanded our research herein to include non-pressurized planar chromatography.

Recent advances in ultrathin layer chromatography (UTLC) indicate that ultrathin layers improve efficiency of planar chromatography while decreasing development time and solvent volume. Notable examples are electrospun polymer layers [16] and electron-beam evaporation of thin SiO2 layers [17]. Other research indicates that advances in the substrates used for capillary flow chromatography show promising results in advancing the technology used in planar chromatography[9]. Additional modernizing advances have occurred in TLC including reduction in particle size (high performance versions, i.e., HPTLC), over-pressure and electrokinetically-driven development, and the aforementioned UTLC [9, 18-20]. Herein we present for the first time original research using lithographically-fabricated uniform pillar arrays for planar chromatography in an open format that are driven by simple capillary action flow. It should be noted that benefits of moderate heterogeneity have been recently reported by Tallarek and coworkers where simulations indicate that at high velocities transverse transport in regular pillar arrays is lacking (20). These confined pillar array systems, as well as spherical particles in tubes, benefit from a small amount of disorder within the system to promote transverse transport and mitigate confinement related dispersion. However, for our unconfined, unpressurized systems with relatively low flow velocities it is not clear that the advantages of moderate disorder are relevant.

Moreover, with open format systems we expect to alleviate some of the problematic issues with pressurized pillar arrays in channels and create new opportunities such as orthogonal 2-D separations and simplified detection. However, the reduction in size and volume of our lithographic-based pillar array platforms relative to traditional TLC creates its own experimental challenges such as uniformly fabricating pillar arrays of greater than 1 cm^2, dealing with heightened solvent evaporation, and the need for introducing very small sample spots. The focus of the current work is fabrication of expansive pillar arrays, studies of solvent transport, methods to create compatible sample spots, and an initial evaluation of band (spot) dispersion.

3.3 Chip design and fabrication of open pillar arrays for separations

To fabricate the initial generation of these planar pillar arrays, a modified version of the technique described in previous publications to generate high-aspect ratio pillar arrays for pressurized systems was used [15]. Standard cleanroom lithographic processing techniques were used in the fabrication process as depicted in Figure (3.3.1). Czochralski grown (p-type) 100mm silicon wafers were used for our top down fabrication process, having an (100) orientation, a thickness ranging from 300 to 500 μm and resistivity between 0.01 and 20 Ω cm.

The 100 mm diameter allowed for ten chips per wafer that were 3 by 1 cm in area. The entire 3 cm^2 chip is a highly ordered array of pillars (Figure (3.3.1)). The pillars were arrayed using CAD software defining the pillars as rhomboids laid out in equilateral triangles, as discussed by Desmet and coworkers [1] using Equation [3.3.1],

$$P = [(2G + 2D)^2 - (G + D)^2]^{1/2} \qquad\qquad [3.3.1]$$

where G is the gap between the pillar sidewalls, D is the pillar diameter and P is the pitch of the pillars. The pillar array parameters that were investigated are listed in Table 3.3.I. To analyze the reduced particle size effect we have varied the pillar dimensions and spacing. The pillar arrays were designed with pillar sizes that range from 1 to 3 μm with a pitch of 2 to 6 μm. To compare these systems with regular packed columns we calculated the external porosity by subtracting the volume of the pillars from the total volume of the chip and determined that this value was comparable to that for some packed columns. The surface area for each pillar array was also approximated in order to estimate analyte loadability and in order to determine concentration volumes for the surface chemistry modification.

Photolithographic patterning was performed using a Quintel, Inc. contact aligner. A double-layer resist system was used (lift-off resist LOR-1A overcoated by positive tone photoresist 955CM-2.1, MicroChem Corp.) which is capable of resolution at the submicron level. Using contact alignment the non-pillared regions are masked off and
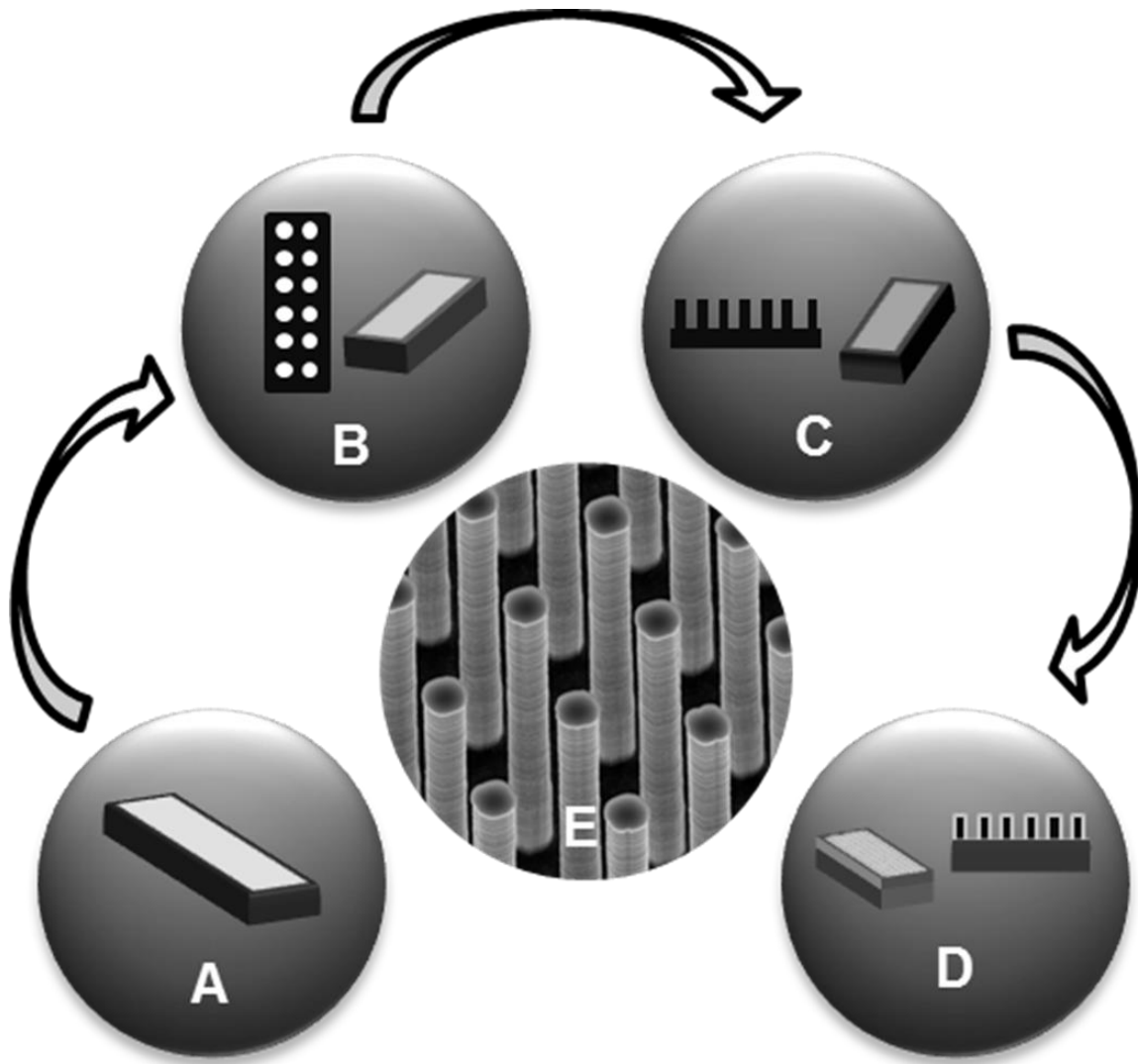
Figure 3.3.1: The fabrication sequence starts with a silicon wafer substrate (A) on which photolithographic patterning is performed (B) followed by DRIE (C) to create the high aspect ratio pillars which are coated with silicon oxide via PECVD (D). An SEM of typical array is shown (E).

Table 3.3.1: Parameters for arrays investigated

Chip Description (all values microns)		$V_P * N_P$[1]	$(V_P / V_C)^2$ *100	$SA_T = SA_P * N_P$[3]
Pillar	Gap	Total Pillar Volume (TV_P)	Void Volume (%)	Surface Area/Chip $(x\ 10^9)$
1	1	1.09E+09	77	4.4
2	1	1.93E+09	60	3.9
2	2	1.09E+09	77	2.2
2	3	6.96E+08	86	1.4
3	3	1.09E+09	77	1.5

[1] V_P indicates the individual pillar volume and N_P is the total number of pillars per array.

[2] V_C is the total volume per pillar array.

[3] SA_T is the total surface area calculated by multiplying the surface area per pillar (SA_P) by the total number of pillars per array.

we expose the wafer to UV light. After development there are holes in the photoresist where the pillars will be etched. Approximately, 15 to 20 nm of chromium was deposited to be used as the etchant mask using an electron beam physical vapor deposition evaporator. The remaining photoresist and excess chromium is then lifted off of the wafer and all that remains on the silicon surface is the hard mask chromium areas that will not be etched. A Bosch process that alternates etching with a passivation layer of fluoropolymer was performed using anisotropic deep reactive ion etching (DRIE) to form pillars that are 15 to 20 μm in height (System 100 Plasma Etcher, Oxford Instruments).

The Bosch process provides anisotropic etching of silicon with scalloped vertical sidewalls and, therefore, increases the surface area of our pillar sidewalls for the separation phase [15]. A thin layer of silicon oxide (~100 nm) was then deposited on the wafer surface using plasma enhanced chemical vapor deposition (PECVD) (System 100 Plasma Deposition Tool, Oxford Instruments). The pillar heights, diameters and pitch were inspected using an FEI Dual Beam scanning electron microscope/focused ion beam (SEM/FIB) (xT Nova Nanolab 200). The processed wafers were scribed and cleaved into individual ~ 1 by 3 cm pillar array chromatographic chips prior to phase modification. A typical array is shown in Figure (3.3.2) where the images on the left are enlarged views of the array on the right to show pillar uniformity.

3.4 Surface modification of the silicon oxide surface

The deposited silicon oxide layer on the pillars served to facilitate subsequent functionalization with silane chemistry. The pillar array was first treated with equal parts of sulfuric and nitric acid to maximize the number of reactive silanol groups on the surface and was then rinsed thoroughly with distilled water and dried at 120 ºC for 18 hours. The stationary phase was synthesized using the method formulated by Hennion et. al. which involved submerging the pillar array in pure octadecyltrichlorosilane (OTS) and heated to 170 ºC for 2 hours [21]. The array was then rinsed with toluene, tetrahydrofuran, a 90/10% ratio of distilled water and
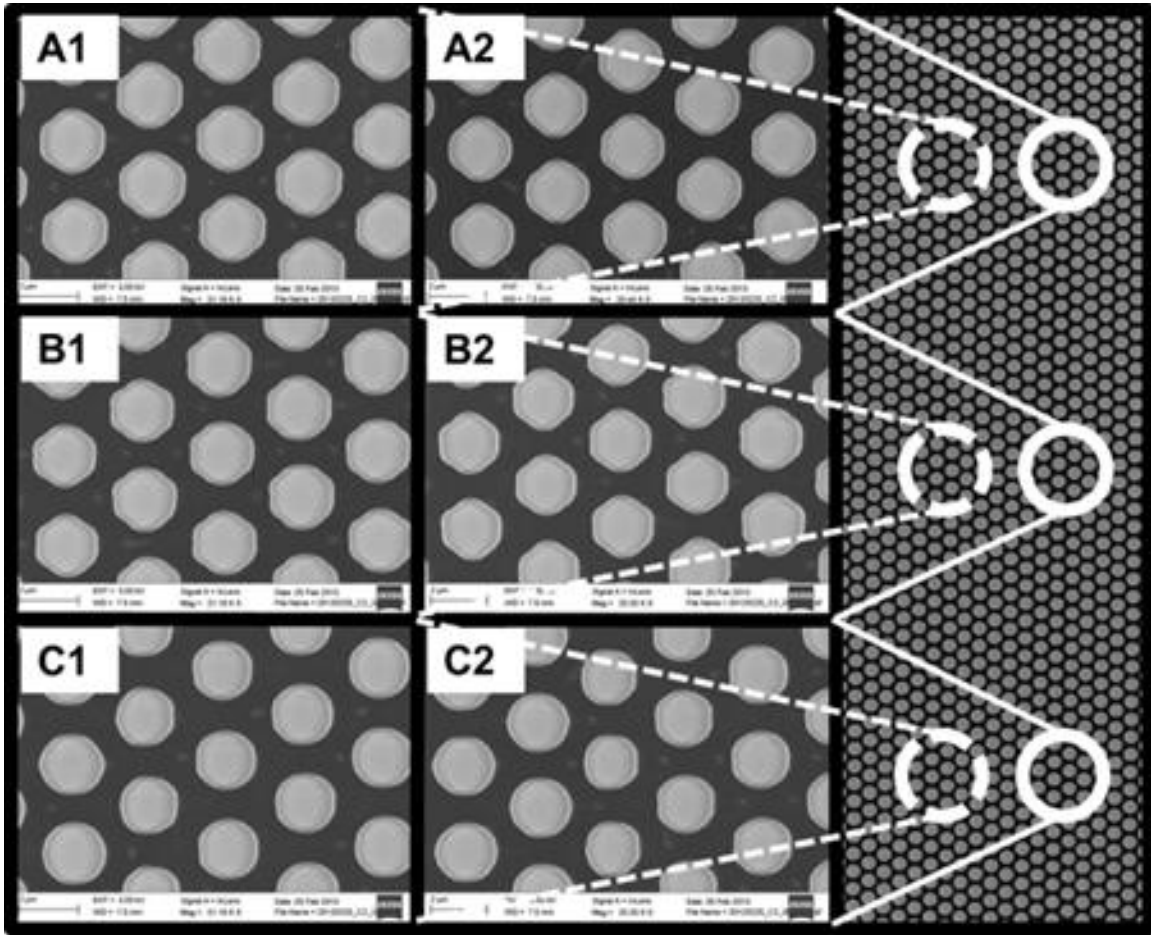
Figure 3.3.2: SEM images of a typical pillar array (pillar dimension of 2 μm with 2 μm pitch). Images A-C are the enlarged areas of the array (right) to show pillar uniformity.

tetrahydrofuran, and finally distilled water. Each rinse was for 10 minutes and repeated twice before continuing to the next rinse stage. This method, when using Partisil packing, yields a maximum carbon content of 23% [21]. Functionalization of the pillar surface with the hydrophobic RP was verified by measuring contact angle (non-pillar area next to the array). The high contact angles observed after C18 phase modification (~135º) confirmed surface modification.

3.5 Development chamber and fluorescent microscope interface

For our initial studies we are using fluorescence detection. To evaluate the analyte development in real time we developed a horizontal development chamber to interface with the fluorescent microscope with a volume of approximately 2 mL. Sample development and detection can be done either simultaneously with horizontal development as performed in these experiments or can be done in the traditional vertical set-up where the plate is developed and then detection is performed in a separate step. The fluorescent imaging is acquired using a Nikon Eclipse E600 and Q-capture software.

3.6 Mobile phase velocity comparison

Capillary action flow in TLC is governed by solvent-stationary phase adhesion and solvent surface tension. The solvent front position in a TLC development process at time t can be related to the planar chromatography system parameters using Equation [3.6.1] where μ_f is the displacement of the solvent front, K_0 is the bed permeability constant, d_p is the diameter of the stationary phase particles, γ represents the surface tension, η the dynamic viscosity and θ, is the contact angle of the mobile phase [9, 22].

$$\mu_f^2 = K_0 t d_p \left(\frac{\gamma}{\eta}\right) \cos\theta \qquad\qquad [3.6.1]$$

This equation has been validated by Guiochon and co-workers for a variety of TLC systems [23, 24] and can be used to predict the relative velocity trend among different solvents. For the common RP solvents shown in Figure (3.6.1A) it was determined that contact angles were small and similar, thus that parameter was
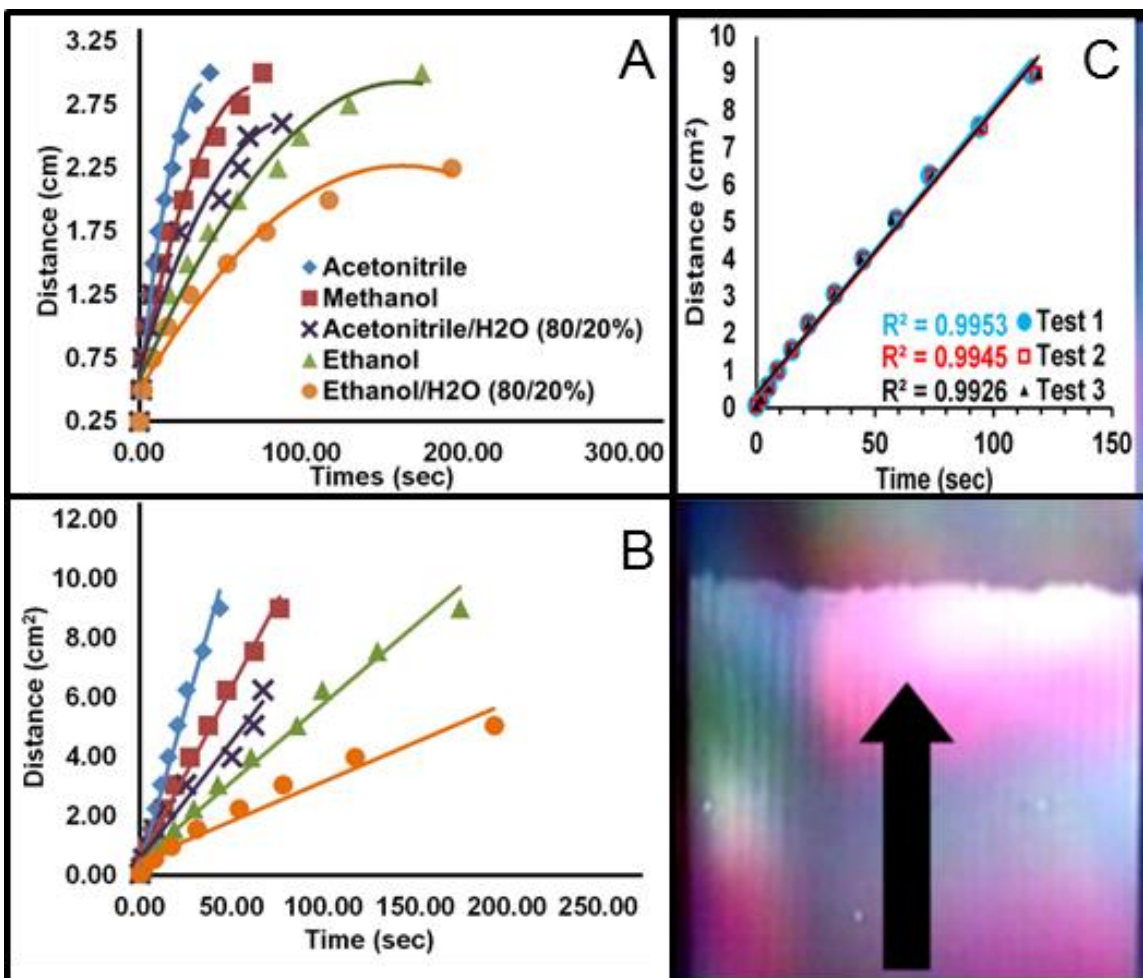
Figure 3.6.1: Solvent comparison for 2μm diameter pillar arrays with 4 μm pitch. (3A) shows the distance of the solvent as a function of time. (3B) represents the squared distance data as a function of time indicating good agreement with Equation [3.6.1]. (3C) is a typical solvent development image with an insert that shows uniformity of L^2 vs t plots.

considered to contribute minimally to the relative velocities. Instead the solvent front velocity is mainly determined by the permeability constant, and the surface tension to viscosity ratio. It has been shown that the permeability constant is much higher for pillar arrays than for more traditional systems [9, 16-19, 25, 26]. In any case the data presented in Figure 3.6.1 is all generated with pillar diameter and pitch being equal to 2 and 4, respectively, thus K_0 is expected to be constant and the relevant influential parameter in the solvent study is, γ/η. As discussed by Poole, an increase in this ratio, as opposed to considering either value individually, is necessary to optimize the plate height for planar chromatography[9]. This ratio (see Table 3.6.1) indicates that the expected trend is consistent with experimental results in that the acetonitrile had the greatest velocity followed by methanol, then ethanol. Also, from Equation [3.6.1], the squared solvent front distance versus time is anticipated to give a linear plot and in Figure (3.6.1B) we can see that the experimental results are consistent with theoretical expectations. Figure (3.6.1C) illustrates that the solvent front for the planar chromatography pillar array is uniform with no apparent anomalies at the array boundries. This is true regardless if the surrounding surface is flat unstructured Si (left) or air (right). The insert in Figure (3.6.1C) indicates that the mobile phase velocity is reproducible for triplicate runs.

3.7 Flow comparisons of pitch variations and to traditional TLC

While the effect of solvent type on flow is straightforward and predictable, the effect of pillar array morphology is a bit more intriguing and requires a more in depth look at Equation [3.6.1]. In TLC, the parameters $\gamma \cos \theta$ influence the capillary action driving force for flow, which can be expected to be constant for a given TLC development process. In TLC that driving force should also scale with the packing bed surface area. Ignoring the effects of internal porosity the surface area should increase with decreasing d_p. The value of the dynamic viscosity, η, influences the hydrodynamic flow resistance. In HPLC this flow resistance is constant and is proportional to vL/d_p^2, where v is mobile phase linear velocity and L is column length. It is important to note that the flow resistance is really dependent on the sizes of the

Table 3.6.1: Relevant properties of solvents studied.

Solvent	Viscosity (η) (mPa·s)	Surface Tension (γ) (mN/m)	(γ/η)	Polarity Index (33) (p')
Ethanol	1.07	22.4	21.5	5.2
Methanol	0.54	22.5	37.9	5.1
Acetonitrile	0.34	29.1	87.2	5.8

gaps between particles with smaller particles yielding smaller gaps. Thus the flow impeding quadratic effect of smaller d_p and the positive effect of smaller values on surface area, hence on the capillary driving force, can be thought to yield the overall linear d_p dependence in Equation [3.6.1]. In TLC the balance of capillary action driving force and hydrodynamic resistance force is achieved early in the development process with large v and is increasingly replaced by the longer development distance (μ_f) as the process proceeds. Our discussion here dismisses the complicating effects of hydrostatic pressure (gravity) and solvent evaporation. Engineered pillar arrays not only provide for high uniformity with a positive effect on flow (larger K_0), but also facilitate a more direct control over flow related surface area and inter-particle (i.e. inter-pillar) gaps. With this in mind, a comparative study was performed to analyze the effect of decreasing the pitch within the system, see Figure (3.7.1A & B). The pillar diameter was held constant at 2 μm and the pitch was varied to produce gaps of 1, 2, and 3 μm with ethanol used as the test solvent. The results of this study indicate that as gaps decrease for constant pillar diameter, the solvent velocity increases as seen in Figure (3.7.1A). Note that as the gap is decreased the surface area that drives the flow process increases (see Table 3.6.1).

Moreover, decreasing the gaps from 3 to 1 μm the distance that solvent must "jump" along the direction of flow between isolated pillars decreases, which may be thought to effectively increase the permeability parameter K_0. The high aspect ratio of the pillars minimize chip floor affects and the capillary flow between the pillars is probably the dominating force. It is certainly true that the hydrodynamic flow resistance increases as the gap decreases but not with a quadratic dependency as predicted by the Poiseuille relationship for flow in a simple capillary tube [27]. The net effect of these factors is a counter intuitive increase in flow with decreasing system size (specifically inter-pillar gaps) as shown in Figure (3.7.1).

To further highlight the advantages of the 2 μm pillar array system with 2 μm gaps (P2G2) when compared to conventional TLC plates, the solvent velocity of a reverse phase TLC plate (Sigma Aldrich C18 silica gel matrix) was recorded using both acetonitrile and ethanol. The solvents were chosen because they represented
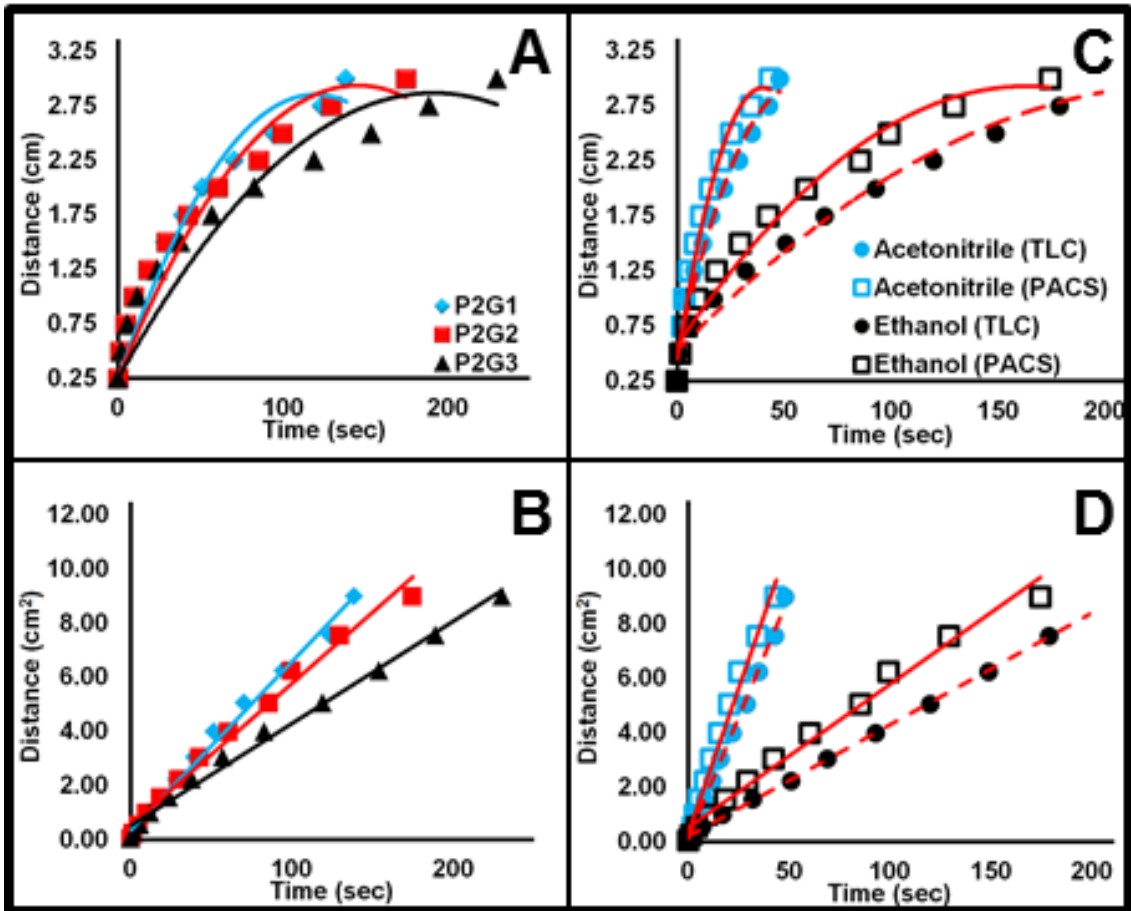
Figure 3.7.1: A & B shows the solvent velocity trend as the pillar diameter to pitch ratio changes, where P indicates the pillar diameter (µm) and G is the gap between pillar sidewalls (µm). Namely that as the pitch to diameter ratio decreases, velocity increases. C & D compares the pillar array chemical separations (PACS) to traditional TLC and indicates that although there is an order of magnitude difference in particle size the pillar array velocity is greater than that for traditional TLC.

the range of the surface tension to viscosity ratio shown in Table 3.6.1. For both solvents the pillar array systems showed an increase in mobile phase velocity over the TLC plates. This increase while modest occurs despite almost an order of magnitude greater TLC particle size compared to the pillar dimensions. Implications of which on efficiency will be discussed later.

3.8 Analyte spotting methods and reproducibility

Critical spotting parameters include sample spot size and reproducibility. Since the overall pillar array size is smaller than typical TLC plates, and our goal is high efficiency, very small sample spots are of paramount importance. Several methods of introducing small spot sizes onto UTLC or TLC substrates have been reported which allow spotting in the low- to sub-mm regime [28-31]. Manipulation of the superhydrophobic nature of our chromatographic system negated the need to use these more elaborate spotting methods. Analytes of interest for chromatographic systems are often only soluble in organic solvents. Spotting with organic solvents on the hydrophobic RP leads to a very large initial spot. To counteract this affect we dissolved our test analytes (standard fluorescent dyes) in methanol and then diluted these samples using aqueous solvents (water or high water content). Two spotting methods that exploit the super hydrophobic character of the arrays were explored; droplet release (from a 1 µL HPLC syringe)/evaporation (Figure (3.8.1A)) and contact transfer (Figure (3.8.1B-upper)). With droplet release it was anticipated that as the droplet evaporates the super hydrophobic mode would shift from the Cassie state, riding on the pillars, to the Wenzel, falling into the pillars [32]. An issue with this technique is that it was difficult to place the droplet in a precise location on the array. Also, with the RP modified pillars the Wenzel mode was often not cleanly observed, hence it is doubtful the sample penetrates the underlying pillars.   The contact transfer spotting method was designed using the 1µL HPLC syringe and a CCD camera to assist in visualization. Using this approach the analyte droplet could easily be placed in specific regions of the array without damaging the pillars with the syringe tip. Fluorescent images of this spotting method indicate that controlling the droplet
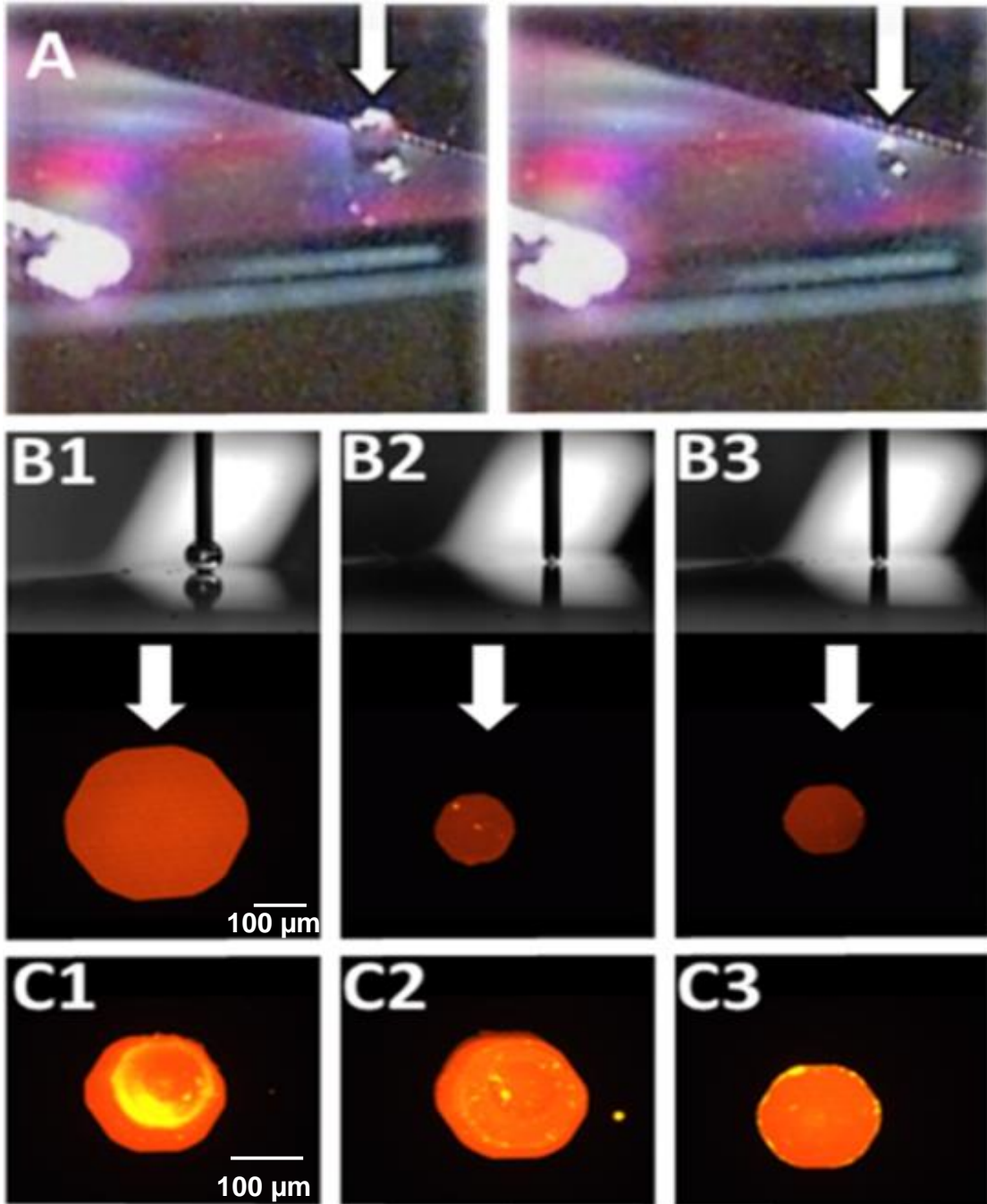
Figure 3.8.1: The droplet release spotting method is demonstrated in (A) while contact spotting with spot size control is seen in (B1-3). (C1-3) shows the reproducibility of the contact spotting method.

volume and contact time allows for sample application of varying spot sizes (Figure (3.8.1B-lower)).

Initial fluorescent microscope imaging indicated that this method was successful, however, upon further investigation it was determined that the images were misleading. Although the spots appeared to be of an appropriate diameter, symmetrical and reproducible the fluorescent images were representative of the contact of the dye with the tops of the pillar. On some occasions the spots take a polygonal shape that mimics the pillar geometry, an effect that has been described by a "pinning" effect during imbibition which causes the solvent droplet to mimic the shape of the pillars within an array at appropriate aspect ratios [33].   However, as with the droplet release method, the hydrophobic nature of the C18 phase and the microstructure pillars discouraged samples of analyte in pure water from entering the pillar array, therefore the underlying spot shape and degree of true analyte loading was uncertain.   It is important to note that during the development process the moving solvent front does not wet the pillar tops, something that is easily observed by noting the spot before and after development. This issue was addressed by adding RP organic modifier to the analyte solution in controlled ratios to determine the appropriate percentage of modification while maintaining a small spot diameter. It was determined that 50-60% Methanol modification allowed for the dye to enter the pillar array while maintaining sufficient hydrophilic nature to maintain small spots. This percentage could change if the array and surface modification is changed. Average spot sizes of approximately 200 µm in diameter were reproducibly observed as shown in Figure (3.8.1C).

3.9 Efficiency analysis: plate height versus μ_f position

While factors that contribute to plate height, H, are extremely complex in planar chromatography, [9, 18] the treatment by Guiochon [34] is generally regarded as comprehensive and is based on the validity of the Van Deemter equation (Equation [3.9.1]) that is common to HPLC theory.

$$H = A + \frac{B}{v} + (C_S + C_M)v \qquad \text{[3.9.1]}$$

Generally, plate height is dependent on eddy diffusion, A, longitudinal diffusion, B, which is influenced by the mobile phase velocity (v) and resistance to mass transfer in both the stationary and mobile phases, Cs and Cm, respectively. Expansion of the Van Deemter equation to include the parameters that influence plate height is shown in Equation [3.9.2].

$$H = 2\lambda d_p + \frac{2\lambda D_M}{v} + \frac{qk'd_f^2 v}{(1+k')^2 D_S} + \frac{\omega d_p^2 v}{D_M} \qquad \text{[3.9.2]}$$

In this equation the critical particle diameter is represented by d_p, the partition coefficient is k', the average film thickness of the stationary phase is d_f, the diffusion coefficients for the stationary and mobile phases are D_S and D_M, and independent factors that are specific to the column packing include q, λ, γ, ω [15, 35].

The eddy diffusion term (A) can be excluded from consideration in the case of perfectly ordered pillar arrays [15]. Also, any broadening contributions from the stationary phase term (C_S) can be excluded for the simplifying case of an unretained solute (k' = 0). Using experimental literature values for pillar arrays we previously reported for γ (0.5) and ω (0.02), [15] the relevant plate height can be estimated based solely on the ubiquitous B and C_m terms by using Equation [3.9.3] [15, 36, 37].

$$H = \frac{2(0.5)D_M}{v} + \frac{0.02d_p^2 v}{D_M} \qquad \text{[3.9.3]}$$

Employing a typical diffusion coefficient (D_M) of 5.0E-6 cm^2/s for the solute and experimental velocities for both the pillar array and the traditional TLC plate (see Figure (3.7.1)) we can compare the predicted plate heights for each system based on position of the solvent front μ_f (Figure (3.9.1A)).

For the pillar array system plate heights are predicted to be significantly smaller than the TLC plates when using identical parameters for the packing factors and only changing the critical particle size (d_p) value and using the experimental velocities. In this case the TLC d_p is taken as the manufacturer's value of 10 μm and polydispersity is not considered. For the pillar array system d_p is taken as the more relevant 1 μm gap. In both systems the solute band is assumed to be located at the
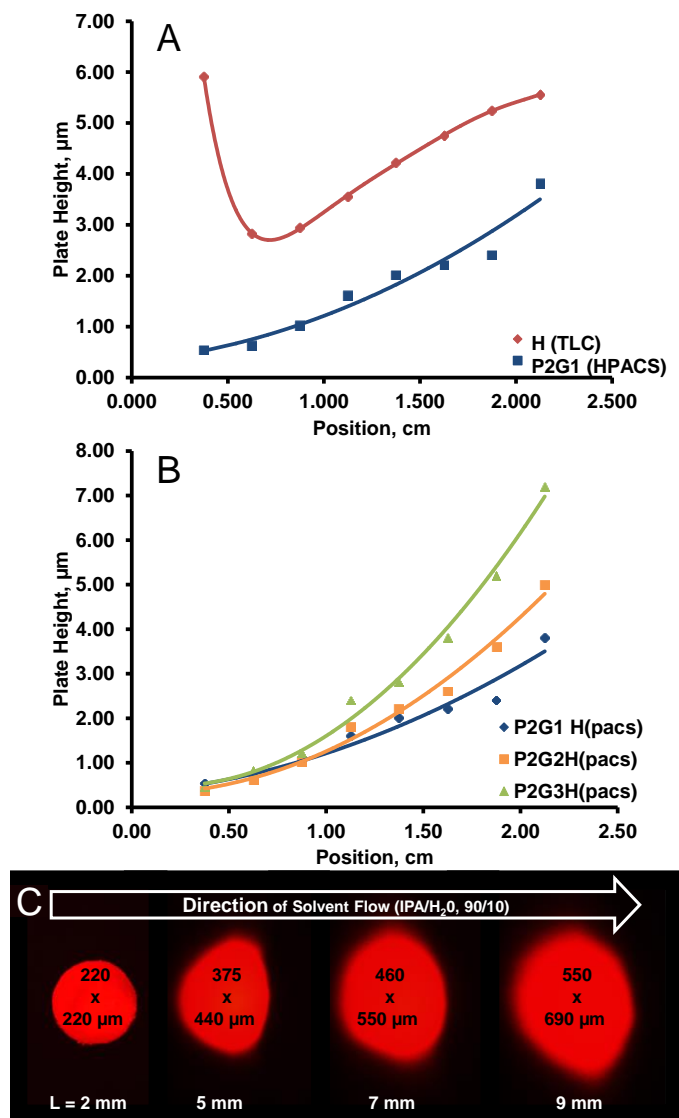
Figure 3.9.1: Van Deemter-like plots of flow rate linear flow velocity dependent of the solvent front versus B and Cm term-based plate height. Experimental flow rates linear flow velocities are taken from the exponential fits in Figure 3.6.1A and C The predicted superior performance of a PACS versus a commercial TLC plate is shown in (A) and (B) demonstrates the effect of PACS gap size, where P represents the pillar diameter (μm) and G indicates the gap betweeen the pillar sidewalls (μM). (C) Evaluation of R6G in real time giving H values of 1.0, 1.4, and 1.7 μm, respectively, from the original spot at 2mm.

71

advancing solvent front but not spatially altered by its proximity to the front. In these treatments of relative efficiency, the difference between the plate heights of these two systems would be expected to be much greater than shown if the actual packing factor terms for TLC were to be used and, in particular, when the eddy diffusion term is also included. Since the linear flow velocity for the pillar array chemical separations (PACS) system is only slightly greater than the TLC case, Figure (3.7.1C & D), at large distances the efficiencies shown in Figure (3.9.1A) are dominated by diffusion. Under these conditions the array platform is only roughly a factor or two better than the TLC case. It is at small distances (rapid flow) that a dominance of the Cm term occurs and the TLC efficiency suffers greatly as seen from the upturn of H shown in the figure. If one were to use smaller particles for TLC to counteract the C_m problem, reductions in flow as predicted by Equation [3.6.1] would exacerbate diffusion problems. Conversely, the unique flow characteristics of the pillar arrays permit small diameter pillars and inter-pillar gaps without evidence of C_m issues for pillar array systems. This behavior is seen when comparing the three different gap sizes shown in Figure (3.9.1B). For all three gaps there is no significant evidence of C_m issues and at longer solvent front distance the fastest moving 2 μm pillar diameter arrays with 1 μm gaps (P2G1) is most efficient. In this treatment we have not considered possible non-development sources of band dispersion; e.g., sample application and detection processes and possible slow solvation as the solvent front encounters sample spots.

3.10 Preliminary experimental evaluation of plate height

An example of band dispersion captured in real time as the analyte moves through the P2G1 pillar array is shown in Figure (3.9.1C). The analyte is rhodamine 6G (1E-7M) applied from a 50/50% methanol/H_2O solution to create a 220 μm diameter spot located 2 mm from the edge of the array. The mobile phase used for development is isopropanol/water (90/10%). A fluorescence microscope signal acquisition time of 1 second allowed for the observation of the analyte at low concentrations without observing a noticeable blurring effect. Spot dispersion in the

direction of solvent flow is minimized in this experiment due to the concentrating effect of the analyte being very near the solvent front, so efficiency was evaluated in the direction perpendicular to that flow. Using these measured spot sizes we expect that diffusion (B-term) is being evaluated and that is deemed appropriate by the treatment in Figure (3.9.1 A&B). Although the bands (especially original spot) are not Gaussian in shape, and the actual spot sizes are prone to interpretation, we use H = μ^2/*distance developed* to estimate efficiency with σ equal to one fourth of the apparent spot size; for example, H_{2-5}= $(115-55)^2$/3000 = 1.2 μm. Similarly for the spots seen at 7 and 9 mm we have H_{2-7}= 1.7 μm, and H_{2-9}= 2.0 μm, respectively, as estimates of plate height (k ≈ 0).

Comparing these values with the expected plate heights in Figure (3.9.1B), the trend of increasing H with slower flow is seen but the actual observed plate heights are a little higher than what was predicted. This could reflect our crude method of evaluating H. More likely, this can be explained by considering the band broadening introduced by non-development factors, in this case solvation of the analyte spot during the initial confrontation with the moving solvent front. Considering band dispersion from both spot solvation (*SS*) and development factors (*DF*) as discussed in the previous section, plate height can be reduced to Equation [3.10.1].

$$H = H_{SS} + H_{DF} \qquad [3.10.1]$$

The uniformity of the pillar array and the low concentration of rhodamine 6G should minimize H_{SS} as compared to TLC. Still it is unreasonable to expect it to be negligible, particularly with the rapid flow early in the development process. As is so often the case, chromatography is a compromise; in this manifestation, spot close to the edge of the array to minimize H_{DF} (B-term here) but spot far from the edge to minimize H_{SS}. Regardless of the rather crude methods of evaluating efficiency used herein, it is clear the initial and developed spots are very small compared to TLC and follow expected trends.

3.11 Conclusion

The research presented herein, for the first time demonstrates that lithographically-produced highly ordered pillar arrays can be used as reusable planar chromatography separation platforms that employ simple capillary flow as the driving force. Both practical and fundamental aspects are discussed and illustrated herein. This open system bypasses issues observed in pressurized pillar array chromatography including sealing of the system. We have incorporated an effective C18 stationary phase functionalization of the arrays that does not cause occlusion between the pillars. Linear flow velocity studies during development reveal a somewhat surprising trend to more rapid flow as pillar size and gap decrease. Rationalization of this trend and its effect on efficiency is presented and point to the value of pillar arrays when compared to more traditional planar platforms for separations. By taking advantage of the superhydrophobic nature of the system we are able to apply sample in very small spots and image the spots and separations with a simple fluorescence microscope. The promising results of these initial studies motivate further reduction in system size, exploration of stationary phases, and modeling in our future work.

3.12 Acknowledgements

3.13 References:

1.   P. Gzil, N. Vervoort, G. V. Baron and G. Desmet, *Analytical Chemistry*, 2003, 75, 6244-6250.
2.   W. De Malsche, D. Clicq, V. Verdoold, P. Gzil, G. Desmet and H. Gardeniers, *Lab on a Chip*, 2007, 7, 1705-1711.
3.   W. De Malsche, H. Eghbali, D. Clicq, J. Vangelooven, H. Gardeniers and G. Desmet, *Analytical Chemistry*, 2007, 79, 5915-5926.
4.   J. De Smet, P. Gzil, N. Vervoort, H. Verelst, G. V. Baron and G. Desmet, *Analytical Chemistry*, 2004, 76, 3716-3726.
5.   B. He and F. Regnier, *Journal of Pharmaceutical and Biomedical Analysis*, 1998, 17, 925-932.
6.   F. E. Regnier, *Journal of High Resolution Chromatography*, 2000, 23, 19-26.
7.   H. Eghbali, W. De Malsche, D. Clicq, H. Gardeniers and G. Desmet, *LC/GC Europe*, 2007, 20.
8.   M. R. Schure, R. S. Maier, D. M. Kroll and H. T. Davis, *Journal of Chromatography A*, 2004, 1034, 79-86.
9.   S. K. Poole and C. F. Poole, *Journal of Chromatography A*, 2011, 1218, 2648-2660.
10.   L. R. Huang, E. C. Cox, R. H. Austin and J. C. Sturm, *Science*, 2004, 304, 987-990.
11.   W. De Malsche, H. Gardeniers and G. Desmet, *Analytical Chemistry*, 2008, 80, 5391-5400.
12.   H. Eghbali, S. Matthijs, V. Verdoold, H. Gardeniers, P. Cornelis and G. Desmet, *Journal of Chromatography A*, 2009, 1216, 8603-8611.
13.   R. M. Tiggelaar, V. Verdoold, H. Eghbali, G. Desmet and J. G. E. Gardeniers, *Lab on a Chip*, 2008, 9, 456-463.
14.   W. De Malsche, S. De Bruyne, J. O. De Beeck, S. Eeltink, F. Detobel, H. Gardeniers and G. Desmet, *Journal of Separation Science*, 2012, 35, 2010-2017.
15.   N. V. Lavrik, L. C. Taylor and M. J. Sepaniak, *Lab on a Chip*, 2010, 10, 1086-1094.
16.   J. E. Clark and S. V. Olesik, *Analytical Chemistry*, 2009, DOI: 10.1021/ac9004293, 4121-4129.
17.   L. W. Bezuidenhout and M. J. Brett, *Journal of Chromatography A*, 2008, DOI: 10.1016/j.chroma.2007.12.089, 179-185.
18.   C. F. Poole, *Journal of Chromatography A*, 2003, DOI: 10.1016 /S0021-9673(03)00435-7, 963-984.
19.   J. Sherma, *Analytical Chemistry*, 2004, 76, 3251-3470.
20.   J. Sherma and B. Fried, *Handbook of Thin-Layer Chromatography*, New York, 3rd edn., 2003.
21.   M. C. Hennion, C. Picard and M. Caude, *Journal of Chromatography*, 1978, 166, 21-35.
22.   A. A. Saha, S. K. Mitra, M. Tweedie, S. Roy and J. McLaughlin, *Microfluidics and Nanofluidics*, 2009, 7, 451-465.
23.   G. Guiochon, *Journal of Chromatography A*, 2007, 1168, 101-168.

24. G. Guiochon, G. Korosi and A. Siouffi, *Journal of Chromatographic Science*, 1980, 18, 324-329.
25. T. J. Kauppila, N. Talaty, P. K. Salo, T. Kotiaho, R. Kostiainen and G. Cooks, *Rapid Communications in Mass Spectrometry*, 2006, 20, 2143-2150.
26. S. Tuomikoski, K. Huikko, K. Grigoras, P. Ostman, R. Kostiainen, M. Baumann, J. Abian, T. Kotiaho and S. Franssila, *Lab on a Chip*, 2002, 2, 247-253.
27. E. W. Washburn, *Physical Review*, 1921, 17, 273-283.
28. W. Streule, T. Lindemann, G. Birkle, R. Zengerle and P. Koltay, *Journal of the Association for Laboratory Automation*, 2004, 9, 300-306.
29. S. C. Powell, *Analytical Chemistry*, 2010, DOI: 10.1021/AC100625S, 3408.
30. D. C. Fenimore and C. J. Meyer, *Journal of Chromatography*, 1979, 186, 555-561.
31. C. K. Byun, X. Wang, Q. Pu and S. Liu, *Analytical Chemistry*, 2007, 79, 3862-3866.
32. T. Koishi, K. Yasuoka, S. Fujikawa, T. Ebisuzaki and X. C. Zeng, *Proceedings of the National Academy of Sciences of the United States of America*, 2009, 106, 8435-8440.
33. L. Courbin, E. Denieul, E. Dressaire, M. Roper, A. Ajdari and H. A. Stone, *Nature Materials*, 2007, 6, 661-664.
34. G. Guiochon and S. Antoine, *Journal of Chromatographic Science*, 1978, 16, 470-481.
35. N. V. Lavrik, L. T. Taylor and M. J. Sepaniak, *Analytica Chimica Acta*, 2011, 694, 6-20.
36. G. Deininger, *Chromatographia*, 1976, 9.
37. C. F. Poole, Elsevier Science B.V., Amsterdam, 2003 edn., 2003.

Chapter 4

Deterministic and stochastic nanoscale pillar arrays for separations

The research presented in Chapter 4 has been adapted from a research article published in journal *Analyst* (Teresa B. Kirchner, Rachel B. Strickhouser, Nahla A. Hatab, Jennifer J. Charlton, Ivan I. Kravchenko, Nickolay V. Lavrik and Michael J. Sepaniak, Analyst, (2015), DOI: 10.1039/c4an02187h*). This chapter focuses on band broadening and plate height in capillary flow driven micro-scale planar chromatographic systems. These unique systems exhibit plate heights around 2 microns and show promise that scaling planar chromatographic systems to these dimensions can offer improvements in efficiency and band broadening when compared to traditional TLC systems.

4.1 Abstract:

The work presented herein evaluates silicon nano-pillar arrays for use in planar chromatography. Electron beam lithography and metal thermal dewetting protocols were used to create nano-thin layer chromatography platforms. With these fabrication methods we are able to reduce the size of the characteristic features in a separation medium below that used in ultra-thin layer chromatography; i.e. pillar heights are 1-2µm and pillar diameters are typically in the 200-400nm range. In addition to the intrinsic nanoscale aspects of the systems, it is shown they can be further functionalized with nanoporous layers and traditional stationary phases for chromatography; hence exhibit broad-ranging lab-on-a-chip and point-of-care potential. Because of an inherent high permeability and very small effective mass transfer distance between pillars, chromatographic efficiency can be very high but is enhanced herein by stacking during development and focusing while drying, yielding plate heights in the nm range separated band volumes. Practical separations of fluorescent dyes, fluorescently derivatized amines, and anti-tumor drugs are illustrated.

4.2 Introduction

When used as planar chromatography separations platforms, periodic and stochastic nanoscale pillar arrays are shown to offer attributes of rapid mass

transport, high chromatographic efficiency that is influenced by development and post development processes, portability, and diminutive

mobile phase and sample requirements. Using clean room fabrication techniques, nano-scale pillar arrays can be fabricated for use as nano-thin layer chromatographic (NTLC) platforms (Figure 4.2.1). As dicussed previously,[1, 2] Electron beam lithography (EBL) permits exquisite control of pillar placement and dimensions to form deterministic pillar arrays (herein, DPA). While the highly ordered systems afforded by this lithography method may be ideal in evaluating effects of changes in pillar dimensions on flow characteristics and furthermore separationefficiency, the EBL process requires expensive equipment and is a slow serial process, the combination creates practical limits as to the size and quantity of fabricated arrays. A far more accesssible approach involves fabrication of stochasitc pillar arrays (SPA) using the thermal dewetting of thin Pt films to create masks [1, 3]. Although these SPA systems do not deliver precise control of pillar morphology, placement, and dimensions, previous work has shown,[1] some control is maintained by varying the Pt film thickness. The SPA systems fabricated and evaluated within this work were tailored, as afforded by the method, to as closely approximate the more dense EBL system. Discussed previously,[1] both the EBL and dewetted Pt fabrication methods are capable of creating pillar arrays with dimensions larger and smaller than the platforms reported herein. These dimensions were partially chosen to create the lowest volume platform while minimizing evaporation and keeping the pillars under a 10:1 aspect ratio to maintain robustness and minimize wicking and spotting damage. In this research we study solvent and analyte transport, chromatographic efficiency, and demonstrate chemically selective separations with DPA- and SPA-NTLC platforms.

Desmet et al. has shown that porous silicon adequately increases surface area in ordered arrays to be used as a liquid chromatography platform for systems that are confined and pressurized [4-7]. Previous research from our group has shown that highly ordered pillar arrays prepared by photolithography in the low µm

regime, and coated with a thin layer of silicon oxide, functionalized with a carbon reverse stationary phase (RP), produced plate heights (H) as low as 0.8 μm in closed pressurized array systems[8] and plate heights on average of 2 μm for capillary-action driven open array systems[9]. Combining previously mentioned fabrication protocols followed by reactive ion etching with a room temperature plasma enhanced chemical vapor deposition process creates a conformal porous silicon oxide (PSO) layer on the pillar surface (Figure 4.2.1) [10, 11]. These unique arrays create a nano-scale platform for RP chromatographic separations. Increasing the accessible surface area of the system and generating substantial surface silanols for bonding with a C18 RP stationary phase (fabrication details in Chapter 5.1, Supporting Information), ultimately achieve an adequate analyte retention .

In our previous pillar array based ultra-thin layer chromatography (UTLC) work we demonstrated that there is an improved H due to a lack of eddy diffusion (ordered arrays) and minimized resistance to mass transfer in the mobile phase (small pillar diameters and inter pillar gaps)[9]. Equally important was a favorable permeability constant (K_0) of these highly ordered systems, avoiding the adverse effects of small packing particles that are observed in traditional TLC, principally slow flow and a concomitant increase in molecular diffusion broadening of

spots. This research was designed to investigate if these trends in flow and H will continue as dimensions are further reduced. It is anticipated that a further reduction in H could occur for these nano-scale systems due to a reduction in feature size as discussed in our previous publications [8, 9, 12, 13], but only if wicking flow is adequate. Further discussion of this topic using the Van Deemter Equation is in Chapter 5, Supporting Information.

Additionally, we employed a semi-empirical model developed by Mai et al. for ordered arrays of silicon pillars[13.] This model derived theoretical wicking velocities for varying pillar dimensions. These velocities allowed us to evaluate the effect of pillar height, diameter, and pitch to make a predicted efficiency. These
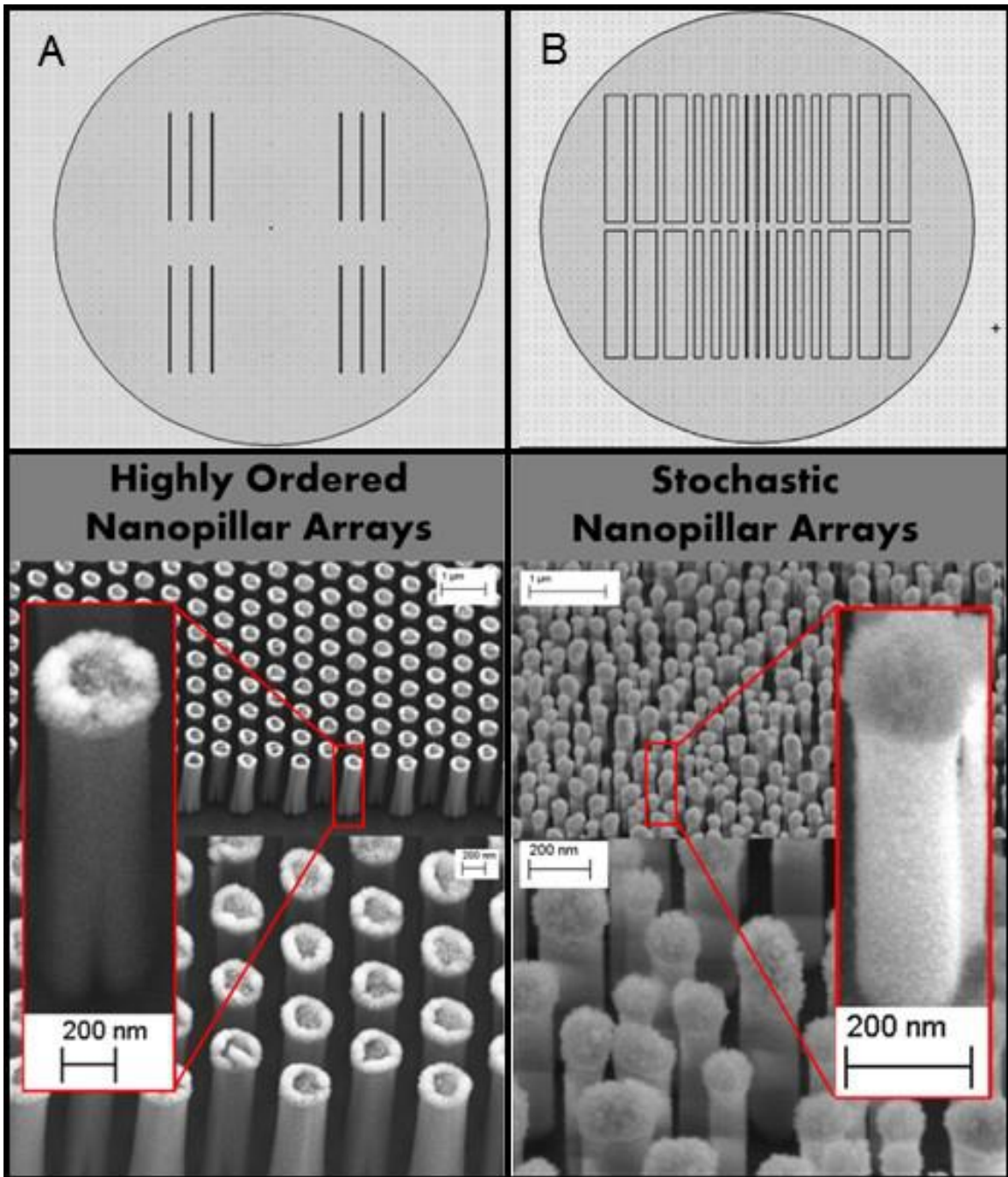
predicted values further directed substrate development. The Mai model

Figure 4.2.1: Wafer layout and SEM images of (A) DPA and (B) SPA patterned   NTLC platforms.

is based on the geometrical parameters of the fabricated substrate, experimentally measured solvent-substrate contact angles, and literature values for solvent viscosity and surface tension. We then predict H for these nano-scale arrays using a typical diffusion coefficients and the modeled velocity for acetonitrile. This yielded values less than 0.5 µm for the NTLC DPA systems, smaller than the H values observed for UTLC systems reported in our previous work[9]. While the flow model does not consider the porous SiO_2 layer and thus only roughly mimics the experiment, this treatment does motivate scaling down into the nano-regime (further information is found in Chapter 5, Supporting Information).

4.3 Solvent velocity studies on NTLC platforms

Rapid flow is essential in generating high efficiency separation platforms for separations. Equation [4.3.1] describes the effects of parameters on flow in traditional planar chromatography. In this equation, μ_f is the

$$\mu_f^2 = K_0 t d_p \left(\frac{\gamma}{\eta}\right) \cos\theta \qquad [4.3.1]$$

displacement of the solvent front, d_p is the diameter of the stationary phase particles, γ represents the surface tension, η the dynamic viscosity and θ, is the contact angle of the mobile phase. The dimensions of the 5 cases investigated (with and without PSO and both types of arrays; DPA and SPA) are summarized in Chapter 5 Supporting Information Table 5.1.1.

Varying pitch is ideal for this study because, for these pillar array systems, the interpillar gap behaves as particle diameter (d_p from Equation 4.3.1) in traditional planar chromatography systems. Figure 4.3.1 illustrates typical solvent behavior for these nanoscale systems. Figure 4.3.1A shows the contact angle of water on PSO on flat silicon before (left) and after (right) functionalization with the C18 RP. The hydrophobic character of the surface indicates successful RP functionalization. Figures 4.3.1B and 4.3.1C are comparisons of the acetonitrile solvent front where the blurriness in the former
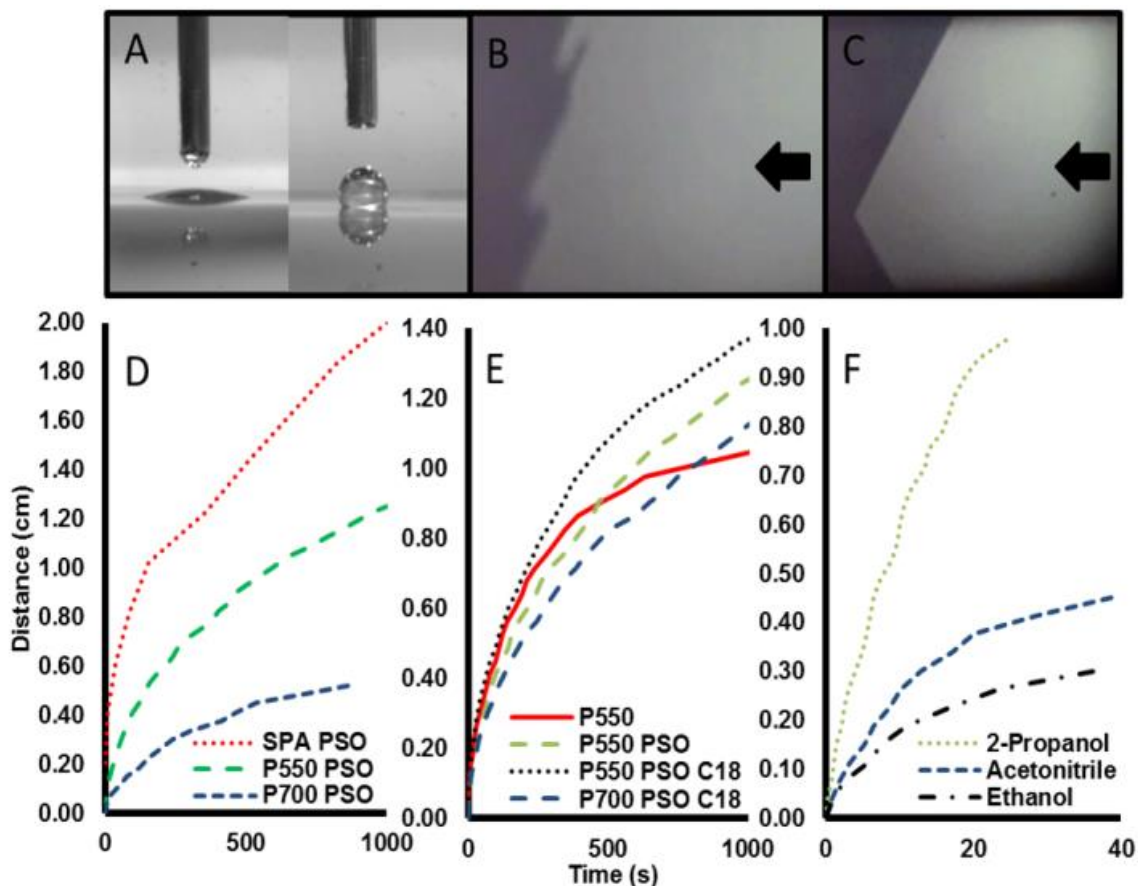
Figure 4.3.1: Microscopy images of (A) water contact angle on non-functionalized PSO (left) and RP functionalized PSO (right), (B) solvent front (direction denoted by arrow) at high velocity early in development, and (C) the front as velocity decreases later in development (DPA case). Velocity plots; (D) comparing DPA pitch variations, P550 with PSO versus P700 with PSO and comparing DPA versus SPA (pillar diameter ~ 200 nm & pitch ~ 550 nm for the SPA PSO case), (E) comparing non-PSO (P550) versus PSO (P550 PSO) DPA and comparing non-functionalized (P550 PSO) versus RP functionalized (P550 PSO C18) and finally comparing pitch with the C18 RP case (550nm versus 700nm). (D) and (E) use benzyl alcohol while (F) uses more traditional solvents for a DPA (P700 PSO C18) system.

is probably due to very rapid wicking early in development. These images show pinning behavior at the solvent front. This behavior self-adjusts during development and should not affect bands significantly behind the solvent front. Due to noticeable evaporation issues with traditional RP mobile phases (Figure 4.3.1F) we used benzyl alcohol as a low vapor pressure mobile phase in experiments that allowed us to identify effects of the pillar array design parameters on their wicking characteristics. In particular, we analyzed how presence of a PSO coating, pitch and degree of order in the arrays affected the observed wicking velocity (Figures 4.3.1D and 4.3.1E). Solvent properties are in Chapter 5, Supporting Information Table 5.7.1.

The results of this analysis show that as the pitch decreases the solvent velocity increases (Figure 4.3.1D, P550 PSO vs P700 PSO). When comparing the SPA to the ordered DPA systems, the former exhibits significantly faster wicking (Figure 4.3.1D). A possible explanation for this behavior may be found in the law of flow resistance in parallel channels as discussed previously for SPA systems[1, 14, 15]. Figure 4.3.1E compares the PSO to the non-PSO arrays. It shows that the solvent velocity is greater as distance increases when compared to the non-PSO for the DPA case. Also, it was observed that the solvent front traveled a greater distance with the addition of PSO. These observations may be due to an increase in nano-capillaries and surface area, the latter benefits chromatographic retention, on the PSO modified surface [16-19]. Figure 4.3.1F is a comparison of the behavior of more traditional RP solvents. The resulting data cannot be explained by Equation [4.3.1] alone, which predicts the wicking velocities in the following order: acetonitrile > ethanol > 2-propanol. This discrepancy is most likely due to effects of more pronounced evaporation of more volatile solvents from the surface of the shallow NTLC platforms.

4.4 NTLC platform efficiency analysis

The H and peak capacity treatment that was used as a predictive exercise to validate the premise for this research was based on the well-known work reported by Guiochon[20, 21] and is often used in planar chromatography. Further

discussion of this treatment can be found in Chapter 5, Supporting Information.

In terms of chromatographic efficiency, evaporation reduces net flow (Figure 4.3.1F) for these nano-scale systems, especially as the development proceeds and, as a consequence, molecular diffusion can become problematic as is the case in traditional TLC. The flow of benzyl alcohol is slow due to an unfavorable γ/η ratio whereas for acetonitrile, with a favorable ratio, the model-predicted flow (see Chapter 5, Supporting Information Figure 5.7.1) is much greater than experimentally observed, presumably due to evaporation.

In spite of these issues with solvent velocity and evaporation the observed efficiencies in our system under different mobile phase conditions as shown in Figure 4.4.1 and 4.4.2 are better than expected. We contend that the traditional Van Deemter efficiency variables give way to fortuitous beneficial effects of *stacking* during development and *focusing* while drying.   For these studies less band dispersion in the direction of the solvent direction was observed.   For example, consider the aspect ratio of the band seen in Figures 4.4.1D, 4.4.2B & 4.4.2D. We propose a stacking phenomenon caused by a gradient of the phase ratio (β = volume mobile phase/volume stationary phase) occurs in the direction of flow during the development. This implies that the phase ratio at the front of the band is smaller than at the tail of the band causing a spatial contraction. Such effects are well known in TLC [22-26], however the scale of the NTLC system is likely to exacerbate the phase ratio issue. When mixed solvents are used uneven evaporation can also play a role.   Although, ideally, we aim to minimize evaporation, there are unique positive effects shown in this work.   Additional observations include a degree of curvature across the band of the DPA (Figure 4.4.2A).   Contributions to this phenomena include solvent considerations (curvature increases when the band is at or near the solvent front) as well as effects of the morphological
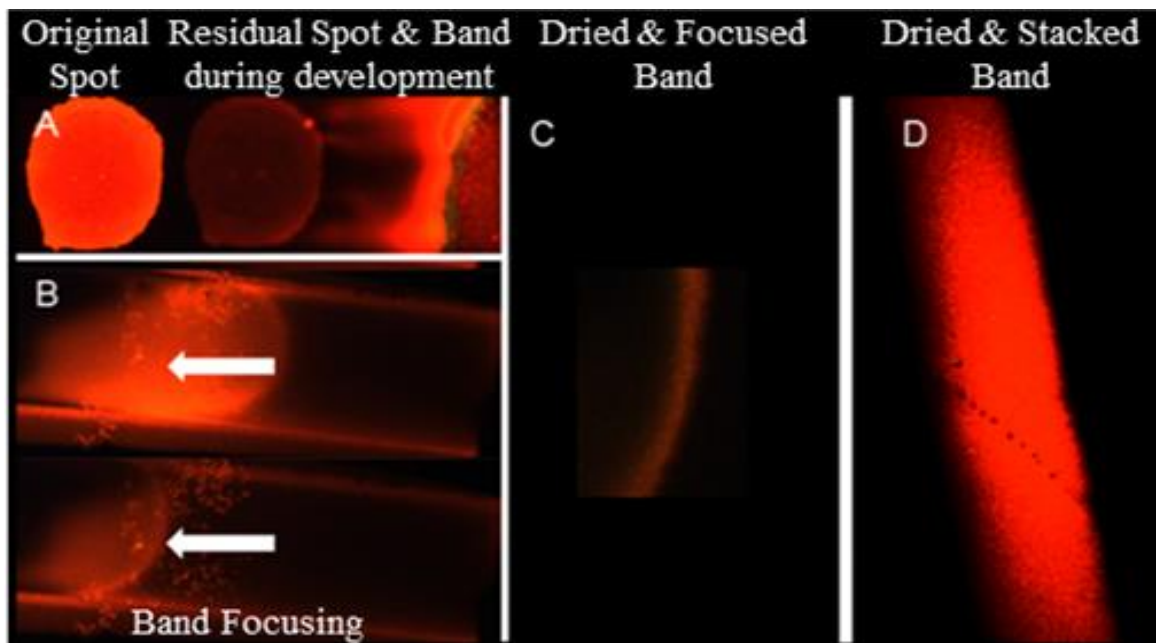
 Figure 4.4.1: Illustration of processes that influence the dispersion (or concentrating) of initially spotted samples of SR640.   (A) and (B) are imaged with mobile phase (ethanol: water & benzyl alcohol) present while (C) and (D) are dried cases. In (A) the solvation of the initial spot exhibits a concentrating effect (400 μm wide DPA, likewise B & C). (B) demonstrates the focusing effect as the solvent (benzyl alcohol) evaporates (note arrows in same position top and bottom). Demonstrated in (C) and (D) are dried bands that are *focused* (400 μm wide DPA, benzyl alcohol), H~100nm (n=3) and *stacked* (SPA, ethanol:water), H~900nm, respectively.
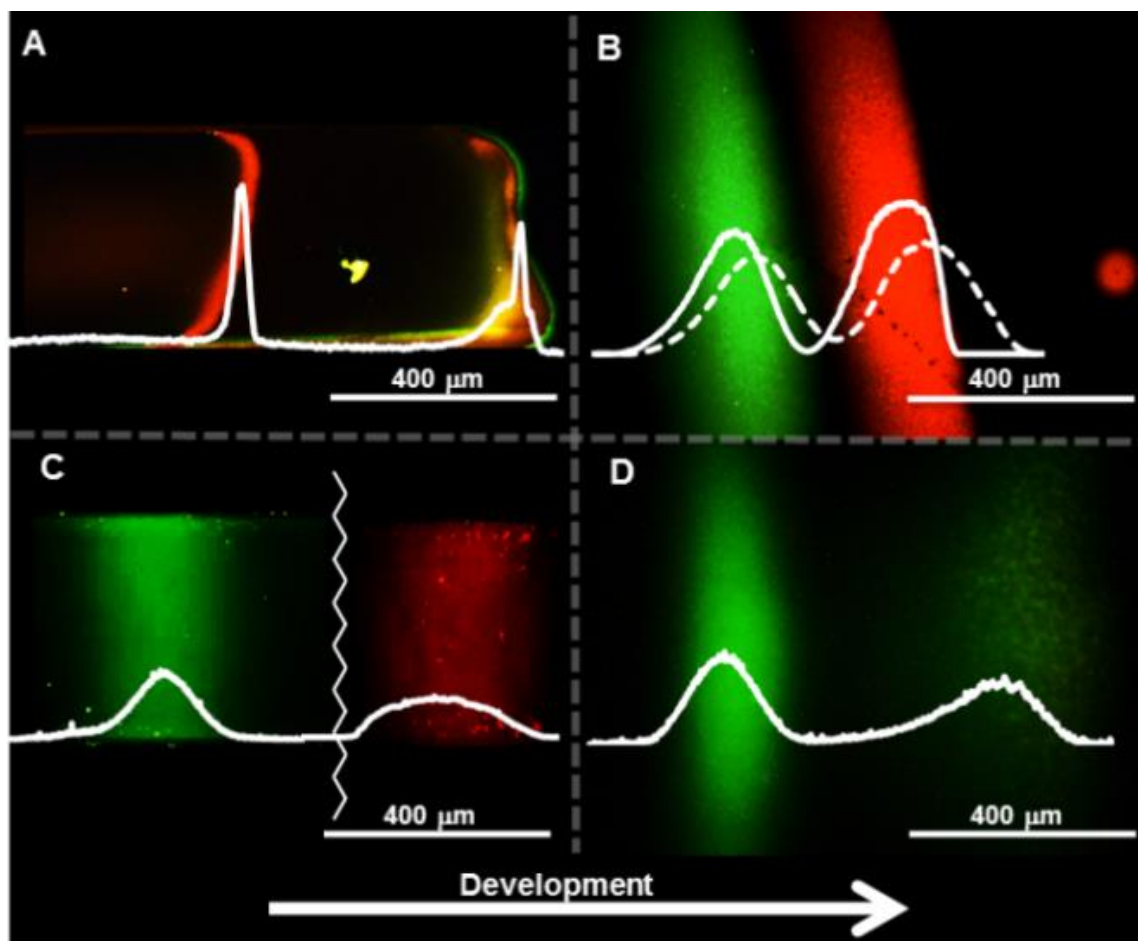
Figure 4.4.2: Illustration of separations using DPA (P450G125) (A) and (C) and SPA (P227G414) (B) and (D) each with 25nm PSO and C18. (A) separation of fluorescent dyes SR 640 (more retained) and FITC (at solvent front), (B) separation of dyes coumarin 102 (more retained) and SR640, (C) separation of anti-tumor drugs D_1 (more retained) and A_1, and (D) separations of fluorescently-derivatized environmental amines n-heptyl amine (more retained) and n-propyl amine.   In (A) slow drying benzyl alcohol is employed as the mobile phase on an array that resulted in very little retention, substantial focusing (H ~ 25 nm) occurs. Conversely, the other separations are performed with (B) ethanol, 80%, (C) 2-propanol, 60%,and (D) ethanol, 70% all in un-buffered water. Chromatographic traces were generated using Image J 1.47V.

heterogeneity of the system at the array boundry (see Figure 5.5.2 in Supporting Information).

It is also important that as the solvent interacts with the initial dried spot, slow solvation kinetics, as described by Poole[24], does not contribute to band broadening. Figure 4.4.1A shows that a concentrating effect is observed as the solvent interacts with the dried spot (note also the image of the pillar top residual after the front passes). While discrete concentrating zones have been implemented in UTLC platforms that also produce concentrating effects[27] our NTLC platforms are morphologically homogeneous (except for at the array boundaries), although there could be an element of overloading contributing to the effect observed in the figure.   Although not done herein, discrete concentrating zones (e.g., thicker PSO layers) could be fabricated into our NTLC platforms as well.

A second type of concentrating effect is focusing of the band after development as the band dries (Figure4.4.1B). The focusing effect is occurring from the solvent front towards the origin. It should be noted that the concentration of the sulforhodamine 640 (SR640) necessary to image the development in rapid real time in Figures 4.4.1A and 4.4.1B was high and is most likely overloading the array and, also, the fluorescence intensity is enhanced by the solvent in comparison to the dry cases (Figure 4.4.1C & 4.4.1D). The focusing effect appears to be solvent dependent in that it has only been observed while using solvents that are viscous and have very low vapor pressure and hence dry relatively slowly. The calculated efficiencies (H) in Figure 4.4.1D (stacking case) and Figure 4.4.1C (focusing case) are approximately 900nm, peak capcacity > 50, and 100nm, peak capacity >150 (n=3), respectively (methods to compute H and approximate peak capacity appear in Chapter 5, Supporting Information). Although it is tempting to equate this focusing with direct coffee ring effects[28, 29], it is noteworthy that the dynamics of evaporation of solute containing bands in this work involve a surface with multiple layers of roughness and a partition capacity for the

analyte. Stacking and focusing are discussed further in Chapter 5, Supporting Information. Focusing and stacking effects are most likely R_f dependent, however, other contributing factors to these effects should be investigated to determine if the processes can be tuned and controlled to maximize resolution. The narrower bandwidth shown in Figure 4.4.1 C versus D is not indicative that DPA are superior to SPA, but rather indicates the increase in efficiency observed in the case of focusing effects. A more thorough discussion on the focusing and stacking effects can be found in Chapter 5, Supporting Information.

4.5 NTLC platform separations

The potential of the NTLC platforms for significant, extremely low volume separations was evaluated. Figures 4.4.2A and 4.4.2B are separations of standard dyes on DPA (sulforhodamine 640 (SR640) and fluorescein isothiocyanate (FITC)) and SPA (SR640 and coumarin 102) platforms, respectively. Figure 4.4.2C is a separation of the anti-tumor drugs Daunorubicin (D_1) and Adriamycin (A_1) on a DPA and Figure 4.4.2D is a separation of fluorescently derivatized environmental amines, 7-nitrobenz-2-oxa-1,3-diazole (NBD)- n-heptyl and n-propyl amine on an SPA. Note that resolution is enhanced (e.g. in Figure 4.4.2B) due to stacking effects and, when generating chromatograms, selecting the central 25% of the stacked band (solid) also improves resolution relative to using the entire band (dashed). In addition to baseline resolution for these separations, plate heights are less than 1 μm and band volumes are in the pL range.z

4.6 Conclusions

We demonstrate herein the fabrication of DPA- and SPA-NTLC platforms that can be made into porous shell-core structures and surface modified with hydrophobic character. The arrays share traits for separations of more traditional approaches but are truly nano in scale and offer attributes of systems at that scale. In particular, NTLC is shown to behave uniquely in terms of solvent and analyte spot transport and dispersion,

producing extremely low volume separations with high efficiency. While issues involving solvent evaporation were observed, it is expected that they can be overcome with further research.

4.7 Acknowledgements

4.8 References

1. J. J. Charlton, N. Lavrik, J. A. Bradshaw and M. J. Sepaniak, *ACS Applied Materials & Interfaces*, 2014.
2. D. M. Tennant, *journal of Vacuum Science Technology*, 2013, 31.
3. R. L. Agapov, B. Srijanto, C. Fowler, D. Briggs, N. V. Lavrik and M. J. Sepaniak, *Nanotechnology*, 2013, 24, 505302-505311.
4. D. Clicq, R. W. Tjerkstra, J. G. E. Gardeniers, A. v. d. Berg, G. V. Baron and G. Desmet, *Journal of Chromatography A*, 2004, 1032, 185-191.
5. W. D. Malsche, D. Clicq, V. Verdoold, P. Gzil, G. Desmet and H. Gardeniers, *Lab on a Chip*, 2007, 7, 1705-1711.
6. W. D. Malsche, H. Gardeniers and G. Desmet, *Analytical Chemistry*, 2008, 80, 5391-5400.
7. R. M. Tiggelaar, V. Verdoold, H. Eghbali, G. Desmet and J. G. E. Gardeniers, *Lab on a Chip*, 2008, 9, 456-463.
8. N. V. Lavrik, L. C. Taylor and M. J. Sepaniak, *Lab on a Chip*, 2010, 10, 1086-1094.
9. T. B. Kirchner, N. A. Hatab, N. V. Lavrik and M. J. Sepaniak, *Analytical Chemistry*, 2013, 85, 11802-11808.
10. J. M. F. Ceiler, P. A. Kohl and S. A. Bidstrup, *Journal of the Electrochemical Society*, 1995, 142, 2067-2071.
11. P.-z. Yang, L.-m. Liu, J.-h. Mo and W. Yang, *Semiconductor Science and Technology*, 2010, 25.
12. N. V. Lavrik, L. T. Taylor and M. J. Sepaniak, *Analytica Chimica Acta*, 2011, 694, 6-20.
13. L. C. Taylor, T. B. Kirchner, N. V. Lavrik and M. J. Sepaniak, *Analyst*, 2012, 137, 1005-1012.
14. O. Reynolds, *Proceedings of the Royal Society of London*, 1883, 35, 84-99.
15. G. Deininger, *Chromatographia*, 1976, 9.
16. A. B. D. Cassie and S. Baxter, *Transactions of the Faraday Society*, 1944, 40, 546-551.
17. H. Kusumaatmaja, C. M. Pooley, S. Girardo, D. Pisignano and J. M. Yeomans, *Physical Review E*, 2008, 77.
18. K. Tsougeni, D. Papageorgiou, A. Tserepi and E. Gogolides, *Lab on a Chip*, 2009, 10, 462-469.
19. R. N. Wenzel, *Industrial and Engineering Chemistry*, 1936, 28, 988-994.
20. G. Guiochon and S. Antoine, *Journal of Chromatographic Science*, 1978, 16, 470-481.
21. , eds. L. Komsta, M. Waksmundzka-Hajnos and J. Sherma, CRC Press, Dec 20, 2015.
22. J. M. Miller, *Chromatography: Concepts and Contrasts*, John Wiley & Sons, Inc., Hoboken, NJ, 2005.
23. C. F. Poole, *Journal of Chromatography A*, 2003, DOI: 10.1016 /S0021-9673(03)00435-7, 963-984.
24. C. F. Poole, *The Essence of Chromatography*, Elsevier Science B.V., Amsterdam, 2003 edn., 2003.
25. S. K. Poole and C. F. Poole, *Journal of Chromatography A*, 2011, 1218, 2648-2660.
26. P. S. Variyar, S. Chatterjee and A. Sharma, in *High-Performance Thin-Layer Chromatography (HPTLC)*, ed. M. Srivastava, Springer, 2011, ch. 2.
27. S. R. Jim, A. J. Oko, M. T. Taschuk and M. J. Brett, *Journal of Chromatography A*, 2011, 1218, 7203-7210.

28. R. D. Deegan, O. Bakajin, T. F. Dupont, G. Huber, S. R. Nagel and T. A. Witten, *Nature*, 1997, 389.
29. B. M. Weon and J. H. Je, *Physical Review*, 2010, 82.

Chapter 5

Supporting information for

"Deterministic and stochastic

nanoscale pillar arrays for

separations"

5.1   Nano-layer array fabrication

The deterministic pillar arrays (DPA) were fabricated using standard cleanroom protocol for electron beam lithography, on silicon wafers using a JEOL JBX-9300FS EBL system. The master CAD file was created using Layout Editor where the pillars were designed to form equilateral triangles as reported in our earlier work[1-5] and by Desmet et. al. [6-10] A 300 nm-thick layer of ZEP520A e-beam resist (ZEON Chemical L.P., Japan) was spun on a 4-in silicon wafer and baked at 180°C for 2 min to harden the resist. The resist was patterned at an acceleration voltage of 100 kV and exposed to a dose of (420-450 µC/cm^2). After exposure, the resist was developed in Xylene for 30 sec, rinsed in isopropyl alcohol for another 30 s and dried under a stream of high-purity nitrogen. Following development, the wafer was exposed to oxygen plasma for 10 sec (Oxford reactive ion etcher) to clean residual resist from the channels[11]. For the lift-off process, a 20 nm Cr layer was first deposited using an electron-beam dual gun evaporation chamber (Thermonics Laboratory, VE-240) equipped with a quartz crystal monitor to measure the thickness. The excess resist and Cr were removed by lift-off using an acetone bath followed by isopropyl alcohol rinse.

The Si anisotropic RIE was carried out in an Oxford PlasmaLab system (Oxford Instruments, UK) at 10 mTorr in a SF6:C4F8:Ar mixture defined by respective flow rates of 58, 25 and 5 sccm. The wafer with Si pillars was then thermally annealed at ~600 ◦C for 10 min in a mixture of hydrogen and argon at a pressure of 735 Torr in a cold wall furnace (Easy Tube 3000, First Nano, Ronkonkoma, NY). Atomic layer deposition of SiO2 was carried out using an Oxford FlexAl tool to coat the resulting Si nanopillars with a 5 nm thick conformal layer. The wafer then was, again, thermally annealed at ~600◦C for 10min in a mixture of hydrogen and argon (10:1) at a pressure of 735 Torr in a cold wall furnace. A thin layer of PSO (~25 nm) was then deposited on the wafer surface using a low temperature plasma enhanced chemical vapor deposition (System 100 Plasma Deposition Tool, Oxford Instruments) method[2]. The pillar dimensions were evaluated using a scanning electron microscope (Carl Zeiss, Merlin).

Table 5.1.1: NTLC – Dimensions (pillar heights 1-2 µm)

Type	Diameter (nm)	Pitch (nm)	PSO
DPA	400	550	No
DPA	400	700	No
DPA	450	550	Yes
DPA	450	700	Yes
SPA	230 (RSD 41%)	640 (RSD 17%)	Yes

The nanoscale stochastic pillar arrays (SPA) were fabricated by using a unique lithography-free approach to fabricating pillar arrays. A thin layer (typically ~ 10 nm) of platinum was deposited on the silicon surface using physical vapor deposition. The Pt layer was then rapidly heated to ~900°C in a cold wall furnace (Easy Tube 3000, First Nano, Ronkonkoma, NY) using a 10:1 ratio of argon and helium (P=735 torr). The thermally processed Pt islands that are created acted as a hard mask and the silicon wafer was then etched using the same anisotropic reactive ion etching and thin film deposition described in the electron beam lithography fabrication above, with further details available in previous work[12, 13]. The dimensions of the 5 cases investigated (with and without PSO and both types of arrays) are summarized in Table 5.1.1. It is noted that the dimensions in the table do not approach the limits of the fabrication techniques used herein. Pillar diameters and gaps can be considerably less than 100nm but may not be as stable as those used.

5.2 C18 Functionalization

The C18 reverse stationary phase was added to the arrays using a method described in our previous work[1] and by Hennion et. al. [14] where the arrays were pretreated using a 50:50 mixture of HNO_3 and HSO_4 acids to increase the number of surface silanols available for the C18 bonding. A 10% solution of the octadecyltrichlorosilane (C18) was prepared in toluene and heated to 170 ºC for 2 hours. The array was then rinsed with toluene, tetrahydrofuran, a 90/10% ratio of distilled water and tetrahydrofuran, and finally distilled water. Each rinse was for 10 minutes and repeated twice before continuing to the next rinse stage.

5.3 Spot and solvent flow imaging

Fluorescence imaging of developed and developing spots for efficiency and separations evaluations was performed using a Nikon Eclipse E600 with Q capture software. Chromatograms were generated from these images using Image J 1.47V (Wayne Rashband, National Institutes of Health, USA) public domain software A . Solvent velocity was recorded using a Watec LCL-211H CCD camera coupled with GrabBee video capture software.

5.4   Evaluation of plate height

Plate heights for these nano-scale systems were evaluated using three different methods. The first two methods were similar to the analysis reported in our previous publication[1]. Both methods calculate H and peak capacity (n)[15] using the following equations:

$$H = \frac{(w_F - w_I)^2}{16d} \qquad \text{[5.4.1]}$$

$$n = 1 + \frac{(\sqrt{N})}{2} \qquad \text{[5.4.2]}$$

Where d is the distance the spot traveled and W_F and W_I are the final and initial spot widths (direction of flow), respectively. For the first method the plate height was evaluated by subtracting the initial spot width from the final width. The second method made the assumption that the initial spot width was infinitesimally small (W_I=0). This was due to the apparent improved efficiencies caused by focusing effects discussed below that caused the final band width to be narrower than the original spot width. The final method used the most prominent Van Deemter (B and Cm) terms that allowed predictions of efficiencies based on the solvent velocity data collected experimentally and modeled in the case of acetonitrile discussed more in Supporting Information. In all cases the calculated H represents a value averaged over the distance traveled. Equation 5.4.2 is used often in chromatography as it relates peak capacity to plate number, N. Herein, N is determined via L/H and is used as a rough approximation of n despite the complication of a changing flow rate (hence efficiency) with position along the NTLC array.

5.5   Development chamber

The horizontal development chamber was designed to minimize volume in order to inhibit evaporation issues. Aluminum metal was machined such that there was a trough of solvent surrounding the nanothin-layer array in order to create a uniform vapor environment. The chamber was sealed using a polydimethylsiloxane gasket and allowed to come to equilibrium. A moveable support was used that allowed for contact with the mobile phase to be made or interrupted to control the development.
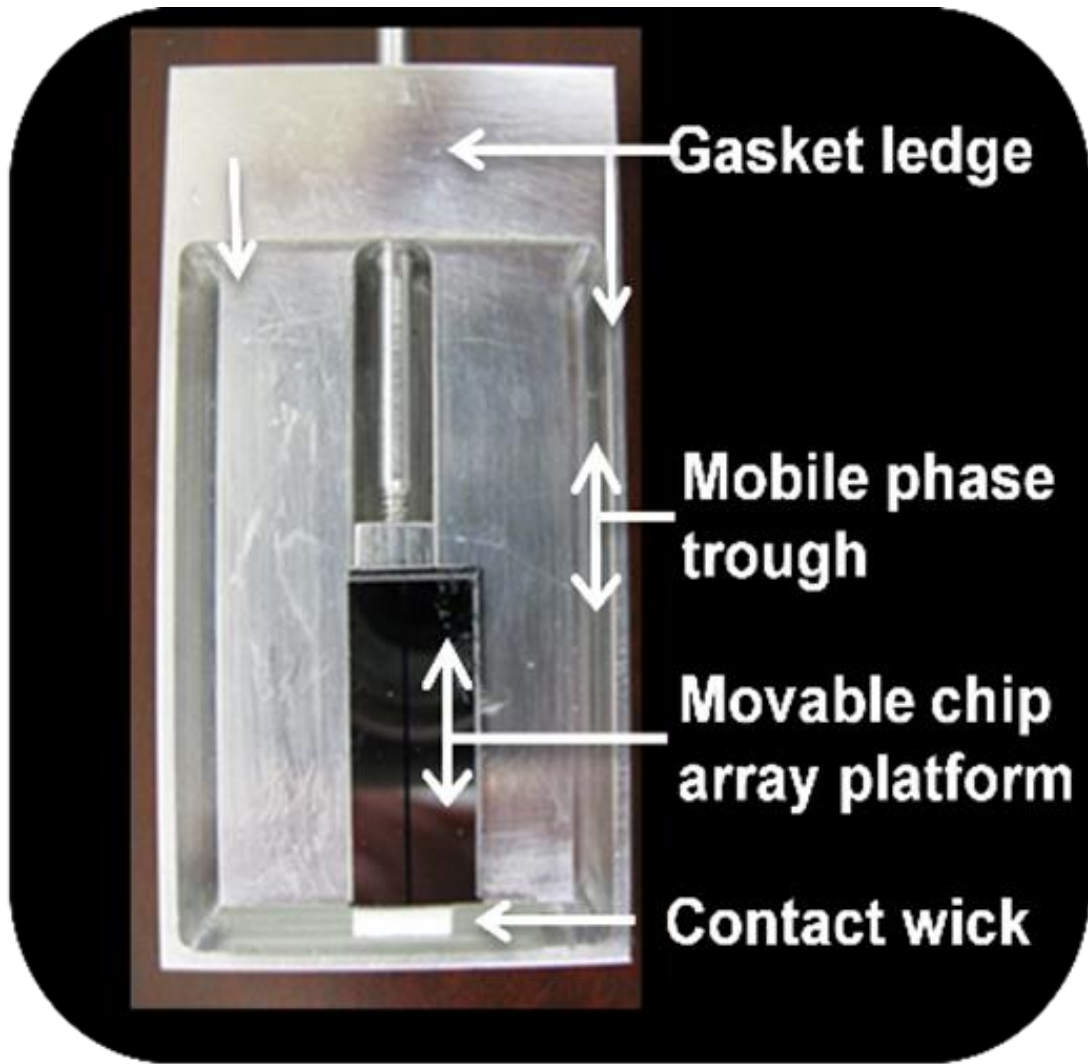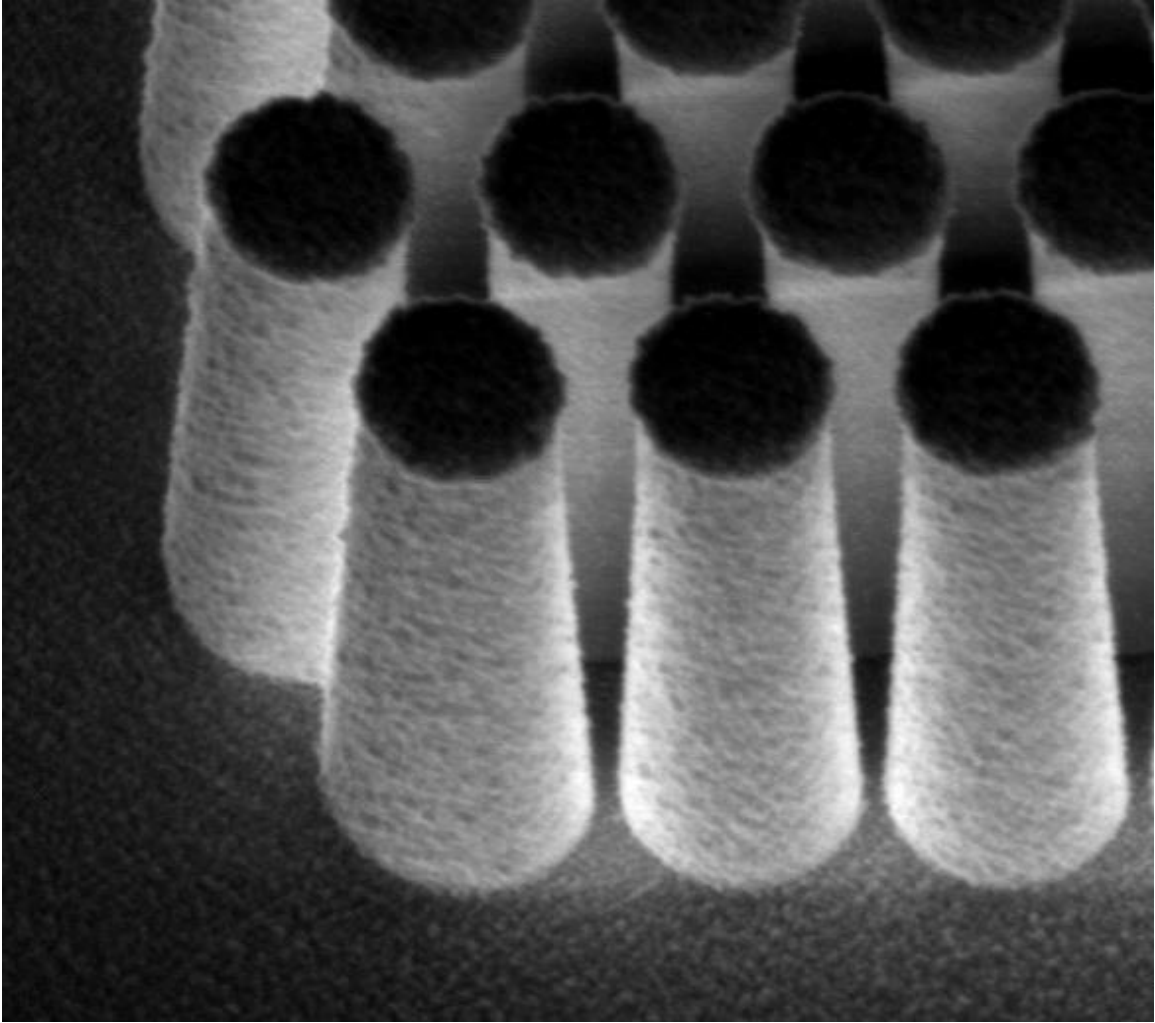
Figure 5.5.1: Horizontal development chamber with mounted EBL array.

Figure 5.5.2: SEM of EBL sidewall.

The volume is < 2mL total and allows for real time analysis of analyte development (SI Figure 5.5.1).

Alternatively, vertical development can also be utilized by mounting the array to a moveable support and sealing inside of a more traditional vertical development chamber. After equilibrium is established the array is lowered to make direct contact with the mobile phase.

Further efforts to minimize evaporation issues within these chromatographic systems will be attempted through a variety of controlled experiments. These include changing the gasket thickness to precisely control the chamber volume and experimentation with temperature control of both the array and the chamber window to allow for the manipulation of solvent (vapor versus liquid) - array interactions in order to minimize evaporation problems. External partial or full saturation of solvent in an ambient gas, with flow in and out of the development chamber, will be pursued to maintain greater control of the local environment proximal to the pillar arrays.

5.6   Image of pillars at the array boundary

After PSO deposition, SI Figure 5.5.2 demonstrates narrower gaps for the pillars that are on the boundary (pillars / no pillars*). A few ro*ws into the array the sidewalls of the pillars are nearly vertical. There is also PSO outside the array that can wick solvent.   This heterogeneity can alter the flow rate in the boundary region of the array and produce irregular band fronts (see Figure 4.4.2A for example). Nevertheless, the central position of the bands remains uniform and due to our ability to select a band region from the center of the dried band this is not detrimental to our analysis. This effect is not seen for the large DW arrays where the band does not encounter a boundary.

5.7   Additional introduction & modeling

As discussed in our previous work the factors that contribute to plate height, H, are complex in planar chromatography [1, 16, 17]. The treatment that was used in order to validate the premise for this research was based on the well-known work proposed by Guiochon [18] and is often used as a thorough analysis for planar chromatography.

Table 5.7.1: Solvent Properties

Solvent	Polarity Index	Surface Tension (γ) mN/m	Viscosity (η) mPa s @25C	γ/ η ratio	Molecular Weight	Vapor Pressure (torr)
Benzyl Alcohol	4.07	39.00 @20C	5.474	7.12	108.14	0.11 @25C
Acetonitrile	5.8	28.66 @ 25C	0.369	77.67	41.05	100 @27C
2-Propanol	3.9	20.93 @ 25C	2.038	10.27	60.10	40 @ 23.8C
Ethanol	5.2	21.97@25C	1.074	20.46	46.07	90@25C

This treatment is based on the validity of the Van Deemter equation (Equation [5.7.1]) that is common to HPLC theory.

$$H = A + \frac{B}{v} + (C_S + C_M)v$$

[5.7.1]

From this equation H is dependent on eddy diffusion, A, longitudinal diffusion, B, which is influenced by the mobile phase velocity (v) and resistance to mass transfer in both the stationary and mobile phases, Cs and Cm, respectively. For the cases of highly ordered pillar arrays the eddy diffusion term (A) should be a minor factor that contributes to band broadening [1, 2]. For k'=0 or very thin stationary phases with rapid kinetics we can further exclude broadening contributions from the stationary phase term (C_S). As done in our previous publication we can use experimental literature values for the packing parameters of the pillar arrays of γ (0.5) and ω (0.02), [1, 2] the relevant plate height can be estimated based solely on the ubiquitous B and C_m terms by using Equation [5.7.2] with experimental or modeled knowledge of solvent velocity [1, 2, 19, 20].

$$H = \frac{2(\gamma)D_M}{v} + \frac{(\omega)d_p^2 v}{D_M}$$

[5.7.2]

To further evaluate the predicted effect on efficiency and to further direct our chromatographic substrate development we derived wicking velocities by using the semi-empirical model developed by Mai et al. for ordered arrays of silicon pillars[21]. This model is based on the geometrical parameters of the fabricated substrate, experimentally measured solvent-substrate contact angles, and literature values for solvent viscosity and surface tension (see Table 5.7.1). Modeled results were compared to the velocities that were experimentally observed in our system. In particular we calculated wicking velocities for acetonitrile and determined that the predicted solvent flow should result in improved plate heights; especially early in the solvent development.

We have estimated the plate heights for these nano-scale arrays using a typical diffusion coefficient (D_M) of 5.0E-6 cm^2/s for the solute, experimental velocities and modeled velocity for acetonitrile. The NTLC system plate heights are predicted to
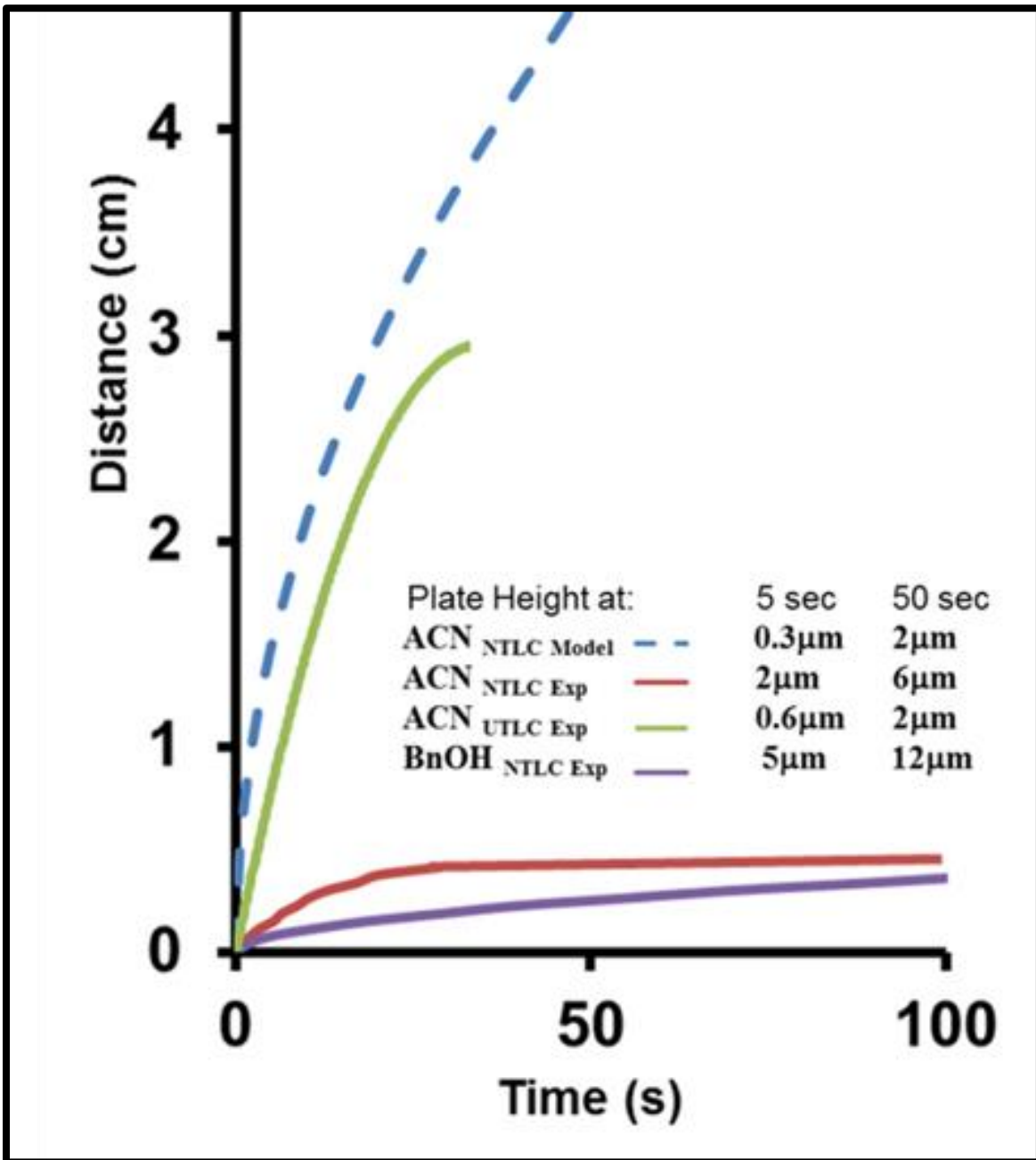
Figure 5.7.2: Mobile phase velocity and predicted plate heights.

be smaller than the UTLC micro scale systems reported in our previous work[1] when using the same parameters for the packing factors and only changing the critical particle size (d_p) value (note: we use the inner pillar gap dimension) and using the modeled velocities for acetonitrile (SI Figure 5.7.1). These predicted plate heights are 0.3μm (NTLC) and 0.6 μm (UTLC) at 5 seconds and 1.7μm for both systems at 50 seconds. While the modeled case does not consider the porous SiO_2 layer and thus only roughly mimics the experiment, this treatment does indicated that the scaling down into the nano-regime from our previous work could potentially yield positive advancements in the field of planar chromatography.

5.8 Stacking

The decrease in phase ratio as one moves from the origin to the solvent front in planar chromatography is well documented for traditional systems [16, 17, 20, 22, 23]. The capillary action driven solvent flow replenishes evaporated solvent most effectively from the solvent reservoir side of the system. The relative effect of evaporation is likely exacerbated for our NTLC (1-2μm depth) relative to UTLC or conventional TLC due to the shallowness of the platform. If we consider Equations [5.8.1] and [5.8.2], as values for the phase ratio β increase smaller k' values for a given partition coefficient (Kc) are observed and this increases flow relative to the mobile phase velocity (v_{mp}) in the band involved (i.e., the zone behind band center can move faster than the zone in front).

$$k' = K_C \frac{V_S}{V_M} \text{ or } \frac{K_C}{\beta} \qquad [5.8.1]$$

$$V_{zone} = \frac{v_{mp}}{(1 + k')} \qquad [5.8.2]$$

Figure 5.8.1 shows stacking effects for one of our test analytes for both TLC and NTLC. The stacking helps to counteract the traditional Van Deemter band broadening contributions and for the NTLC case plate heights that are significantly lower in the direction of propagation than predicted from the Van Deemter Equation. A beneficial stacking effect is seen in the resolution of the bands in Figure 4.4.2B for which isotopic band broadening would have left the bands largely unresolved.
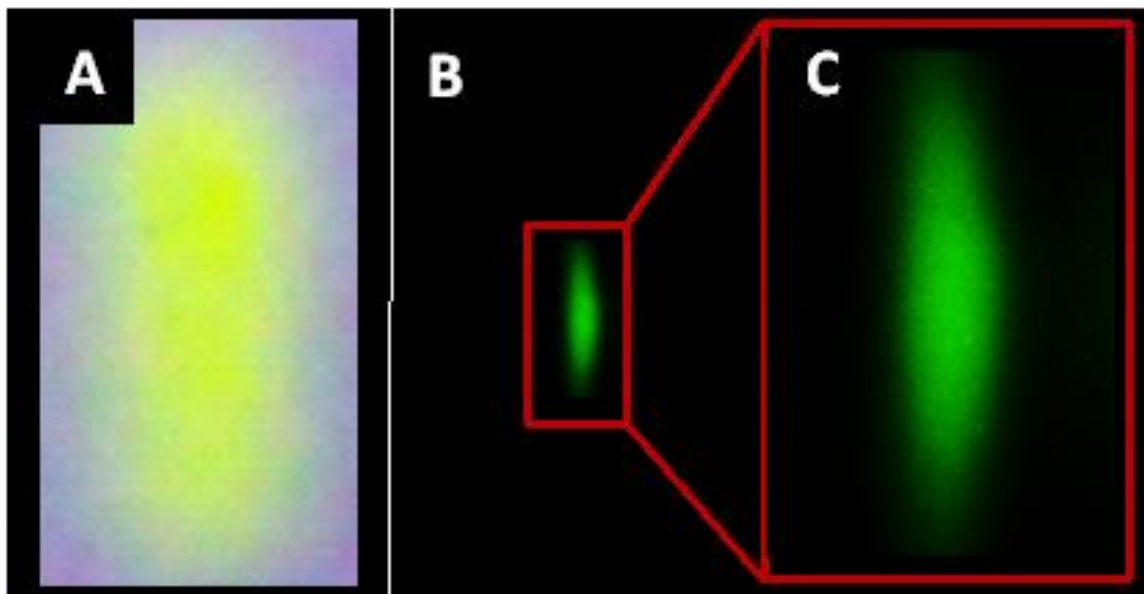
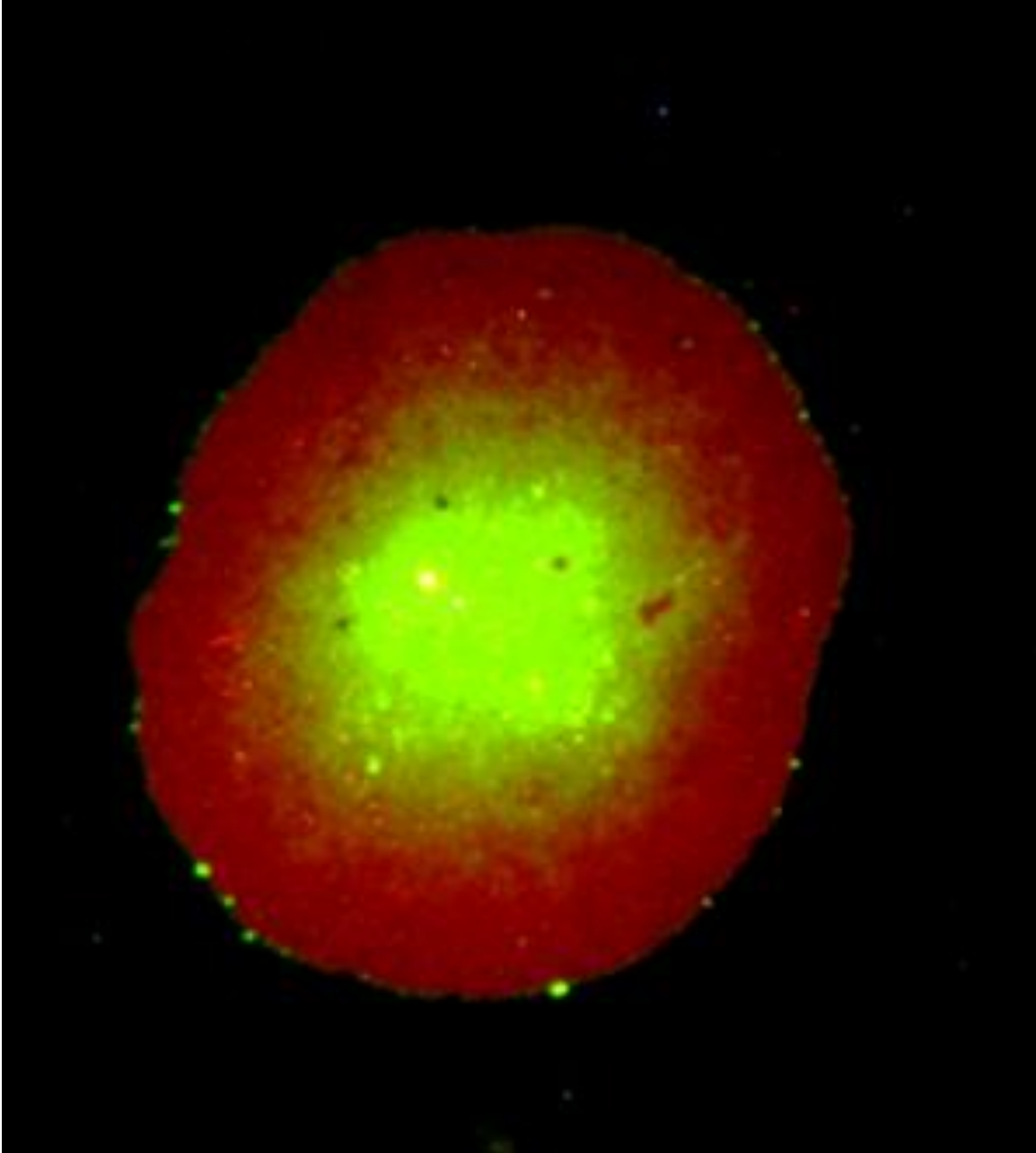**Figure 5.8.1: Illustration of stacking phenomena for NBD-heptyl amine; (A) reversed phase TLC case (spot width in flow direction ~2,300 μm), (B) stochastic array case (spot width ~400 μm), (C) B magnified ~ 4X.**

Figure 5.9.1: Image of spotted FITC and Rhodamine sample showing spatially defined drying.

5.9 Focusing

The focusing effects observed during the band drying are not easily understood for our complex morphologies. The traditional coffee ring effect moves solute (usually particles) toward the perimeter of a drying droplet. This occurs as the droplet edge is pinned and evaporation at the perimeter produces a replenishing outward flow from the center[23]. In some cases such flows can be reversed by Marangoni and other effects[24]. In fact we have observed preferred perimeter deposition of solute at times during sample spotting. SI Figure 5.9.1 is one of the more informative of these observations. For this spotting procedure we take advantage of the superhydrophobic nature of the array and continuously deliver sample solution from a small gauge needle syringe into a very small (typically 200-250 µm) spot on the array[1]. The process can take tens of seconds during which fresh solution is added and replenishes evaporation at the perimeter of the spot. As evaporation occurs at the perimeter, solute should be driven by phase distribution into the stationary phase leaving the equivalent of a coffee ring effect. However, if the perimeter becomes saturated then the solute will be retained in the liquid phase and this can lead to a more uniform spot or even a preference of solute in the center of the spot. These effects seem to occur in SI Figure 5.9.1 for a two component mixture observed with microscope settings that observe both dyes. The red Rhodamine dye has a larger k', a lower concentration, and appears more at the perimeter.   Conversely the FITC green dye has a smaller k' (less affinity for the stationary phase), a higher concentration to facilitate detection, and appears more in the center of the spot. These observations of phase distribution and non-linear isotherm behavior may help explain the focusing shown in Figure 4.4.1B, C and 4.4.2A. In Figure 4.4.1B a very high concentration of dye was used to observe the process in real time and it appears that the dye is being swept along with the receding drying front. Presumably the stationary phase is saturated to the right of the front in the figure.   In Figure 4.4.1C the R_f is approximately 0.5 (apparent H ~ 100nm). whereas in Figure 4.4.2A the focused band is near the solvent front and is focused more tightly (apparent H < 100nm).   Clearly the focusing effect is very

system and condition dependent and it remains to be determined if it can be harnessed for practical chromatographic good.

5.10 Acknowledgements

5.10 References:

1. T. B. Kirchner, N. A. Hatab, N. V. Lavrik and M. J. Sepaniak, *Analytical Chemistry*, 2013, 85, 11802-11808.
2. N. V. Lavrik, L. C. Taylor and M. J. Sepaniak, *Lab on a Chip*, 2010, 10, 1086-1094.
3. N. V. Lavrik, L. T. Taylor and M. J. Sepaniak, *Analytica Chimica Acta*, 2011, 694, 6-20.
4. L. C. Taylor, T. B. Kirchner, N. V. Lavrik and M. J. Sepaniak, *Analyst*, 2012, 137, 1005-1012.
5. L. C. Taylor, N. V. Lavrik and M. J. Sepaniak, *Analytical Chemistry*, 2010, 82, 9549-9556.
6. W. De Malsche, D. Clicq, V. Verdoold, P. Gzil, G. Desmet and H. Gardeniers, *Lab on a Chip*, 2007, 7, 1705-1711.
7. W. De Malsche, S. De Bruyne, J. O. De Beeck, S. Eeltink, F. Detobel, H. Gardeniers and G. Desmet, *Journal of Separation Science*, 2012, 35, 2010-2017.
8. W. De Malsche, H. Eghbali, D. Clicq, J. Vangelooven, H. Gardeniers and G. Desmet, *Analytical Chemistry*, 2007, 79, 5915-5926.
9. W. De Malsche, H. Gardeniers and G. Desmet, *Analytical Chemistry*, 2008, 80, 5391-5400.
10. J. De Smet, P. Gzil, N. Vervoort, H. Verelst, G. V. Baron and G. Desmet, *Analytical Chemistry*, 2004, 76, 3716-3726.
11. S. M. Wells, S. D. Retterer, J. M. Oran and M. J. Sepaniak, *ACS Nano*, 2009, 3, 3845-3853.
12. R. L. Agapov, B. Srijanto, C. Fowler, D. Briggs, N. V. Lavrik and M. J. Sepaniak, *Nanotechnology*, 2013, 24, 505302-505311.
13. J. J. Charlton, N. Lavrik, J. A. Bradshaw and M. J. Sepaniak, *ACS Applied Materials & Interfaces*, 2014.
14. M. C. Hennion, C. Picard and M. Caude, *Journal of Chromatography*, 1978, 166, 21-35.
15. F. Gritti and G. Guiochon, *Journal of Chromatography A*, 2012, 1221, 2-40.
16. C. F. Poole, *Journal of Chromatography A*, 2003, DOI: 10.1016 /S0021-9673(03)00435-7, 963-984.
17. S. K. Poole and C. F. Poole, *Journal of Chromatography A*, 2011, 1218, 2648-2660.
18. G. Guiochon and S. Antoine, *Journal of Chromatographic Science*, 1978, 16, 470-481.
19. G. Deininger, *Chromatographia*, 1976, 9.
20. C. F. Poole, *The Essence of Chromatography*, Elsevier Science B.V., Amsterdam, 2003 edn., 2003.
21. T. T. Mai, C. Q. Lai, H. Zheng, K. Balasubramanian, K. C. Leong, P. S. Lee, C. Lee and W. K. Choi, *Langmuir*, 2012, 28, 11465-11471.
22. J. M. Miller, *Chromatography: Concepts and Contrasts*, John Wiley & Sons, Inc., Hoboken, NJ, 2005.

23.   P. S. Variyar, S. Chatterjee and A. Sharma, in *High-Performance Thin-Layer Chromatography (HPTLC)*, ed. M. Srivastava, Springer, 2011, ch. 2.

Chapter 6

Concluding Remarks

6.1 Conclusion:

Development of chip based separations is a rapidly growing field. The miniaturization of chromatographic platforms has applications in healthcare as point-of-care devices and lab-on-chip devices for many industries. Also, fundamental understanding of fluid flow (capillary driven, electrokinetic, pressurized) and analyte interactions in these miniaturized devices is critical in the advancement of this type of analysis as well as other areas where understanding fluid dynamics in relation to micro- and nano- scale systems is relevant.

Fabrication of the devices described in this disseratation are not trivial and the optimization of many parameters was necessary in order to successfully complete this research. Initial research was performed to optimize mobile phase velocity by investigating the pillar aspect ratio and inter-pillar spacing. It was determined that high-aspect ratio pillars were appropriate for both the micro- and nano- scale arrays investigated in this research. Inter-pillar spacing was successfully reduced to 1 micron for the deterministic photolithographic array and 250nm for the deterministic EBL arrays. The stochastic arrays investigated had a range of inter-pillar gaps that bounded the 250nm range. Initial work indicated that the surface area of the pillar arrays was insufficient for analyte retention without further modification. This issue was resolved by changing the surface modification parameters for silicon oxide from a high temperature (~200°C) to a room temperature deposition process. This created a porous silicon oxide layer on the pillar surface that greatly increased the surface area for reverse phase (C18) stationary phase surface siloxane chemistry. Another benefit of the silicon oxide deposition is that this process increased the stability of the pillars making these arrays more robust. This fabrication process, including C18 RP functionalization, is a reproducible method that allows for the production of numerous reusable chromatographic substrates on one silicon wafer. The fabrication methods outlined in this work serves as a guide for future fabrication of similar devices.

Sample application for UTLC has been highlighted as one of the limitations that is critical to overcome for this chromatographic process to become more

mainstream[1]. Development of a spotting method that demonstrate the ability to create reproducible sample spots that are less than 200 microns (micro- scale arrays) and 400nm (nano- scale arrays) within these arrays was critical to the advancement of this and similar research. Taking advantage of the super-hydrophobic nature of these systems allowed for the development of a novel method of low volume sample application that did not require any additional automated instrumentation that is commonly used for such low volumes.

Another observation made during the course of this work was that spot solvation kinetics does not increase band broadening as the mobile phase initially interacts with the analyte. With these low spot volumes the mobile phase readily dissolve the analyte and lifts it into the remainder of the dry spot causing a concentration of the original spot into a very narrow band for development.

Deterministic silicon pillar arrays have been used in pressurized chromatography and the results from these studies indicate that, for these highly ordered systems, a reduction in particle size does not result in a reduction in mobile phase velocity. The fabrication methods for these arrays allow for precise control of pillar morphology, size, placement and height. This dissertation focuses on the effect of scaling planar chromatography systems down to the low micron and nano- scale in non-pressurized, capillary flow driven systems . Effects on velocities, and efficiency were studied using the low micron plates and velocity, efficiency and resolution was evaluated using both deterministic and stochastic nano- scale systems.

The deterministic micro-scale arrays discussed in Chapter 3 of this work showed significant promise due to rapid solvent wicking through these arrays as the dimensions were reduced in comparison to traditional TLC. The preliminary research discussed in this chapter illustrates both practical and fundamental aspects of this research. This results presented herein indicate that lithographically-produced highly ordered pillar arrays can be used as reusable planar chromatography separation platforms with mobile phase capillary flow.   This open system bypasses issues observed in pressurized pillar array chromatography including sealing of the system[2-

[4]. Of significant importance a C18 stationary phase functionalization of the arrays has been incorporated that does not cause occlusion between the pillars. Surprisingly, the linear flow velocity studies during development reveal a trend to more rapid flow as pillar size and gap decrease.   Discussion of this trend on the effects on efficiency are presented and indicate that these arrays perform better when scaling down to these ultra-thin layers when compared to traditional TLC platforms. The superhydrophobic nature of these systems, due to both the micro- structured features and the carbon RP stationary phase, enables analyte sampling in very small spots. Imaging of these spots and separations was possible using a simple fluorescence microscope.   The results from these initial studies motivated the subsequent scaling down to the nano- regime and, also, shows promise in research where utilizing the these micro- systems and investigating a reduction in the inter- pillar gaps would be interesting.

Scaling down to the nano-regime was non-trivial in both the fabrication of these miniaturized devices and working with extremely low mobile phase and analyte volumes. In Chapter 4 we have demonstrated the fabrication of both deterministic and stochastic nanothin-layer chromatographic platforms. Using a room temperature porous silicon oxide deposition method we have created a porous shell-core structures that have been functionalized with a carbon reverse phase stationary phase. These systems have produced extremely low volume separations with high efficiency. Although, these systems have issues regarding solvent evaporation it seems that the resulting phase ratio gradient has generated a unique focusing and stacking effect that is beneficial to efficiency. Most significantly these systems resulted in bands that were highly efficient and resulted in significant separations of analytical laser test dyes, environmentally significant NBD-derivatized amines, and, biologically relevant chemotherapy drugs (Adriamycin and Daunorubicin).

The work presented herein has optimized fabrication parameters, sampling methods and has highlighted critical areas that require more optimization for future work (i.e. development chamber and evaporation effects). Future work in this area

should include the aforementioned issues and also investigation of further scaling of the inter-pillar gaps and investigation into other methods to improve surface area.

6.2 References:

1. S. C. Powell, *Analytical Chemistry*, 2010, DOI: 10.1021/AC100625S, 3408.
2. L. C. Taylor, Ph.D., University of Tennessee, 2012.
3. L. C. Taylor, T. B. Kirchner, N. V. Lavrik and M. J. Sepaniak, *Analyst*, 2012, 137, 1005-1012.
4. L. C. Taylor, N. V. Lavrik and M. J. Sepaniak, *Analytical Chemistry*, 2010, 82, 9549-9556.

Vita

Teresa was born in Warner Robins, GA in April, 1977. She was raised on a farm outside of Perry, GA, which fostered her curiosity of science. She moved north of Atlanta as a teenager and graduated from Johnson Comprehensive High School in 1995. She received an A.S. from Gainesville Community College (2004) and a B.S. from North Georgia College and State University (2007). After graduating from North Georgia, Teresa studied analytical chemistry and chemometrics under Dr. Paul Gemperline at East Carolina University. Teresa continued her graduate studies at the University of Tennessee under Dr. Michael J. Sepaniak where she will graduate with a Ph.D. in May, 2015. She is currently working as an R&D analytical chemist for BAE Systems in Kingsport, TN.